

Determination of the Cabibbo-Kobayashi-Maskawa matrix element $|V_{cb}|$

Giulia Ricciardi

Dipartimento di Fisica E. Pancini, Università di Napoli Federico II and
I.N.F.N. Sezione di Napoli,
Complesso Universitario di Monte Sant'Angelo, Ed. 6, Via Cintia, 80126 Napoli, Italy
E-mail: giulia.ricciardi@na.infn.it

Marcello Rotondo

Laboratori Nazionali dell'INFN di Frascati, Via Enrico Fermi 40, 00040 Frascati
(Roma), Italy
E-mail: marcello.rotondo@lnf.infn.it

Nov 2019

Abstract.

In this review we present and discuss the determination of the magnitude of the Cabibbo-Kobayashi-Maskawa (CKM) matrix parameter V_{cb} . The CKM matrix parametrizes the weak charged current interactions of quarks in the Standard Model (SM), and a precise determination of its elements has always been one of the most important targets of particle physics. The precise knowledge of the $|V_{cb}|$ value plays a pivotal role in testing the flavour sector of the SM and in the analyses of the unitarity of the CKM matrix.

The SM does not predict the values of the CKM matrix elements, which have to be extracted by experimental data. Given the variety of channels that allow the extraction of $|V_{cb}|$, different theoretical and experimental techniques are mustered for the $|V_{cb}|$ determination. The exertion toward precision represents not only a significant test of our theoretical procedures but a stimulus towards better detection performances.

The most precise measurements of $|V_{cb}|$ come from semileptonic decays, that being tree level at the lowest order in the SM are generally considered unaffected by physics beyond the SM. After summarizing the characteristics of the SM that set the frame for the determination of $|V_{cb}|$, we discuss inclusive and exclusive semileptonic B decays. We analyze the $|V_{cb}|$ extraction methods and recent results, detailing both the theoretical and experimental techniques, and, finally, outline future prospects. We also comment on exclusive decays into heavy leptons, on the observables $R(D)$ and $R(D^*)$, and on decays to excited B -meson states.

Contents

1	Introduction	5
2	The flavour scenario	6
2.1	The Yukawa terms in the SM Lagrangian	6
2.2	Electroweak currents after SSB	8
2.3	The Cabibbo-Kobayashi-Maskawa matrix	9
2.4	The unitarity triangles	11
3	Semileptonic B-meson decays	13
3.1	Inclusive decays	14
3.1.1	Heavy Quark Expansion	15
3.1.2	Mass schemes	17
3.2	Exclusive decays into light leptons	18
3.2.1	Form factors	20
3.2.2	Zero recoil and beyond	22
3.3	Exclusive decays into heavy leptons	24
3.4	Decays to excited D -Meson states	26
4	Experimental techniques	28
4.1	B -hadron production	28
4.1.1	B -Factories	28
4.1.2	Hadron Colliders	30
4.2	Semileptonic measurements at B-Factories	32
4.2.1	Soft pion from D^*	33
4.2.2	B tagging	34
4.3	Semileptonic measurements at LHCb	35
4.3.1	Techniques for kinematic reconstruction	37
5	Inclusive V_{cb} determination	38
5.1	Moment measurements	39
5.1.1	Hadron moments	40
5.1.2	Lepton moments	40
5.2	Results	41
6	Exclusive V_{cb} determination	43
6.1	Unitarity bounds	43
6.2	BGL and CLN parametrizations	45
6.3	The $B \rightarrow D^* \ell \nu_\ell$ channel	47
6.3.1	Belle untagged measurement	48
6.3.2	BaBar tagged measurement	51
6.3.3	Results	53

<i>CONTENTS</i>	4
6.4 $B \rightarrow D\ell\nu_\ell$ channel	55
6.4.1 Belle tagged analysis	56
6.4.2 Results	56
6.5 Direct measurement of $ V_{ub}/V_{cb} $	58
6.6 The $ V_{cb} $ puzzle	60
7 Future prospects	62
8 Bibliography	64

1. Introduction

Nowadays accuracy in measurements and theoretical calculations of physical observables is indispensable to check the Standard Model (SM) and explore the small region of parameters space left to its extensions, at our energies. The increase in precision demands an accurate knowledge of the parameters of the Cabibbo-Kobayashi-Maskawa (CKM) matrix, which are not predictable within the SM, and must be extracted by data. In the last decades, a large effort has gone towards their determination, mostly driven by increasingly higher statistics at new and improved facilities, accompanied by more complex and sophisticated theoretical computations.

Among the CKM matrix elements, V_{cb} takes central stage. Its role is pivotal in the unitarity analyses of the CKM matrix. The so-called unitarity clock, the circle around the origin in the $\bar{\rho}-\bar{\eta}$ plane, is proportional to the ratio $|V_{ub}/V_{cb}|$, and $|V_{cb}|$ normalizes the whole unitarity triangle. Relations between $|V_{cb}|$ and other observables can be exploited to estimate their values, within or beyond the SM, and an accurate determination of $|V_{cb}|$ is necessary for their correct assessment. One example are B decays originated by flavour changing neutral currents, such as rare radiative $B \rightarrow X_s \gamma$ or semileptonic $B \rightarrow X_s \ell^+ \ell^-$ decays, where X_s are hadronic states with strangeness different from zero. In the SM, the $b \rightarrow s$ quark transitions cannot occur at tree level, but start at one loop, mediated by the so-called penguin diagrams, with an up-type quark running in the loop. Top and charm quark contributions are proportional to $V_{tb}V_{ts}^*$ and $V_{cb}V_{cs}^*$ respectively (unitarity can be used to cancel $V_{ub}V_{us}^*$ in the rate). Other examples are in the kaon sector, where ϵ_K , ϵ'/ϵ and branching ratios of rare kaon decays depend sensitively on values of $|V_{cb}|$ (and $|V_{ub}|$) [1].

The semileptonic decays of beauty hadrons, dominated at the quark level by the weak transition $b \rightarrow c \ell \nu_\ell$, are used to determine with high precision the magnitude of the matrix element V_{cb} . The heavy mass of the B meson allows to exploit simplifications in the limit of infinite quark mass and to better separate perturbative and non-perturbative regimes. Another advantage is that semileptonic decays are mediated at leading order in perturbation theory tree-level processes. The exchange of a new physics (NP) particle is strongly constrained at tree level. A clean determination of CKM parameters from tree level processes is therefore a valuable input for other NP more sensitive estimates. Past, present and future B factories have provided and will provide an unparalleled level of precision in branching ratios and related observables, and LHCb is following suit.

There are two approaches to determine $|V_{cb}|$, which allow almost equally precise measurements: the inclusive and the exclusive approach. In the inclusive approach, the $B \rightarrow X_c \ell \nu_\ell$ decays, where X_c , the hadronic state originated by the charm quark, is not reconstructed in any specific final state. Sufficiently inclusive quantities can be expressed as a double series in α_s and Λ_{QCD}/m_b , in the framework of the Heavy Quark Expansion (HQE). In the exclusive approach, one consider decays where a specific hadronic final state is reconstructed, as $B \rightarrow D \ell \bar{\nu}_\ell$ and $B \rightarrow D^* \ell \bar{\nu}_\ell$ decays. The inclusive and exclusive semileptonic determinations rely on different theoretical calculations and on different

experimental techniques which have, to a large extent, uncorrelated statistical and systematic uncertainties. This independence makes their expected agreement a useful test of our understanding of both experiments and theory. Since at least three decades, there is a tension among the $|V_{cb}|$ values, depending on whether they are extracted using exclusive or inclusive semileptonic channels. In the present general scenario of data in optimal agreement within the SM, this tension is intriguing, and alone motivates, in our view, more and more precise theoretical and experimental investigations.

In this paper we review the theoretical background and the experimental techniques relevant for the $|V_{cb}|$ determination. In section 2 we introduce the flavour sector of the SM Lagrangian and the CKM matrix. In section 3 we discuss exclusive and inclusive semileptonic decays (into light and heavy leptons) and the theoretical tools necessary for their analyses. In section 4 we review the experimental techniques used at the B -Factories and LHCb to study semileptonic decays, pointing out the various sources of systematic uncertainties. Sections 5 and 6 are devoted to inclusive and exclusive $|V_{cb}|$ determinations, respectively. Finally, in section 7, we examine future prospects at Belle-II and LHCb facilities, and future theoretical directions of development.

2. The flavour scenario

2.1. The Yukawa terms in the SM Lagrangian

The SM is a gauge field theory describing the electromagnetic, weak interactions and strong interactions of quarks and leptons. It has supported calculations of physical quantities with unflinching precision for the past 50 years. Although there are challenges that the SM does not address, a complete, coherent framework, in agreement with data, which encompasses and extends the SM, has still to emerge.

The SM formulation was obtained after a great deal of experimental data and theoretical conjectures. A main feature, the universality of coupling, for quarks as well as for leptons, implied the existence of some powerful underlying symmetries, which were understood as characteristic of a gauge theory.

The (exact) gauge symmetry of the electroweak (EW) interactions is $SU(2)_L \otimes U(1)_Y$, while the (exact) gauge symmetry satisfied by the strong interactions is color $SU(3)_c$. As a whole, the SM Lagrangian is invariant under $SU(2)_L \otimes U(1)_Y \otimes SU(3)_c$ gauge transformations. Fields in the SM Lagrangian are classified according to irreducible representations of this gauge group. The gauge symmetry of the SM is spontaneously broken to $SU(3)_c \times U(1)_{em}$, where $U(1)_{em}$ is the electromagnetic gauge group.

Gauge invariance in the SM Lagrangian leads one to expect massless vector bosons. Such impasse, mostly debated in the sixties, is surmounted by the so-called Higgs mechanism. According to the Higgs mechanism, the vector bosons W^\pm and Z^0 couple through the EW covariant derivative D_μ to a newly introduced complex scalar ϕ . The dynamics is described by adding to the massless Lagrangian a gauge invariant term \mathcal{L}_ϕ

for the field ϕ

$$\mathcal{L}_\phi = (D_\mu \phi)^\dagger D^\mu \phi - V(\phi) \quad (1)$$

where

$$V = +\mu^2 \phi^\dagger \phi - \frac{\lambda}{4} (\phi^\dagger \phi)^2 \quad (2)$$

Here μ^2 and λ are positive real arbitrary coefficients. The Higgs (or Brout-Englart-Higgs) field behaves as a doublet under the $SU(2)_L$ symmetry and has hypercharge 1/2. When ϕ gets a vacuum expectation value different from zero (spontaneously symmetry breaking), the SM Lagrangian acquires extra terms which are precisely mass terms for the Higgs and the W^\pm and Z^0 bosons. The photon remains massless.

A similar mechanism is also adopted to give mass to quarks and charged leptons. Other gauge invariant terms involving the complex Higgs, the so called Yukawa terms, are added to the Lagrangian in a way that after SSB they include mass terms for charged fermions.

The most general $SU(2)_L \otimes U(1)_Y$ invariant term of dimension four involving the Higgs doublet ϕ and quarks is given, for the first generation of quarks, by

$$\mathcal{L}_{Y_d} = -Y^{(d)} \bar{q}_L \phi d_R + h.c. \quad (3)$$

where $h.c.$ stands for Hermitian conjugate and q_L is the $SU(2)_L$ fundamental doublet, with $q = (u, d)$. The fermion fields have been decomposed into chirality eigenstates, that is

$$u = u_L + u_R, \quad d = d_L + d_R \quad (4)$$

where $(P_{L(R)} = (1 \mp \gamma_5)/2)$

$$\begin{aligned} u_{L(R)} &= P_{L(R)} u & \bar{u}_{L(R)} &= \bar{u} P_{R(L)} \\ d_{L(R)} &= P_{L(R)} d & \bar{d}_{L(R)} &= \bar{d} P_{R(L)} \end{aligned} \quad (5)$$

The gauge symmetry does not constrain the boson-fermion $Y^{(d)}$ coupling, referred as Yukawa coupling, which is a complex number completely arbitrary. After the insertion of the vacuum expectation value $\langle \phi \rangle = (0, v/\sqrt{2})$, bilinear fermion terms for the d quark field follow naturally, since

$$\begin{aligned} \mathcal{L}_{Y_d} &= -Y^{(d)} \bar{q}_L \phi d_R - Y^{(d)*} \bar{d}_R \phi^\dagger q_L \rightarrow \\ &\quad -\frac{v}{\sqrt{2}} \left(Y^{(d)} \bar{d}_L d_R + Y^{(d)*} \bar{d}_R d_L \right) \end{aligned} \quad (6)$$

In order to give mass to the u -quark as well, $\phi_C \equiv i\tau_2 \phi^*$, the charge conjugate of ϕ , is introduced. We can write

$$\mathcal{L}_{Y_u} = -Y^{(u)} \bar{q}_L \phi_C u_R + h.c. \quad (7)$$

and repeat the above reasoning.

Summarizing, the most general Yukawa Lagrangian involving scalars and quarks is given, for the first generation, by

$$\mathcal{L}_Y = -Y^{(d)} \bar{q}_L \phi d_R - Y^{(u)} \bar{q}_L \phi_C u_R + h.c. \quad (8)$$

where ϕ and ϕ_C are Higgs doublets of hypercharge $Y = 1/2$ and $Y = -1/2$, respectively. We have excluded terms of dimension higher than four because of the requirement of renormalizability. Similar terms in the Lagrangian, with analogously arbitrary couplings, can be built to give mass to the charged leptons within the SM.

After spontaneous symmetry breaking (SSB), in the case of 3 generations of quarks, the Yukawa term can be written as

$$\mathcal{L}_Y = - \sum_{i,j=1}^3 \left(M_{ij}^{(d)} \bar{d}_L^i d_R^j + M_{ij}^{(u)} \bar{u}_L^i u_R^j \right) + h.c. \quad (9)$$

where

$$M_{ij}^{(d(u))} \equiv Y_{ij}^{(d(u))} \frac{v}{\sqrt{2}} \quad (10)$$

and $Y_{ij}^{(d(u))}$ are three by three Yukawa matrices. The up-type quarks have been indicated with $u^i \in (u, c, t)$ and the down-type quark with $d^i \in (d, s, b)$. By writing \mathcal{L}_Y in matrix form we have

$$\mathcal{L}_Y = - \bar{\hat{d}}_L M^{(d)} \hat{d}_R - \bar{\hat{u}}_L M^{(u)} \hat{u}_R + h.c. \quad (11)$$

where $\hat{u} \equiv (u, c, t)$ and $\hat{d} \equiv (d, s, b)$. These are flavour eigenstates, that is states participating in gauge interactions, but not yet mass eigenstates. Indeed, the $M^{(u)}$ and $M^{(d)}$ matrices are not necessarily Hermitian, nor there is an a priori theoretical reason that they should be diagonal in the generation index. By what is known in mathematics as a singular value decomposition, they can be both made hermitian and diagonal by a bi-unitary transformation

$$U_L^{u\dagger} M^{(u)} U_R^u = M_D^u \quad U_L^{d\dagger} M^{(d)} U_R^d = M_D^d \quad (12)$$

where M_D^u and M_D^d are diagonal with positive eigenvalues and $U_{L(R)}^{u(d)}$ are unitary matrices. It corresponds to the transformations of the quark states

$$\begin{aligned} \hat{u}_L &\rightarrow U_L^u \hat{u}_L & \hat{u}_R &\rightarrow U_R^u \hat{u}_R \\ \hat{d}_L &\rightarrow U_L^d \hat{d}_L & \hat{d}_R &\rightarrow U_R^d \hat{d}_R \end{aligned} \quad (13)$$

The new states are the physical ones, since the mass matrix is diagonal in that basis. For each of these states the usual mass term of the form $-m_i u_L^i u_R^i$ has appeared in the SM Lagrangian.

2.2. Electroweak currents after SSB

The change from flavour to mass quark eigenstates (13) in the Yukawa sector has to be registered by other sectors of the Lagrangian. One can easily observe that the neutral and electromagnetic currents remain invariant, since they couple separately up-type and down-type quarks. On the contrary, the charged current interactions are affected by this change of basis.

In the massless SM, the part of the Lagrangian describing the hadronic exchanges of charged bosons W^\pm reads

$$\mathcal{L}_{CC} = g(W_\mu^+ J_W^{\mu+} + W_\mu^- J_W^{\mu-}) \quad (14)$$

where g is the EW charge and the charged weak current, $J_W^{\mu+}$, is defined as

$$J_W^{\mu+} = \frac{1}{\sqrt{2}} \sum_{i=1,2,3} \bar{u}_{iL} \gamma^\mu d_{iL} \quad (15)$$

$J_W^{\mu-}$ is its Hermitian conjugate. If we consider the EW current $J_W^{\mu+}$, after the change of basis (13) we have

$$\sum_{i=1}^3 \bar{u}_L^i \gamma^\mu d_L^i = \bar{\hat{u}}_L \gamma^\mu \hat{d}_L \rightarrow \bar{\hat{u}}_L U_L^{u\dagger} \gamma^\mu U_L^d \hat{d}_L = \bar{\hat{u}}_L \gamma^\mu V \hat{d}_L \quad (16)$$

The right-hand side is expressed in terms of the quark mass eigenstates and includes a new matrix V , the Cabibbo-Kobayashi-Maskawa (CKM) matrix, defined as

$$V \equiv U_L^{u\dagger} U_L^d \quad (17)$$

It is a unitary matrix, being the product of unitary matrices, and it parameterizes the change of basis (13). One can proceed similarly for $J_W^{\mu-}$.

Summarizing, the charged current terms in the Lagrangian become

$$\mathcal{L}_{CC} = \frac{g}{\sqrt{2}} (W_\mu^+ \bar{\hat{u}}_L \gamma^\mu V \hat{d}_L + W_\mu^- \bar{\hat{d}}_L \gamma^\mu V^\dagger \hat{u}_L) \quad (18)$$

in terms of the quark mass eigenstates. In this new Lagrangian the fields are physical, mass eigenstates, and in the SM they can reassume, without ambiguity, the previous names, that is $\hat{u} \equiv (u, c, t)$ and $\hat{d} \equiv (d, s, b)$. On the other hand, a new unitary matrix, the CKM matrix, whose elements are otherwise completely arbitrary, has appeared in the SM.

2.3. The Cabibbo-Kobayashi-Maskawa matrix

In the SM, the CKM matrix is a key element in describing the flavour dynamics. As seen above, it is unitary, but this is its only theoretical constraint. The parameters of the CKM, which can be complex, have to be determined experimentally, and there is no a priori theoretical way to determine their values within the SM framework. The CKM matrix V induces flavour-changing transitions inside and between generations in the charged sector at tree level. By contrast, there are no flavour-changing transitions in the neutral sector at tree level. We can write

$$V = \begin{pmatrix} V_{ud} & V_{us} & V_{ub} \\ V_{cd} & V_{cs} & V_{cb} \\ V_{td} & V_{ts} & V_{tb} \end{pmatrix} \quad (19)$$

Due to the unitarity, not all the entries of the CKM matrix are independent. The independent parameters are four in the case of three generations, and can be interpreted as three rotation angles and one phase. There are several equivalent parameterization of the CKM matrix. A common one is

$$V = \begin{pmatrix} c_{12}c_{13} & s_{12}c_{13} & s_{13}e^{-i\delta} \\ -s_{12}c_{23} - c_{12}s_{23}s_{13}e^{i\delta} & c_{12}c_{23} - s_{12}s_{23}s_{13}e^{i\delta} & s_{23}c_{13} \\ s_{12}s_{23} - c_{12}c_{23}s_{13}e^{i\delta} & -c_{12}s_{23} - s_{12}c_{23}s_{13}e^{i\delta} & c_{23}c_{13} \end{pmatrix}, \quad (20)$$

where $c_{ij} = \cos \theta_{ij}$ and $s_{ij} = \sin \theta_{ij}$, with i and j labeling families that are coupled through that angle ($i, j = 1, 2, 3$). This CKM parametrization can be seen as the product of three rotations, with the phase put on the smallest element. The rotation angles may be restricted to lie in the first quadrant, provided one allows the phase δ to be free. As a consequence, c_{ij} and s_{ij} can all be chosen to be positive. The angle θ_{12} is generally called the Cabibbo angle (θ_C), and $\sin \theta_C \simeq 0.22$, corresponding to a value $\theta_C \simeq 13^\circ$. The angle of mixing between the second and the third family is $\theta_{23} \simeq 2^\circ$, and between the first and the third is $\theta_{13} \simeq 0.2^\circ$. The phase δ is constrained by measurements of the CP violation in K decays to be in the range $0 < \delta < \pi$. Its value is approximately $\delta \simeq 1.2$. In this parameterization, the s_{ij} are simply related to directly measurable quantities

$$\begin{aligned} s_{13} &= |V_{ub}| \\ s_{12} &= |V_{us}| / \sqrt{1 - |V_{ub}|^2} \sim |V_{us}| \\ s_{23} &= |V_{cb}| / \sqrt{1 - |V_{ub}|^2} \sim |V_{cb}| \end{aligned} \quad (21)$$

where we have set $|V_{ub}| \ll 1$, as indicated by data.

According to experimental evidence, the CKM matrix has a hierarchical structure. Transitions within the same generation are characterized by matrix elements of order $O(1)$. Transitions between the first and second generations are suppressed by a factor of $O(10^{-1})$, between the second and third generations by a factor of $O(10^{-2})$ and between the first and third generations by a factor of $O(10^{-3})$. This hierarchy has prompted another useful parameterization, the so-called Wolfenstein parameterization [2], based on a series expansion in the small parameter $\lambda = |V_{us}|$. At the lowest order

$$V = \begin{pmatrix} 1 - \lambda^2/2 & \lambda & A\lambda^3(\rho - i\eta) \\ -\lambda & 1 - \lambda^2/2 & A\lambda^2 \\ A\lambda^3(1 - \rho - i\eta) & -A\lambda^2 & 1 \end{pmatrix} + O(\lambda^4). \quad (22)$$

This parametrization corresponds to a particular choice of phase convention which eliminates as many phases as possible and puts the one remaining complex phase in the matrix elements V_{ub} and V_{td} . In this parametrization the unitarity of the matrix is explicit, up to λ^3 corrections. The real, independent, parameters A , ρ and η are known to be roughly of order unity, while λ , that is essentially the sine of the Cabibbo angle, s_{12} , is a small number, of order 0.2. Relative sizes of amplitudes depending on CKM parameters can be roughly estimated by counting powers of λ in the Wolfenstein parametrization.

It is convenient to express the Wolfenstein parameters through phase convention-independent quantities

$$\begin{aligned} s_{12}^2 &= \lambda^2 = \frac{|V_{us}|^2}{|V_{ud}|^2 + |V_{us}|^2} \\ s_{23}^2 &= A^2 \lambda^4 = \frac{|V_{cb}|^2}{|V_{ud}|^2 + |V_{us}|^2} \end{aligned}$$

$$\bar{\rho} + i\bar{\eta} = -\frac{V_{ud}V_{ub}^*}{V_{cd}V_{cb}^*} \quad (23)$$

where $\bar{\rho}$ and $\bar{\eta}$ are two new parameters that substitute ρ and η . These relations ensure that the CKM matrix written in terms of λ , A , $\bar{\rho}$, and $\bar{\eta}$ is unitary to all orders in λ [3]. When terms of the $\mathcal{O}(\lambda^6)$ are neglected, we have

$$V_{\text{CKM}} \simeq \begin{pmatrix} 1 - \frac{1}{2}\lambda^2 - \frac{1}{8}\lambda^4 & \lambda & A\lambda^3(\bar{\rho} - i\bar{\eta}) \\ -\lambda + \frac{1}{2}A^2\lambda^5[1 - 2(\bar{\rho} + i\bar{\eta})] & 1 - \frac{1}{2}\lambda^2 - \frac{1}{8}\lambda^4(1 + 4A^2) & A\lambda^2 \\ A\lambda^3[1 - (\bar{\rho} + i\bar{\eta})] & -A\lambda^2 + \frac{1}{2}A\lambda^4[1 - 2(\bar{\rho} + i\bar{\eta})] & 1 - \frac{1}{2}A^2\lambda^4 \end{pmatrix} \quad (24)$$

Since we have defined

$$s_{13}e^{i\delta} = V_{ub}^* = A\lambda^3(\rho - i\eta) \quad (25)$$

the following relation holds

$$\rho + i\eta = \left(1 + \frac{\lambda^2}{2}\right) \bar{\rho} + i\bar{\eta} + \mathcal{O}(\lambda^4) \quad (26)$$

Thus one can reproduce the CKM matrix (24) at the same order in ρ and η by the substitutions $\bar{\rho} \rightarrow \rho$ and $\bar{\eta} \rightarrow \eta$ in all entries, except V_{td} where the substitution is $(\bar{\rho} + i\bar{\eta}) \rightarrow (1 - \frac{1}{2}\lambda^2)(\rho + i\eta)$.

2.4. The unitarity triangles

The unitarity of the CKM matrix implies

$$\begin{aligned} \sum_{i=1}^3 |V_{ij}|^2 &= 1 \quad j = 1, 2, 3 \\ \sum_{i=1}^3 V_{ji}V_{ki}^* &= \sum_{i=1}^3 V_{ij}V_{ik}^* = 0 \quad j, k = 1, 2, 3 \quad j \neq k \end{aligned} \quad (27)$$

The equalities for the off-diagonal terms are sums of three complex numbers, depending on the four CKM parameters. They are

$$V_{ud}V_{us}^* [\mathcal{O}(\lambda)] + V_{cd}V_{cs}^* [\mathcal{O}(\lambda)] + V_{td}V_{ts}^* [\mathcal{O}(\lambda^5)] = 0 \quad (28)$$

$$V_{ud}^*V_{cd} [\mathcal{O}(\lambda)] + V_{us}^*V_{cs} [\mathcal{O}(\lambda)] + V_{ub}^*V_{cb} [\mathcal{O}(\lambda^5)] = 0 \quad (29)$$

$$V_{us}V_{ub}^* [\mathcal{O}(\lambda^4)] + V_{cs}V_{cb}^* [\mathcal{O}(\lambda^2)] + V_{ts}V_{tb}^* [\mathcal{O}(\lambda^2)] = 0 \quad (30)$$

$$V_{cd}^*V_{td} [\mathcal{O}(\lambda^4)] + V_{cs}^*V_{ts} [\mathcal{O}(\lambda^2)] + V_{cb}^*V_{tb} [\mathcal{O}(\lambda^2)] = 0 \quad (31)$$

$$V_{ud}V_{ub}^* [\mathcal{O}(\lambda^3)] + V_{cd}V_{cb}^* [\mathcal{O}(\lambda^3)] + V_{td}V_{tb}^* [\mathcal{O}(\lambda^3)] = 0 \quad (32)$$

$$V_{ud}^*V_{td} [\mathcal{O}(\lambda^3)] + V_{us}^*V_{ts} [\mathcal{O}(\lambda^3)] + V_{ub}^*V_{tb} [\mathcal{O}(\lambda^3)] = 0 \quad (33)$$

In these relations it is indicated in parenthesis the order of each term in the expansion parameter λ . These equalities give way to a geometric representation in terms of $\bar{\rho}$, $\bar{\eta}$, A and λ , since in the complex plane they can be geometrically represented by triangles, all characterized by the same area [4]. Only the last two of the six triangles corresponding to these equalities have sides of the same order of magnitude, $\mathcal{O}(\lambda^3)$ (i.e., the triangles are not squashed). In particular, the triangle defined by (32), rescaled by a factor

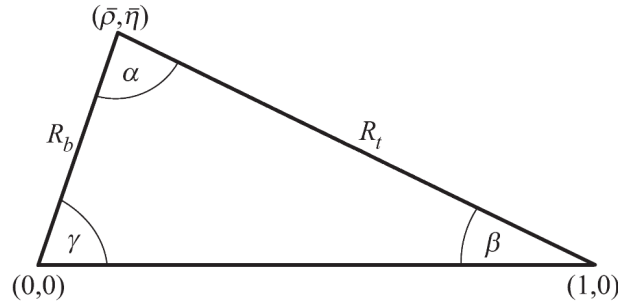


Figure 1. The unitarity triangle in the complex plane.

$V_{cd}V_{cb}^*$ is commonly referred to as the unitarity triangle (UT) (see figure 1). Because it involves the term $V_{cd}V_{cb}^*$ and $V_{ud}V_{ub}^*$, the UT arises naturally in analyses involving B mesons. With the bases of the UT normalized to unity, the coordinates of the UT apex are $(\bar{\rho}, \bar{\eta})$. The sides R_b and R_t are given by the magnitudes of

$$\begin{aligned} R_b &= \frac{V_{ud}V_{ub}^*}{V_{cd}V_{cb}^*} = \left(1 - \frac{\lambda^2}{2}\right) \frac{1}{\lambda} \frac{V_{ub}^*}{|V_{cb}|} \\ R_t &= \frac{V_{td}V_{tb}^*}{V_{cd}V_{cb}^*} = \frac{1}{\lambda} \frac{V_{td}}{|V_{cb}|} \end{aligned} \quad (34)$$

As can be seen, a special role is played by $|V_{cb}|$, which normalizes the UT triangle. Due to its economical structure in terms of only four parameters, the CKM matrix can be determined experimentally by exploiting several different flavour changing decays or processes related to neutral-meson mixing. One tries to measure as many observable as possible, in function of the UT triangle parameters, over-constraining the shape of the triangle and testing that it closes. The consistency of the various measurements probes the consequences of unitarity in the three generations SM and discrepancies with the SM expectations signal the possibility of NP in some observable. An extensive program of measurements of the UT parameters has been carried through at different experiments since the nineties. Due to the complexity of non-perturbative strong interactions, it is convenient to analyze processes with a limited number of hadrons in the initial or final state, as semileptonic B decays into one hadron, or observables (typically ratios) for which uncertainties due to such QCD effects reduce or cancel. Besides, since the potential sensitivity to NP is limited for tree-level processes, they are often preferred to fix the CKM parameters. Tree level processes are f.i. the semileptonic B decays into charmed states, mediated by the quark decay $b \rightarrow c \ell \nu_\ell$ at the lowest order in the SM. The results from tree-level processes can be used as input for precise SM predictions of rare, loop-induced processes. Since the start of the analyses on the UT triangle, there has always been an intensive strain to combine all available measurements (global

analysis) in order to obtain statistically meaningful constraints on the CKM parameters, in the framework of the SM and some of its extensions[‡].

3. Semileptonic B -meson decays

Semileptonic B decays are the processes of election when it comes to a precise determination of the magnitude of the CKM matrix element V_{cb} . At the lowest order in the SM, semileptonic B decays are mediated by the a tree level quark decay, the $b \rightarrow c \ell \nu_\ell$ decay, whose amplitude is proportional to V_{cb} , as illustrated in figure 2. The presence of leptons in the final states simplifies the QCD analyses, since hadronic and leptonic currents factorize.

There are two methods for $|V_{cb}|$ determination with semileptonic B decays, taking the name from the hadronic processes involved. In the so-called exclusive method, $|V_{cb}|$ is extracted by studying exclusive decays, in particular $B \rightarrow D^{(*)} \ell \nu_\ell$. Having only one hadron in the final state facilitates the analysis (e.g. no final state rescattering). The inclusive method refers to the investigation of the inclusive semileptonic decay $B \rightarrow X_c \ell \nu_\ell$ decays, where the final state X_c is an hadronic state originated by the charm quark. The inclusive and exclusive determinations rely on different theoretical calculations and make use of different techniques which, to a large extent, have uncorrelated experimental uncertainties. Comparing the results of these two largely independent approaches represents also a powerful test of our understanding of hadron dynamics. We detail both approaches in the following.

[‡] A systematic program in this direction is carried on by the CKMfitter [5] and UTfit collaborations [6].

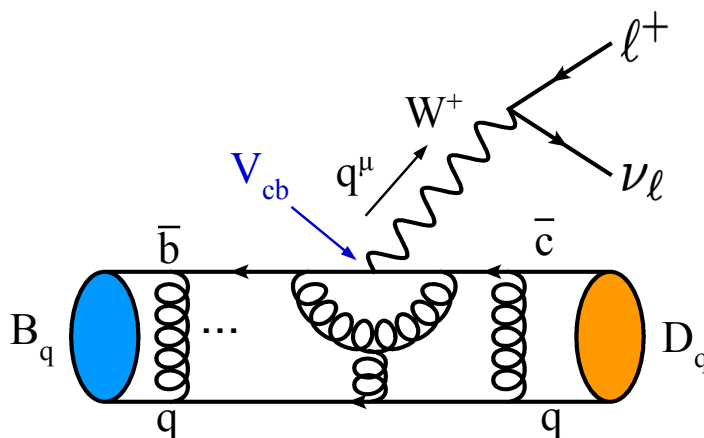


Figure 2. Diagram of the $B_q \rightarrow D_q \ell^+ \nu_\ell$ decay. The amplitude of this process is proportional to V_{cb} . The transfer four-momentum q^μ is given by $q^\mu \equiv p_B^\mu - p_D^\mu = p_\ell^\mu - p_\nu^\mu$. The diagram is at the lowest order in the weak interactions and the gluon configuration depicted is merely indicative.

3.1. Inclusive decays

In inclusive $B \rightarrow X_c \ell \nu_\ell$ decays, the final state X_c is an hadronic state originated by the charm quark. Inclusive decays can be interpreted as a sum over all possible hadronic final states; the details of the hadronic final states are lost, and transition amplitudes are expected to be sensitive only to the dynamics of the initial B meson. Quark-hadron duality is generally assumed, which means, loosely speaking, that the inclusive hadronic observables, when integrated over large enough portions of phase space, are described in terms of the underlying parton-level processes, provided all possible sources of corrections stemming from QCD are properly accounted for §.

Both perturbative and non-perturbative QCD interactions affect decay processes in an essential way. A basic tool to disentangle their contributions to the decay amplitude in a systematic fashion is provided by the operator product expansion (OPE). The OPE formalism allows us to express the non-perturbative physics in terms of B meson matrix elements of local, gauge invariant, operators, and the perturbative physics in terms of Wilson coefficients, which can be computed as a series in a perturbative QCD coupling α_s . In other terms, the OPE separates the physics associated with soft scales (parametrized by the matrix elements of the local operators) from that associated with hard scales, which determine the Wilson coefficients. Semileptonic B decays have an intrinsic large 'dynamic' scale of energy release of the order of the b -quark mass, while the soft scale is of the order of the hadronic scale Λ_{QCD} . The large hierarchy between these two scales leads naturally to Λ_{QCD}/m_b as an expansion parameter of non-perturbative effects and to a description of the heavy b -quark in the framework of the Heavy Quark Effective Theory (HQET) (for a review see f.i. [9]).

Jumping to the conclusions, sufficiently inclusive quantities (typically the total semileptonic width and the moments of the kinematic distributions) can be expressed as a double series in α_s and Λ_{QCD}/m_b . This expansion is referred to as Heavy Quark Expansion (HQE). The expansion for the total semileptonic width takes the form

$$\begin{aligned} \Gamma(B \rightarrow X_c \ell \nu) = & \frac{G_F^2 m_b^5}{192 \pi^3} |V_{cb}|^2 [c_3 \langle O_3 \rangle + \\ & + c_5 \frac{\langle O_5 \rangle}{m_b^2} + c_6 \frac{\langle O_6 \rangle}{m_b^3} + O\left(\frac{\Lambda_{QCD}^4}{m_b^4}, \frac{\Lambda_{QCD}^5}{m_b^3 m_c^2}, \dots\right)] \end{aligned} \quad (35)$$

Here c_d ($d = 3, 5, 6 \dots$) are short distance coefficients, calculable in perturbation theory as a series in the strong coupling α_s , and O_d denote local operators of (scale) dimension d . The hadronic expectation values of the operators encode the nonperturbative corrections and can be parametrized in terms of HQE parameters, whose number grows with powers of Λ_{QCD}/m_b . The leading term is given by the free b -quark decay (parton model). A remarkable feature of (35) is the absence of a contribution of order $1/m_b$, due to the absence of an independent gauge invariant operator of dimension four. The power corrections start at $O(\Lambda_{QCD}^2/m_b^2)$, and are comparatively suppressed. The fact that nonperturbative, bound state effects in inclusive decays are strongly suppressed (at

§ For reviews on quark-hadron duality see f.i. [7, 8]

least two powers of the heavy quark mass) explains a posteriori the success of parton model in describing such processes. Due to the relative sizes of the b and c quarks, at higher orders in the expansion, terms suppressed by powers of m_c also appear, starting with $O(\Lambda_{QCD}^5/m_b^3 m_c^2)$.

Similar expansions give the moments of distributions of charged-lepton energy, hadronic invariant mass and hadronic energy. As most experiments can detect the leptons only above a certain threshold in energy, the charged-lepton energy moments are defined as

$$\langle E_\ell^n \rangle = \frac{1}{\Gamma_{E_\ell > E_{cut}}} \int_{E_\ell > E_{cut}} E_\ell^n \frac{d\Gamma}{dE_\ell} dE_\ell \quad (36)$$

where E_ℓ is the charged lepton energy in the $B \rightarrow X_c \ell \nu_\ell$ decays, n is the order of the moment, $\Gamma_{E_\ell > E_{cut}}$ is the semileptonic width above the energy threshold E_{cut} and $d\Gamma/dE_\ell$ is the differential semileptonic width as a function of E_ℓ . The hadronic mass moments are

$$\langle m_X^{2n} \rangle = \frac{1}{\Gamma_{E_\ell > E_{cut}}} \int_{E_\ell > E_{cut}} m_X^{2n} \frac{d\Gamma}{dm_X^2} dm_X^2 \quad (37)$$

Other moments (and cuts on other observables) can be defined in a similar way. It is sometimes convenient to employ central moments, computed relative to the averages $\langle E_\ell \rangle$ and $\langle m_X^2 \rangle$, that is

$$l_n(E_{cut}) \equiv \langle (E_\ell - \langle E_\ell \rangle)^n \rangle \quad h_n(E_{cut}) \equiv \langle (m_X^2 - \langle m_X^2 \rangle)^n \rangle \quad (38)$$

Let us stress that the HQE is valid only for sufficiently inclusive measurements and away from perturbative singularities, therefore the relevant quantities to be measured are global shape parameters (moments of various kinematic distributions) and the total rate. While the general structure of the expansion is the same for all the above mentioned observables, the perturbative coefficients are in general different.

Details on HQE will be given in section 3.1.1 and the sensitivity of rates and momenta to the definition of quark masses briefly discussed in section 3.1.2. In section 5 we will draw conclusions on the inclusive $|V_{cb}|$ extraction.

3.1.1. Heavy Quark Expansion In order to discuss the characteristics and the status of the HQE in $B \rightarrow X_c \ell \nu_\ell$ decays, let us go back to the expansion for the total semileptonic width in (35). The hadronic expectation values of the local operators O_d are the (normalized) forward matrix elements, written in the short-hand notation as

$$\langle O_d \rangle \equiv \frac{\langle B | O_d | B \rangle}{2m_B} \quad (39)$$

where m_B is the B meson mass, included in the definition for the normalization and dimensional counting. This set of operators, built with dimensional criteria using HQFT b quarks fields, is basically the same set of operators, albeit with different weights, that appears in other B decay rates as well as distributions. While we can easily identify these operators and their dimensions, we cannot compute their hadronic expectation

values from first principles, and we have to express them in function of a number of HQET parameters, which increases with powers of $1/m_b$.

The lowest-order terms of HQE are the dimension-three operators. In the HQET formalism, v_μ is the B -meson velocity ($v^2 = 1$, $v_0 > 0$) and $b_v(x) = e^{-im_b v \cdot x} b(x)$ is the b field whose space time dependence is determined by the residual momentum $k_\mu = p_\mu - m_b v_\mu$, which is due to binding effects of the heavy quark inside the heavy B meson, and it is of order Λ_{QCD} . Owing to Lorentz invariance and parity there are only two combinations which can appear, namely $O_3 = \bar{b}_v \not{v} b_v$ and $O_3 = \bar{b}_v b_v$. Since the operators b_v differ from the full QCD operators only by a phase redefinition, the equalities $\bar{b}_v \not{v} b_v = \bar{b} \not{v} b$ and $\bar{b}_v b_v = \bar{b} b$ hold. The matrix element of the former is

$$\langle B | \bar{b} \not{v} b | B \rangle = v^\mu \langle B | \bar{b} \gamma_\mu b | B \rangle = v^\mu (2m_B v_\mu) = 2m_B \quad (40)$$

The penultimate equality follows because $\bar{b} \gamma_\mu b$ is the conserved b quark number current. The hadronic expectation value of the operator $\bar{b}_v b_v$ between the heavy meson states can be expanded in $1/m_b$, finding that it differs from the hadronic expectation value of the operator $\bar{b}_v \not{v} b_v$ by terms of order $1/m_b^2$. Thus the matrix elements of the dimension-three contribution are known; they incorporate the parton model result which dominates asymptotically, i.e. for $m_b \rightarrow \infty$.

At order $1/m_b^0$ in the HQE, that is at the parton level, the perturbative corrections up to order α_s^2 to the width and to the moments of the lepton energy and hadronic mass distributions are known completely [10–16]. The terms of order $\alpha_s^{n+1} \beta_0^n$, where β_0 is the first coefficient of the QCD β function, $\beta_0 = (33 - 2n_f)/3$, have also been computed following the Brodsky-Lepage-Mackenzie (BLM) procedure [13, 17].

By using the equation of motion in HQET, one can check that there are no matrix elements of dimension four operators that occur in the HQE. This means that there are no corrections suppressed by a single power of Λ_{QCD}/m_b .

The next order is Λ_{QCD}^2/m_b^2 , and at this order the HQE includes two operators, called the kinetic energy and the chromomagnetic operator. Their matrix elements, μ_π^2 and μ_G^2 , respectively, are defined as

$$\begin{aligned} \mu_\pi^2 &\equiv \frac{1}{2m_B} \langle B | \bar{b}_v \vec{\pi}^2 b_v | B \rangle \\ \mu_G^2 &\equiv \frac{1}{2m_B} \langle B | \bar{b}_v \frac{i}{2} \sigma_{\mu\nu} G^{\mu\nu} b_v | B \rangle \end{aligned} \quad (41)$$

where $\vec{\pi} = -i\vec{D}$, D^μ is the covariant derivative and $G^{\mu\nu}$ is the gluon field tensor. The matrix element μ_π^2 is naturally associated with the average kinetic energy of the b quark inside the B meson while the matrix element μ_G^2 is connected to the $B^* - B$ hyperfine mass splitting. Both matrix elements generally depend on a cut-off μ chosen to separate soft and hard physics, which can be implemented in different ways, or schemes. Perturbative corrections to the coefficients of the kinetic operator [18, 19] and the chromomagnetic operator [20–22] have been evaluated at order α_s .

Two independent parameters, $\rho_{D,LS}^3$, are also needed to describe matrix elements of operators of dimension six, that is at order $1/m_b^3$. Their coefficients have long been

known at tree level, i.e. neglecting perturbative corrections [23]. Very recently an analytical calculation of the α_s corrections for the coefficient ρ_D^3 has been presented [24].

Starting at order Λ_{QCD}^3/m_b^3 , terms with an infrared sensitivity to the charm mass appear, at this order as a $\log m_c$ contribution [25–27]. At higher orders these contributions, sometimes dubbed intrinsic charm contribution, in form of powers of Λ_{QCD}/m_c , have to be considered as well. Indeed, roughly speaking, since $m_c^2 \sim O(m_b \Lambda_{QCD})$ and $\alpha_s(m_c) \sim O(\Lambda_{QCD})$, contributions of order $\Lambda_{QCD}^5/m_b^3 m_c^2$ and $\alpha_s(m_c) \Lambda_{QCD}^4/m_b^2 m_c^2$ are expected comparable in size to contributions of order Λ_{QCD}^4/m_b^4 .

Presently, the matrix elements have been identified and estimated up to the order $1/m_b^4$ and $1/m_b^5$ [28–30]. In HQE the number of independent parameters needed to describe the nonperturbative physics of matrix elements grows with the order in $1/m_b$. At dimension seven and eight, nine and eighteen independent matrix elements appear, respectively, and for higher orders one has an almost factorial increase of the number of independent parameters.

3.1.2. Mass schemes In QED, the location of the divergence in the propagator of the electron can be taken as a physical definition of the electron mass, and it is indicated as on-shell or pole mass. This definition is not naturally extended to quarks, which are confined and can never be seen as asymptotic states. While not measurable per se due to confinement, one can still define a pole mass for quarks in a formally consistent way within perturbation theory. However, this mass will be plagued by ambiguities related to non-perturbative effects in QCD, the so-called renormalon ambiguities (for a review see f.i. [31]), when related to observable quantities. Alternative definitions of mass for a quark can be used, each with its own advantages and disadvantages, but all requiring a careful description of the adopted framework (prescription or scheme).

The HQE nonperturbative parameters depend on the heavy quark mass, although sometimes the infinite mass limit of these parameters is taken. They are affected by the particular theoretical scheme that is used to define the quark masses.

A commonly used definition of the mass of the quark is the minimal subtraction (MS) mass, which corresponds to the running renormalized mass in perturbative QCD, when, in dimensional regularization, the finite parts of the relevant counterterms are set to zero. In the $\overline{\text{MS}}$ subtraction scheme, also $\ln(4\pi)$ and γ_E factors are subtracted off. The $\overline{\text{MS}}$ prescription has the advantage of computational simplicity. The mass $m_b^{\overline{\text{MS}}}(\mu)$ depends on a scale μ and it is not affected by renormalon ambiguities. It is sometimes referred as a short-distance mass, since it is well defined in the infrared regime. The $\overline{\text{MS}}$ is quite appropriate for describing heavy flavour production, but not for treating heavy meson decays, where the dynamics is characterized by scales lower than the heavy scale m_b .

Alternative scheme have been proposed, sometimes referred as threshold schemes; we list the most commonly used to describe heavy quarks in heavy mesons. In the kinetic scheme [32–34], the so-called “kinetic mass” $m_b^{\text{kin}}(\mu)$ is the mass entering the non-relativistic expression for the kinetic energy of a heavy quark. It is defined by

introducing an explicit factorization scale, and subtracting the physics at scales below this scale from the quark-mass definition. More technically, its definition requires using heavy-quark sum rules for semileptonic $b \rightarrow c$ decays in the small velocity (SV) limit.

Other examples of threshold schemes are the PS (Potential subtracted) scheme [35] and the 1S scheme [36–38]. The PS mass and the kinetic mass are similar, in the sense that they both subtract out the troublesome infrared part by introducing an explicit factorization scale. The PS scheme is based on the properties of nonrelativistic quark-antiquark systems, whose dynamics depend on the total static energy. The contribution to the potential from the region of small momenta, identified as the source of the leading renormalon, is subtracted from the PS mass. The 1S mass is defined as half the energy of the 1S state Υ state calculated in perturbation theory. In the 1S scheme there is a mismatch with the usual perturbation theory, overcome by a working tool, the so-called ‘ Υ expansion’, whose validity has been questioned [39].

3.2. Exclusive decays into light leptons

In this section we discuss the exclusive semileptonic CKM favoured $B \rightarrow D^{(*)}\ell\nu_\ell$ decays, when $\ell = e, \mu$. Neglecting lepton masses, their SM differential ratios can be written as

$$\begin{aligned} \frac{d\Gamma}{dw}(B \rightarrow D^*\ell\nu_\ell) &= \frac{G_F^2}{48\pi^3}(m_B - m_{D^*})^2 m_{D^*}^3 \chi(w)(w^2 - 1)^{\frac{1}{2}} |V_{cb}|^2 |\eta_{EW}|^2 |\mathcal{F}(w)|^2 \\ \frac{d\Gamma}{dw}(B \rightarrow D\ell\nu_\ell) &= \frac{G_F^2}{48\pi^3}(m_B + m_D)^2 m_D^3 (w^2 - 1)^{\frac{3}{2}} |V_{cb}|^2 |\eta_{EW}|^2 |\mathcal{G}(w)|^2 \end{aligned} \quad (42)$$

where m_X is the mass of the X meson, p_X its 4-momentum and w is the recoil parameter, defined as $w = p_B \cdot p_{D^{(*)}}/(m_B m_{D^{(*)}}) = v_B \cdot v_{D^{(*)}}$; v_B and $v_{D^{(*)}}$ are the 4-velocities of the initial and final-state mesons. The recoil parameter is related to the energy transferred to the leptonic pair $q^2 = (p_B - p_{D^{(*)}})^2 = (p_\ell + p_{\nu_\ell})^2$, namely $w = (m_B^2 + m_{D^{(*)}}^2 - q^2)/(2m_B m_{D^{(*)}})$. In the B meson rest frame the expression for w reduces to the Lorentz boost $w = \gamma_{D^{(*)}} = E_{D^{(*)}}/m_{D^{(*)}}$. The values of the recoil parameter are limited by kinematics. The superior limit occurs when $q^2 = q_{min}^2 = m_\ell^2$, that is at $w = (m_B^2 + m_{D^{(*)}}^2)/(2m_B m_{D^{(*)}})$, assuming massless leptons. The inferior limit (the zero recoil point) is at $w = 1$, and corresponds at $q_{max}^2 = (m_B - m_{D^{(*)}})^2 \simeq 11 \text{ GeV}^2$. Intuitively an higher q^2 (lower w) corresponds to an higher mass of the virtual W boson, which, at the two-body decay level, implies a lower “kick” to the $D^{(*)}$.

In figure 3, we give an illustration of the kinematics of the decays at low and high q^2 in the B meson rest frame. These simple pictures can be useful to gain some intuition about semileptonic B decays. For example the large *helicity* suppression at zero recoil of $B \rightarrow D\ell\nu_\ell$ decay compared to $B \rightarrow D^*\ell\nu_\ell$ decay, can be easily understood: the lepton and the neutrino are back to back, this means that the component of the total angular momentum of the leptons along their line of flight is unity and cannot be compensated by the pseudoscalar D meson. At the other extreme, $q^2 \approx 0$, where the hadron recoil velocity is maximum, the lepton and the neutrino are parallel and their combined spin along this direction is null. For the $B \rightarrow D^*\ell\nu_\ell$ decays this means that the D^* is fully polarized having null spin projection along the lepton direction.

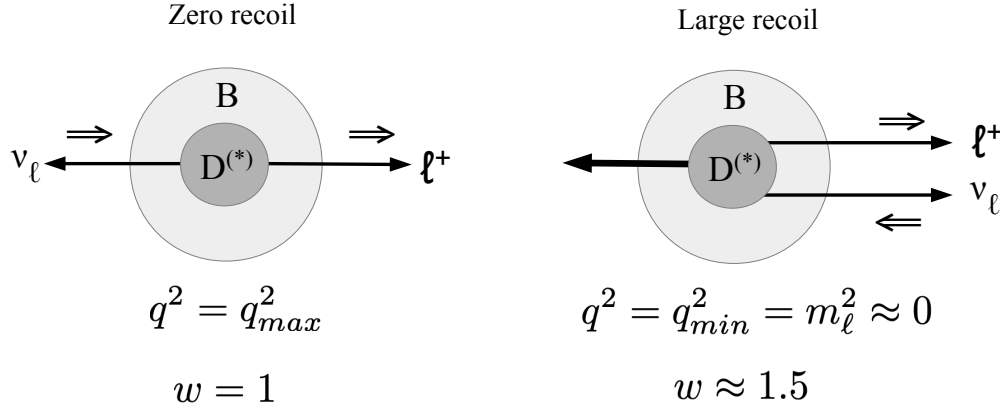


Figure 3. In the "zero recoil" kinematic configuration the hadron is at the rest in the B meson rest frame, so the two leptons are produced back to back. In the "large recoil" limit the leptons are produced parallel and opposite to the hadron that acquires the largest momentum. The spin of the right-handed neutrino and the left-handed positron are also depicted.

As seen in (42), the differential cross sections are proportional to

- the squared modulus of the CKM matrix element: $|V_{cb}|^2$
- a single form factor, $\mathcal{F}(w)$ and $\mathcal{G}(w)$, for $B \rightarrow D^* \ell \nu_\ell$ and $B \rightarrow D \ell \nu_\ell$, respectively
- η_{EW} , a structure-independent correction factor that accounts for electroweak effects [40]. In the literature, a long-distance EM radiation effect (Coulomb correction) is sometimes added to this factor [41]
- a phase space factor, $(w^2-1)^{1/2}$ and $(w^2-1)^{3/2}$ for $B \rightarrow D^* \ell \nu_\ell$ decays and $B \rightarrow D \ell \nu_\ell$ decays, respectively, that vanish at the zero recoil point. For $B \rightarrow D^* \ell \nu_\ell$ there is an additional phase space factor $\chi(w)$

$$\chi(w) = (w+1)^2 \left(1 + \frac{4w}{w+1} \frac{m_B^2 - 2w m_B m_{D^*} + m_{D^*}^2}{(m_B - m_{D^*})^2} \right) \quad (43)$$

The hardship of the extraction of $|V_{cb}|$ is due to the presence of the form factors, which cannot be computed in the framework of perturbation theory. In the heavy quark limit ($m_{b/c} \rightarrow \infty$), that is to lowest order in heavy quark effective theory, heavy quark symmetries predict that both form factors equal a single universal Isgur-Wise function, $\mathcal{F}(w) = \mathcal{G}(w) = \xi(w)$, which is absolutely normalized to unity at zero recoil, that is $\xi(w=1) = 1$. This property has an intuitive reason. The no-recoil point corresponds to the kinematical situation where the D meson stays at rest in the rest frame of the decaying B ($v = v'$); the decaying b -quark, at rest, is transformed into a c -quark, also at rest. The light hadronic cloud does not notice the flavour change $b \rightarrow c$ and it is transferred from the B to the D meson with probability one. The form factor function is identical for $B \rightarrow D$ and $B \rightarrow D^*$ transitions, because these are related by the heavy-quark spin symmetry. For a realistic analysis, corrections to the heavy-quark limit have

to be considered. At zero recoil, the heavy quark symmetries also provide the structure of the symmetry breaking non-perturbative corrections at finite heavy quark mass m , which start at order $1/m^2$ and $1/m$ for the $\mathcal{F}(w = 1)$ and $\mathcal{G}(w = 1)$ form factors, respectively.

In order to extract $|V_{cb}|$, we need not only to compute the form factors, but also to measure experimental decay rates. The advantage in the computation of the form factors provided by the heavy quark symmetries at $w = 1$ has the hindrance that the differential rates in (42) vanish at zero-recoil. Thus one needs to extrapolate the experimental points taken at $w \neq 1$ to the zero recoil point $w = 1$, using a parameterization of the dependence on w of the form factors, which introduces additional uncertainties. In other words, the $|V_{cb}|$ determination may proceed according to the following steps:

- 1) theoretical determination of the form factors \mathcal{F}/\mathcal{G} at zero recoil $w = 1$;
- 2) theoretical parametrization of the w dependence;
- 3) experimental measurements of the exclusive decays rates at non-zero recoil points, yielding the products $|\eta_{EW}|^2 |\mathcal{F}(w)|^2 |V_{cb}|^2$ or $|\eta_{EW}|^2 |\mathcal{G}(w)|^2 |V_{cb}|^2$;
- 4) extrapolation of the experimental points to zero recoil and $|V_{cb}|$ extraction.

Since a few years there is an endeavor to amend this strategy, by calculating form factors directly at non-zero recoil points, with evident advantages on the extraction of $|V_{cb}|$. Some results are already available in the $B \rightarrow D\ell\nu_\ell$ channel.

Several parameterizations for the momentum dependence of the form factors are on the market. Traditionally, the form factors are parameterized with an explicit pole and a sum of effective poles, see f.i. Ball and Zwicky [42, 43] and Becirevic and Kaidalov [44]. Although these parameterizations capture some known properties of form factors, in general they do not allow an easy quantification of systematic uncertainties. Recent determinations adopt a more systematic approach that aims at exploiting the positivity and analyticity properties of two-point functions of vector currents. In these parametrizations w is mapped onto a complex variable z via the conformal transformation $z = (\sqrt{w+1} - \sqrt{2})/(\sqrt{w+1} + \sqrt{2})$. The form factors may be written in form of an expansion in z , which converges rapidly in the kinematical region of heavy hadron decays. The coefficients of the expansions are subject to unitarity bounds based on analyticity. To this type belong the CLN (Caprini-Lellouch-Neubert) [45], the BGL (Boyd-Grinstein-Lebed) [46] and the BCL (Bourrely-Caprini-Lellouch) [47] parameterizations. Further details will be given in section 6.1. The experimental measurements of the form factors are described in sections 6.3 and 6.4 for the $B \rightarrow D^*\ell\nu_\ell$ and $B \rightarrow D\ell\nu_\ell$, respectively.

3.2.1. Form factors From the field theory point of view, it is convenient to define form factors as coefficients of independent Lorentz structures appearing in the hadronic transition matrix elements. In the framework of HQET, the independent Lorentz 4-vectors are the velocities of the two mesons, rather than their momenta. This can be intuitively understood by considering that in the heavy flavour limit, $m_{b,c} \rightarrow \infty$ (m_b/m_c

fixed), when the weak current changes the flavour $b \rightarrow c$, the light degrees of freedom inside the meson become aware of the change in the heavy quark velocities, $v_B \rightarrow v_{D^{(*)}}$ ($v_B \equiv p_B/m_B$, $v_{D^{(*)}} \equiv p_{D^{(*)}}/m_{D^{(*)}}$), rather than of the change in momenta. Since the only scalar formed from the velocities ($v_B^2 = v_{D^{(*)}}^2 = 1$ by definition) is $w = v_B \cdot v_{D^{(*)}}$, we can set [9]

$$\begin{aligned} \frac{\langle D|V^\mu|B \rangle}{\sqrt{m_B m_D}} &= h_+(w)(v_B + v_D)^\mu + h_-(w)(v_B - v_D)^\mu \\ \frac{\langle D^*|V^\mu|B \rangle}{\sqrt{m_B m_{D^*}}} &= h_V(w)\varepsilon^{\mu\nu\rho\sigma}v_{B\nu}v_{D^*\rho}\epsilon^*_\sigma \\ \frac{\langle D^*|A^\mu|B \rangle}{\sqrt{m_B m_{D^*}}} &= ih_{A_1}(w)(1+w)\epsilon^{*\mu} - i[h_{A_2}(w)v_B^\mu + h_{A_3}(w)v_{D^*}^\mu]\epsilon^* \cdot v_B \end{aligned} \quad (44)$$

where ϵ^* is the D^* polarization vector, which respects the equality $\sum_{\alpha=1}^3 \epsilon_\alpha^{*\mu} \epsilon_\alpha^{*\nu} = -g^{\mu\nu} + v_{D^*}^\mu v_{D^*}^\nu$. In the conventional, relativistic normalization of the meson states $|B(D^{(*)})\rangle$, the factor $1/\sqrt{m_{B(D^{(*)})}}$ on the left side of Eqs. (44) is omitted; its addition pertains to a mass independent renormalization [9].

In the heavy flavour limit there is only one form factor, the Isgur-Wise function $\xi(w)$ [48, 49]. In that limit, the form factors become

$$h_+(w) = h_V(w) = h_{A_1}(w) = h_{A_3}(w) = \xi(w) \quad h_-(w) = h_{A_2}(w) = 0 \quad (45)$$

The form factor $\mathcal{G}(w)$ in (42) can be expressed as a combination of $h_+(w)$ and $h_-(w)$ [9]

$$\mathcal{G}(w) = h_+(w) - \frac{m_B - m_D}{m_B + m_D} h_-(w) \quad (46)$$

Similarly, the form factor $\mathcal{F}(w)$ can be written as [9]

$$\begin{aligned} \mathcal{F}(w) &= \left\{ 2(1 - 2wr + r^2) \left[h_{A_1}^2 + \left(\frac{w-1}{w+1} \right) h_V^2 \right] + \right. \\ &\quad \left. + [(1-r)h_{A_1} + (w-1)(h_{A_1} - h_{A_3} - rh_{A_2})]^2 \right\} \times \\ &\quad \times \left\{ (1-r)^2 + \frac{4w}{w+1}(1 - 2wr + r^2) \right\}^{-1} \end{aligned} \quad (47)$$

where $r = m_{D^*}/m_B$. The form factor $\mathcal{F}(w)$ is dominated by the axial vector form factor h_{A_1} as $w \rightarrow 1$. It is sometimes convenient to define two ratios of the form factors

$$R_1 = \frac{h_V}{h_{A_1}} \quad R_2 = \frac{h_{A_3} + rh_{A_2}}{h_{A_1}} \quad (48)$$

In the infinity mass limit, heavy quark spin symmetry implies that $R_1 = R_2 = 1$, independently of the w value.

With respect to comparison with experimental results, the above definition of form factors is not the most convenient, since the combinations of form factors most easily obtained from data are those appearing in a sum of squares in the differential rates, namely, the helicity amplitudes. They are particular linear combinations of the original form factors, and thus simply form a different basis for the description of the matrix elements. In the $B \rightarrow D^* \ell \nu_\ell$ decay, one can use three helicity amplitudes, labeled H_\pm and H_0 , corresponding to the three polarization states of the D^* , two transverse and one

longitudinal. The form factor $\mathcal{F}(w)$ can be expressed in terms of the helicity amplitudes as

$$\chi(w)|\mathcal{F}(w)|^2 = \frac{1 - 2wr + r^2}{12m_B m_{D^*}(1 - r)^2} \left(H_0^2(w) + H_+^2(w) + H_-^2(w) \right) \quad (49)$$

The helicity amplitudes, in turn, depend on the $h_x(w)$ form factors

$$\begin{aligned} H_0(w) &= \frac{\sqrt{m_B m_{D^*}}}{1 - 2wr + r^2} (w + 1) [(w - r)h_{A_1}(w) - (w - 1)(rh_{A_2}(w) + h_{A_3}(w))] \\ H_{\pm}(w) &= \sqrt{m_B m_{D^*}}(w + 1) \left[h_{A_1}(w) \pm \sqrt{\frac{w - 1}{w + 1}} h_V(w) \right] \end{aligned} \quad (50)$$

Other details on the w dependence of form factors and helicity amplitudes will be given in section 6.2.

3.2.2. Zero recoil and beyond Since more than a decade, the lattice community performs computations of the $B \rightarrow D^{(*)}$ form factors. The difficulties related to heavy fermions on lattice can be naïvely summarized by observing that direct simulation of high mass such $ma \geq 1$, where a represent a lattice spacing, gives discretization errors out of control. As of today $m_b \sim 1/a$ and no direct simulation is possible. The main way out is the usage of effective theories, as HQET [48] and Non-Relativistic QCD (NRQCD) [50]. In broad terms, they eliminate high degrees of freedom, aided by systematic expansions in Λ_{QCD}/m_b . The downside is the introduction of new sources of errors (matching of HQET to QCD, renormalization, control of extrapolation, etc.) to take care of.

Another common approach to non-perturbative calculations of form factors are QCD sum rules. The sum rules are based on the general idea of calculating a relevant quark-current correlation function and relating it to the hadronic parameters of interest via a dispersion relation. They have reached wide application for calculation of exclusive amplitudes and form factors in the form of light cone sum rules (LCSR), employing light-cone OPE of the relevant correlation functions. Uncertainties may originate from the truncation of the expansions, the input parameter uncertainties, and the assumption of quark-hadron duality. Direct sum rules calculations, without extrapolations, hold in the kinematic region of large recoil (small q^2), where the lattice calculation are substantially more difficult, and are in this respect complementary to lattice analyses.

Let us now report recent results in literature, starting from the $B \rightarrow D^* \ell \nu_\ell$ channel, which is less suppressed in the phase space and whose branching fractions are more precise (even twice) in the majority of experimental measurements.

The form factor for the $B \rightarrow D^* \ell \nu$ channel, in the lattice unquenched $N_f = 2 + 1$ approximation has been estimated at zero recoil. The FNAL/MILC collaboration, which used Wilson fermions for both c and b heavy quarks, gives [41]

$$\mathcal{F}(1) = 0.906 \pm 0.004 \pm 0.012 \quad (51)$$

The first error is statistical and the second one is the sum in quadrature of all systematic errors. The total uncertainty is around the (1-2)% level. The largest error is the heavy quark discretization error related to the Fermilab action.

A more recent value of the lattice form factor $\mathcal{F}(1)$ has been presented by the HPQCD collaboration, which used the fully relativistic HISQ (Highly improved staggered quarks) action for light, strange and charm quarks and the NRQCD action for the b quark [51]

$$\mathcal{F}(1) = 0.895 \pm 0.010 \pm 0.024 \quad (52)$$

Both the results in (51) and (52) are in good agreement. Another recent calculation by HPQCD focuses on $B_s \rightarrow D_s^* \ell \nu_\ell$ [52]. They use the HISQ action for all valence quarks in order to perform the normalizations of all required currents non-perturbatively and avoid a large source of systematic uncertainty. From their result for $\mathcal{F}_s(1)$ they extract $\mathcal{F}(1)$ by using the $\mathcal{F}(1)/\mathcal{F}_s(1)$ ratio computed in their older paper [51], and obtain [52]

$$\mathcal{F}(1) = 0.914 \pm 0.024 \quad (53)$$

in agreement with all previously mentioned determinations.

At the current level of precision, it would be important to extend form factor unquenched calculations for $B \rightarrow D^*$ semileptonic decays to non-zero recoil, in order to reduce the uncertainty due to the extrapolation to $w = 1$. Indeed, at finite momentum transfer, only old quenched lattice results are available [53]. Stimulated by this objective, theory work on lattice is rapidly progressing. Preliminary blinded results at non-zero recoil are already available from the Fermilab/MILC collaboration [54, 55]. The LANL/SWME collaboration is working to reduce the discretization error by using an improved version of the Fermilab action, the Oktay-Kronfeld action [56]. The work in progress of the JLQCD collaboration is based on Möbius domain-wall quarks, at zero and non-zero recoil, from $N_f = 2 + 1$ QCD [57].

In alternative to lattice, older form factor estimates are available via zero recoil sum rules, giving [58, 59]

$$\mathcal{F}(1) = 0.86 \pm 0.02 \quad (54)$$

in good agreement with the lattice value in (51), but slightly lower in the central value. Recently, information on all form factors parametrizing matrix elements of the basis of dimension-six operators, including those appearing only in connection of new physics effects, has become available in the framework of QCD LCSR [60], and exploited for $|V_{cb}|$ determinations from $B \rightarrow D^{(*)} \ell \nu_\ell$ decays [61].

For the $B \rightarrow D \ell \nu_\ell$ decays, lattice-QCD calculation of the hadronic form factors at non-zero recoil have become available since 2015 ||. In [63] the FNAL/MILC collaboration has calculated the form factors for a range of recoil momenta and parametrized their dependence on momentum transfer using the BGL z -expansion. Two months later, new results on $B \rightarrow D \ell \nu_\ell$ form factors at non-zero recoil were announced by the HPQCD Collaboration [64]. Their results are based on NRQCD action for bottom and the Highly Improved Staggered Quark (HISQ) action for charm quarks, together with $N_f = 2 + 1$ MILC gauge configuration.

|| Prior results at non-zero recoil were only available in the quenched approximation [62].

Given an experimental determination, the $B_s \rightarrow D_s \ell \nu_\ell$ decay can supply a new method for precisely determining $|V_{cb}|$. Lattice QCD calculations of $B_s \rightarrow D_s$ form factors have already been performed at high q^2 , close to zero recoil, where statistical errors are smaller [65–68]. The signal/noise degrades exponentially as the spatial momentum of the meson in the final state grows. Systematic errors from missing discretisation (and relativistic) corrections also grow away from zero recoil. Very recently, the HPQCD Collaboration has presented a lattice QCD determination of the $B_s \rightarrow D_s \ell \nu_\ell$ scalar and vector form factors over the full physical range of momentum transfer [69]. They work with a highly improved quark action and cover a range of values of the lattice spacing that includes very fine lattices and results from lighter than physical b quarks.

3.3. Exclusive decays into heavy leptons

Exclusive B decays into τ leptons were first observed by the Belle Collaboration in 2007 [70]. Subsequent measurements by BaBar and Belle reported branching fractions above-yet consistent with-the SM predictions until 2012, when a significant excess over the SM expectation was reported by BaBar [71]. The discrepancy with the SM persists today, triggering a relevant amount of theoretical analyses. Measurements and predictions are usually quoted as branching fraction ratio

$$R(D^{(*)}) \equiv \frac{\mathcal{B}(B \rightarrow D^{(*)} \tau \nu_\tau)}{\mathcal{B}(B \rightarrow D^{(*)} \ell \nu_\ell)} \quad (55)$$

where the denominator is the average for $\ell \in \{e, \mu\}$. This ratio is typically used instead of the absolute branching fraction of $B \rightarrow D^{(*)} \tau \nu_\tau$ decays, in order to cancel uncertainties common to the numerator and the denominator. These include the CKM matrix element and several theoretical uncertainties on hadronic form factors and experimental reconstruction effects.

The ratio (55) tests the couplings of the charged gauge bosons to the different lepton families. A discrepancy with the SM predictions challenges the universality of the SM couplings, and indicates physics beyond the SM. Although this ratio cannot be used to determine $|V_{cb}|$ directly, its knowledge is still useful, indirectly, since possible new physics couplings would affect high precision semileptonic analyses aimed at $|V_{cb}|$ extraction.

In 2012-2013 the BaBar collaboration measured $R(D^{(*)})$ by using its full data sample [71, 72], and reported a significant excess over the SM expectation. In 2015 the Belle collaboration reported a measurement of $R(D)$ and $R(D^*)$ [73], using the hadronic B -tagging in an analysis similar to the BaBar one. In the same year, LHCb collaboration reported the first measurement of $R(D^*)$ in pp collisions [74]. Both these measurements were above the SM expectations. Since then other measurements have been performed; here we report the full list:

- (i) $R(D)$ and $R(D^*)$ with τ reconstructed in the $\tau \rightarrow \ell$ mode ($\ell \in \{e, \mu\}$), and using the hadronic B -tagging approach: BaBar 2012 [71, 72], Belle 2015 [73];

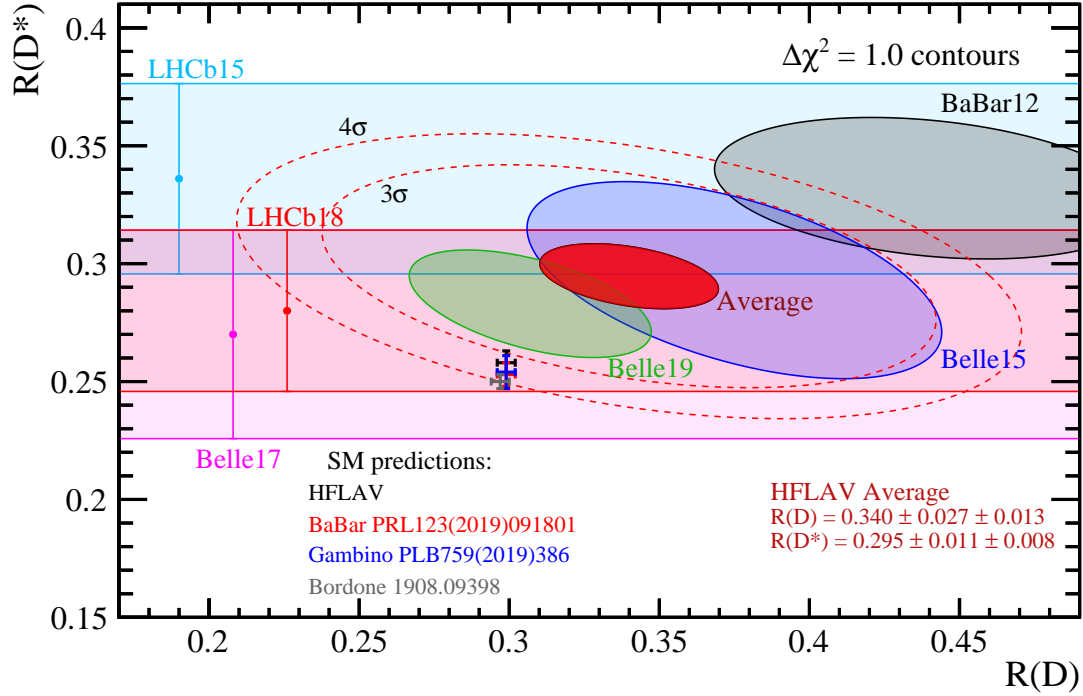


Figure 4. Measurements of $R(D)$ and $R(D^*)$ and their two-dimensional HFLAV average [79]. Contours correspond to $\Delta\chi^2 = 1$, i.e., 68% CL for the bands and 39% CL for the ellipses. The black point with errors is the average of the SM predictions used by HFLAV and obtained from [80–83]. This prediction and the experimental average, deviate from each other by 3.1σ . The dashed ellipses correspond to a 3σ (99.73%) and 4σ contours. Also very recent predictions are reported.

- (ii) $R(D^*)$ with the τ reconstructed in $\tau \rightarrow \mu$ mode: LHCb 2015 [74];
- (iii) $R(D^*)$ with $\tau \rightarrow \ell$, using the semileptonic B -tagging: Belle [75] (this measurement has been superseded by the more recent combined $R(D)$ and $R(D^*)$ measurement [76] using the same tagging approach);
- (iv) $R(D^*)$ and τ polarization with the τ reconstructed in hadronic $\tau \rightarrow \pi(\pi^0)\nu_\tau$ decay mode, and using the hadronic B -tagging: Belle 2016 [77];
- (v) $R(D^*)$ with τ reconstructed in the hadronic $\tau \rightarrow 3\pi(\pi^0)\nu_\tau$ mode: LHCb 2017 [78];
- (vi) $R(D)$ and $R(D^*)$ with $\tau \rightarrow \ell$, using the semileptonic B -tagging: Belle 2019 [76].

By averaging the measurements [71, 73, 74, 76–78], the HFLAV Collaboration has found [79]

$$\begin{aligned} R(D^*) &= 0.295 \pm 0.011 \pm 0.008 \\ R(D) &= 0.340 \pm 0.027 \pm 0.013 \end{aligned} \tag{56}$$

where the first uncertainty is statistical and the second one is systematic. The average and the individual measurements included are shown in figure 4.

Several theoretical predictions for $R(D^*)$ in the SM have been performed, starting from 2012 [84]. Some of them use the data presented by the Belle collaboration in 2017 [85] and the BGL parameterization ¶ [81–83]. Their results are generally consistent with the older predictions, and their arithmetic average, as given by the HFLAV collaboration [79], is

$$R(D^*) = 0.258 \pm 0.005 \quad (57)$$

In the case of $R(D)$, lattice SM predictions by FNAL/MILC [63] and HPQCD [64] collaborations have been averaged by the FLAG collaboration, yielding $R(D) = 0.300 \pm 0.008$ [86]. Like for $R(D^*)$, there are more recent calculations [80, 81, 83] that have performed analyses combining experimental data on $B \rightarrow D\ell\nu_\ell$ decays from Belle and Babar, and theory calculation; their arithmetic HFLAV average is [79]

$$R(D) = 0.299 \pm 0.003 \quad (58)$$

The HFLAV predictions (57) and (58) are reported in figure 4. The averages for $R(D)$ and $R(D^*)$ in (56) exceed the SM values by about 1.4σ and 2.5σ , respectively. If one considers both deviations, the tension rises to about 3.1σ .

More recent SM predictions [61, 87, 88], while compatible with the previous calculations, are slightly on the lower side, resulting in discrepancies with the HFLAV average between 3.3 and 3.9σ . We show in figure 4 also these more recent predictions.

3.4. Decays to excited D -Meson states

The interest in semileptonic B decays to excited states of the charm meson spectrum derives mostly by the fact that they contribute as a background to the direct decay $B \rightarrow D^{(*)}\ell\nu$ at the B factories, and, as a consequence, as a source of systematic error in the $|V_{cb}|$ measurements. Precise knowledge of the properties of the excited D meson states is important to reduce uncertainties in the measurements of semileptonic decays.

The spectrum of mesons consisting of a charm and a \bar{u} or \bar{d} (open charm mesons) is poorly known. A QCD framework for their analysis can be set up by using HQET. In the limit of infinite heavy quark mass, the spin of the heavy quark \vec{s}_h is conserved and decouples from the total angular momentum of the light degrees of freedom \vec{j}_l , which becomes a conserved quantity as well. The separate conservation in strong interaction processes of \vec{s}_h and \vec{j}_l permits a classification of heavy mesons of given radial (principal) quantum number according to the value of \vec{j}_l . Mesons can be collected in doublets: the two states in each doublet (spin partners) have total angular momentum $\vec{J} = \vec{j}_l + 1/2 \hat{s}_h$ and parity $P = (-1)^{L+1}$, since $\vec{j}_l \equiv \vec{L} + \vec{s}_l$, where \vec{L} is the orbital angular momentum and \vec{s}_l the spin of the light degrees of freedom. Within each doublet the two states are degenerate in the limit of infinite heavy quark mass,

The low-mass spectrum includes the ground states, with principal (radial) quantum number $n = 1$ and $L = 0$ (1S, in the spectroscopic notation), which implies $j_l^P = \frac{1}{2}^-$.

¶ They were prompted by the debate on the different parameterizations outlined in section 6.3.3.

The ground state doublet consists of two states with $J^P = (0^-, 1^-)$, that is D and D^* mesons⁺.

When $L = 1$, there are four states ($1P$ states), which are generically referred to as D^{**} ^{*}. The doublet having $j_l^P = \frac{1}{2}^+$ is named (D_0^*, D_1) and corresponds to $J^P = (0^+, 1^+)$. These states are identified with $D_0^*(2300)$ (it was $D_0^*(2400)$, see [89]) and $D_1(2430)$. The doublet having $j_l^P = \frac{3}{2}^+$ is named (D_1, D_2^*) and corresponds to $J^P = (1^+, 2^+)$. These states are identified with $D_1(2420)$ and $D_2^*(2460)$. For the states with $j_l = \frac{3}{2}$, the two-body decay $D^{**} \rightarrow D^{(*)}\pi$ must be in the D-wave to conserve j_l . Therefore, the width should be narrow and relatively easy to observe. $D_1(2420)$ and $D_2^*(2460)$ have relatively narrow widths, about 30 MeV, and have been observed and studied by a number of experiments since the nineties. In contrast, for the state with $j_l = \frac{1}{2}$ the same two-body decay should proceed in S-wave, and widths should be wide. Therefore, $D_0^*(2300)$ and $D_1(2430)$ are more difficult to detect due to the large width, about 200-400 MeV, and were not observed prior to the B -factory era. The state $D_0^*(2300)$ has been studied by Belle, BaBar and LHCb collaborations in exclusive B decays [90–94], while the state $D_1(2430)$ has been observed by Belle collaboration [90], but its production in semileptonic B decays, studied by BaBar [95] and Belle [96] gives contradictory results.

When a new state is observed, the concept of a heavy quark spin doublet is the guiding principle to understand the nature of the observed state. However, the spectroscopic identification for heavier states is not very clear. In 2010 BaBar has observed, for the first time, candidates for the radial excitations (2S) of the D^0 , D^{*0} and D^{*+} , as well as the $L = 2$ excited states of the D^0 and D^+ [97]. Resonances in the 2.4-2.8 GeV/ c^2 region of hadronic masses have also been identified at LHCb [92–94, 98].

Limits in the experimental scenario concerning B decays into excited states are mirrored by theoretical ambiguities. The analyses from Belle [96] and BaBar [99], which combined one additional pion to the ground and first excited states, revealed a couple of interesting anomalies.

The first is the fact the $B \rightarrow D^{**} \rightarrow D^{(*)}\pi l \nu_l$ branching fraction is composed of approximately equal contributions from the $j_l = 1/2$ and $j_l = 3/2$ states. This is unexpected as most theoretical calculations, using sum rules [100, 101], quark models [102–105] (but not constituent quark models, see f.i. [106]), OPE [107, 108], indicate that the narrow width states dominate over the broad D^{**} states (the “1/2 vs 3/2” puzzle).

The other puzzle is that the sum of the measured semileptonic exclusive rates having $D^{(*)}$ in the final state is less than the inclusive one (“gap” problem) [96, 99]. Indeed, decays into $D^{(*)}$ make up $\sim 70\%$ of the total inclusive $B \rightarrow X_c l \bar{\nu}$ rate and decays into $D^{(*)}\pi$ make up another $\sim 15\%$, leaving a gap of about 15%. This is in contrast to the

⁺ The naming convention followed is to use $D^*(mass)$ to denote the states having $P = (-1)^J$, that is $J^P = 0^+, 1^-, 2^+, \dots$ (natural spin-parity) and with $D(mass)$ all the others (unnatural spin-parity).

^{*} Sometimes in literature this term is extended to include all particles in the low-mass spectrum except the ground states.

situation with the tauonic channels, where the branching fractions of the $B \rightarrow D^{(*)}\tau\nu_\tau$ saturate the inclusive $B \rightarrow X_c\tau\nu_\tau$ rate measured at LEP [89]. BaBar used the full dataset to improve the precision on decays involving $D^{(*)}\pi l\nu$ and to search for $D^{(*)}\pi\pi l\nu$ decays [109]. These results have assigned about 0.7% to the $D^{(*)}\pi\pi l\nu$ branching ratio, reducing the significance of the gap from 7σ to 3σ .

One possible weakness common to most theoretical approaches is that they are derived in the heavy quark limit and corrections might be large. For instance, it is expected that $1/m_c$ corrections induce a significant mixing between the two D_1 states, which could soften the 1/2-3/2 puzzle [110]. The possibility of a larger than expected contribution of the first radial excitation of the D^* to the B semileptonic decay into charmed mesons has also been advanced [111, 112]. However, no firm conclusion can be drawn until more high quality data on the masses and the widths of the orbitally excited D meson states become available.

4. Experimental techniques

4.1. B -hadron production

The b -hadrons can be produced in different experimental environments: from e^+e^- annihilation, collisions of protons or proton-antiproton annihilation. The most recent results on b -hadron semileptonic decays come from e^+e^- experiments operating at the energy of the $\Upsilon(4S)$ and from pp collision at LHC.

Understanding the features of the b -hadron production in various environments is crucial to understand the experimental setup and analysis techniques developed to study semileptonic decays. In the following we focus on the b -hadron production mechanism at the B -Factories and pp colliders.

4.1.1. B -Factories Studies of B meson decays have been performed at e^+e^- colliders working at the center-of-mass energy of $\sqrt{s} = 10.58$ GeV, which corresponds to the mass of the $\Upsilon(4S)$ resonance. The first two experiments working at this resonance were ARGUS (at DORIS accelerator) and CLEO (at CESR).

The next generations of e^+e^- colliders have been the modern B -Factories, BaBar and Belle, designed to collect data produced in the collisions at PEP-II and KEKB, respectively. A detailed description of both BaBar and Belle, their performances and their analysis methods can be found in [113].

The main characteristic of the B -Factories was the very high luminosity (2 order of magnitude higher than older e^+e^- colliders) achieved by the machines PEP-II and KEKB. The experiments BaBar and Belle stopped their operations in 2008 and 2010, respectively. However, a decade later, many analyses are still ongoing to exploit the full dataset collected by these two experiments. The measurements of $|V_{cb}|$ are dominated by the B -Factories.

At B -Factories, the B -mesons are produced through the decay of the $\Upsilon(4S)$. An

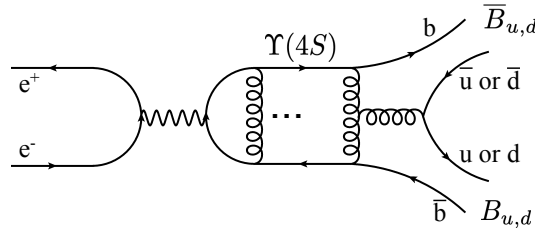


Figure 5. B mesons at B -Factories are produced from the decays of the $\Upsilon(4S)$.

illustration of the process involved is shown in figure 5. The $\Upsilon(4S)$ is the lightest $b\bar{b}$ resonance with mass above the $B\bar{B}$ pair production \ddagger . This resonance decays almost exclusively in a couple of B -meson pairs. The probabilities to produce $B^0\bar{B}^0$ and B^+B^- from $\Upsilon(4S)$ decays are about the same. The ratio of the branching fraction decays f_{+-}/f_{00} differs slightly from unity because of the small difference due to Coulomb effect, which increase the rate when oppositely charged states are present in the final state. The current average value is $f_{+-}/f_{00} = 1.058 \pm 0.024$ [89].

Because of the small mass difference between the $\Upsilon(4S)$ state and $B\bar{B}$ pairs, the B -mesons are produced with very small momentum in the $\Upsilon(4S)$ center of mass. In particular the B -meson momentum is $|\vec{p}_B| \simeq 320 \text{ MeV}$. For this reason the decay products of the two B 's are produced almost isotropically in the $\Upsilon(4S)$ rest frame. Evens like these are usually called *spherical*.

The integrated luminosity collected at $\Upsilon(4S)$ energy was 426 fb^{-1} and 711 fb^{-1} at BaBar and Belle, respectively. The integrated luminosity collected by ARGUS and CLEO were only 0.2 fb^{-1} and 16 fb^{-1} , respectively. The high luminosity has been paramount to study CP violation in B mesons decay, because it allows the study of rare processes, with branching ratios of the order of $10^{-4} \div 10^{-6}$. The need to measure time-dependent properties of the B meson decays has driven the design of the B -Factories. A unique characteristic of the B -Factories was the asymmetric energies of the colliding beams, so the $\Upsilon(4S)$ was produced boosted. The boost allowed a better spatial separation of the two B meson decay vertices. For example, in BaBar the boost was $\beta\gamma \approx 0.55$, resulting in an average distance between the two B meson decay vertex of $250 \mu\text{m}$ which was in the capability of the vertex detector.

At the energy \sqrt{s} corresponding to the $\Upsilon(4S)$ mass, the cross section of $e^+e^- \rightarrow \Upsilon(4S)$ is about 1.06 nb , resulting is about $1.1 \times 10^6/\text{fb}^{-1}$ $B\bar{B}$ pairs. But at this energy, Only about one forth of all the hadronic events produced are $\Upsilon(4S)$, the rest non- $B\bar{B}$ events. The cross section for some important processes at $\sqrt{s} = 10.58 \text{ GeV}$ are reported in table 1. These events are a background to the study of B meson decays, called *continuum background*. In general they are rejected exploiting the differences between

\ddagger The $\Upsilon(4S)$ is above the $B\bar{B}$ pair mass, so the decays proceed through strong decays which dominate over radiative or weak decays. The $\Upsilon(4S)$ is accessible at e^+e^- colliders because the process $e^+e^- \rightarrow \gamma^* \rightarrow b\bar{b}$ allows only states with $J^{PC} = 1^{--}$ quantum numbers.

Table 1. The cross section for some relevant processes at different colliders. The collected integrated luminosity for some of the experiments is reported in parenthesis.

Collider	Process	cross section	experiments
$e^+e^- \rightarrow \Upsilon(4S)$	$b\bar{b}$	1.06 nb	BaBar (426 fb ⁻¹)
	$c\bar{c}$	1.30 nb	Belle (711 fb ⁻¹)
	$d\bar{d}, u\bar{u}, s\bar{s}$	2.09 nb	
$e^+e^- \rightarrow Z$	$b\bar{b}$	6.6 nb	ALEPH, DELPHI (0.14 fb ⁻¹), OPAL, L3
pp 7, 8 TeV	$b\bar{b}$ $2 < \eta < 5$	72 μb	LHCb (3 fb ⁻¹)
	$b\bar{b}$ total	295 μb	CMS, ATLAS (25 fb ⁻¹ each)
pp 13 TeV	$b\bar{b}$ $2 < \eta < 5$	144 μb	LHCb (6 fb ⁻¹)
	$b\bar{b}$ total	600 μb	CMS, ATLAS (150 fb ⁻¹ each)
$p\bar{p}$ 1.96 TeV	$b\bar{b}$ $ \eta < 1$	30 μb	CDF, D0 (10 fb ⁻¹ each)

decays of the $\Upsilon(4S)$ and the decays of the $e^+e^- \rightarrow q\bar{q}$. As said before, the B mesons are produced almost at rest in the $\Upsilon(4S)$ frame, so the decay products have a spherical topology, while in $e^+e^- \rightarrow q\bar{q}$ processes the tracks coming from the fragmentation of the two quarks produces a topology with two opposite jets. Furthermore, the average number of particles produced in the quark hadronization in $e^+e^- \rightarrow q\bar{q}$ processes is smaller than in $\Upsilon(4S) \rightarrow B\bar{B}$ processes. The suppression of the continuum background is thus performed requiring a minimum number of tracks, usually three or four, and applying global event shape criteria that allow to separate jet-like events from more spherical events.

Even with these requirements, the continuum, mainly the contribution from $e^+e^- \rightarrow c\bar{c}$, remain an important background in many semileptonic analyses. Therefore part of the data (about one tenth) are taken at a center of mass about 50 MeV below the $\Upsilon(4S)$ mass in order to have pure continuum events needed for the study of the background. The study of these continuum events, corrected for the luminosity and for the small energy difference, can be used to predict both the absolute scale and the correct kinematics of the continuum background events.

As we will see in section 4.2.2, many semileptonic analyses gain a lot by an approach called *B-tagging* where the signal B meson is reconstructed together with the second B meson present in the event. The *B-tagging* is very effective in suppressing the continuum background, and more generally, to clean the event reconstruction.

4.1.2. Hadron Colliders At LHC the production mechanism of b -quarks are the quark annihilation $q\bar{q} \rightarrow b\bar{b}$ and gluon fusion processes $q\bar{q}, gg \rightarrow b\bar{b}$, with the latter ones largely dominating [114]. At leading order in perturbation theory $O(\alpha_s)$, we can draw the tree diagram corresponding to the quark-antiquark annihilation and the flavour creation diagrams shown in figure 6, that is the gluon fusion diagrams in the t -, u - and s -channel

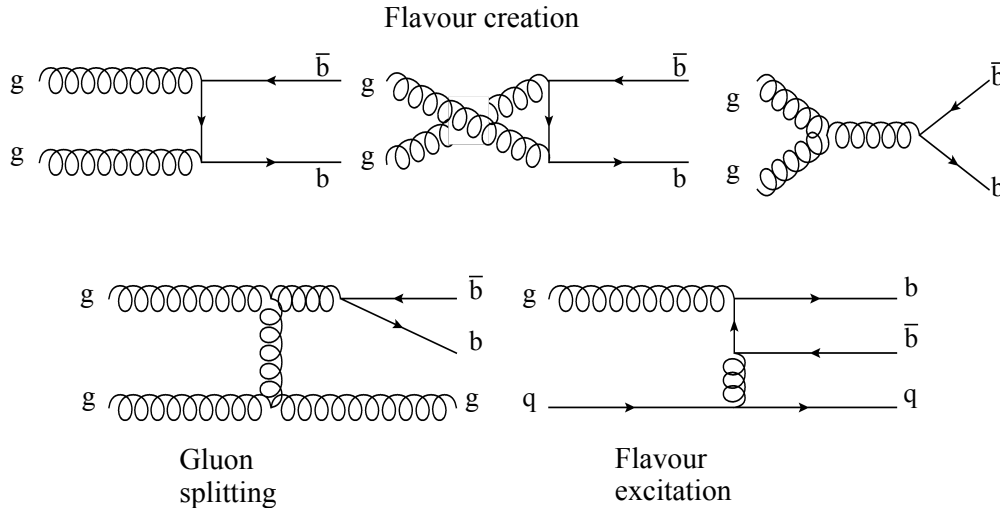


Figure 6. The leading order heavy flavour production processes dominant at LHC.

(from left to right). The $q\bar{q} \rightarrow b\bar{b}g$ parton process and the processes described by the gluon splitting and the flavour excitation diagrams depicted in figure 6 are order $O(g_s\alpha_s)$ in perturbation theory.

The different processes have different final state kinematics: the flavour creation yields $b\bar{b}$ pairs that are almost back to back and with symmetric transverse momentum p_T ; the flavour excitation produces $b\bar{b}$ pairs with highly asymmetric p_T ; the gluon splitting produces $b\bar{b}$ pairs with small opening angle and small p_T . In the forward (and backward) direction the gluon splitting is the dominant process. The LHCb detector is designed to take advantage of this feature [115].

The particle acceptance region covered by the LHCb experiment is the very forward one with pseudorapidity η in the range $2 < \eta < 5$. The pseudorapidity η of a particle is defined as $\eta = -\ln(\tan \theta/2)$, where θ is the angle of the particle three-momentum \vec{p} relative to the positive direction of the beam axis. The acceptance region at LHCb corresponds only to 4% of the full solid angle, but the collected $pp \rightarrow b\bar{b}$ events represent about 25% of the total cross section. The visible b -hadron cross section in the pseudorapidity range $2 < \eta < 5$ has been measured to be $72 \mu\text{b}$ at 7 TeV and almost double at 13 TeV being about $144 \mu\text{b}$ [116].

The general purpose experiments CMS and ATLAS have an acceptance limited to the more central region $|\eta| < 2.2$, which correspond to an efficiency of about 40% for the the $pp \rightarrow b\bar{b}$ processes. Semileptonic B meson decays have not yet been studied at these experiments.

Various important result on B meson semileptonic decays have instead been provided by CDF and D0 experiments, that took data provided by $p\bar{p}$ collisions at 1.96 TeV at Tevatron. In table 1 we report a list of relevant cross section, at different facilities.

The produced b -quark can hadronize, with different probabilities, called *production*

fractions, into a full spectrum of b -hadrons, mainly B^0 , B^+ , B_s , Λ_b . The measured fraction of B^0 and B^+ , in the LHCb acceptance region, is about 36% [79], while the ratio between the B_s and the $B^0 + B^+$ mesons production rate, $f_s/(f_d + f_u)$, is about 0.12 and it has been observed to be slightly dependent on the B_s transverse momentum itself [117]. The Λ_b production fraction, respected to $B^0 + B^+$ production has been measured and it is $f_{\Lambda_b}/(f_u + f_d) \approx 0.26$. A strong dependence of transverse momentum of the observed to be strongly dependent on the transverse momentum of Λ_b has been observed [117]. In the LHCb acceptance range, the production rates $B^0 : B^+ : B_s : \Lambda_b$ are approximately in the ratio $0.36 : 0.36 : 0.09 : 0.19$, with small fractions (10^{-3}) of B_c and other b -baryons (10^{-2}).

The production fractions are crucial to determine the branching ratios of different hadron B decays. For instance, the number of events $N(H_b)$ produced in the LHCb acceptance, of a semileptonic process like $H_b \rightarrow H_c \ell \nu_\ell$, is given by

$$N(H_b) = 2 L \sigma(b\bar{b}) \epsilon_{LHCb} f_{H_b} \mathcal{B}(H_b \rightarrow H_c \ell \nu_\ell) \mathcal{B}(H_c) \quad (59)$$

where L is the integrated luminosity, $\sigma(b\bar{b})$ the total $b\bar{b}$ cross section, ϵ_{LHCb} the detector acceptance, f_{H_b} the production fraction of the H_b hadron species, $\mathcal{B}(H_b \rightarrow H_c \ell \nu_\ell)$ is the branching fraction of the process we are considering, and $\mathcal{B}(H_c)$ is the branching fraction of the c -hadron decay channel used to reconstruct H_c .

4.2. Semileptonic measurements at B -Factories

Generally speaking, the reconstruction of the decays driven by the partonic decay $b \rightarrow c \ell \nu_\ell$ requires an efficient and reliable reconstruction of the lepton ℓ , where the lepton can be an electron or a muon. In the case of the exclusive reconstruction of the final hadronic state, an high efficiency reconstruction and identification of its decay products is also required. Some analyses also require the reconstruction of the other particles of the events, for example to infer the kinematics of the missing neutrino or reduce the combinatorial background in the signal reconstruction. At B -Factories the acceptance of the detectors is an important feature. Their geometry is solenoidal around the interaction point. Detailed descriptions of the B -Factories and of their detectors can be found in [118, 119] and [120]. Here we just briefly describe the most important subdetectors for the study of B -meson semileptonic decays:

- (i) a multilayer silicon detector allows the reconstruction of the tracks very close to the interaction point. This is crucial for the decay vertex reconstruction and for the tracking of very low momentum tracks;
- (ii) a low-mass drift chamber used for charged track reconstruction. The drift chamber allows a precise measurement of the momenta and the identification, through the measurement of the energy loss (dE/dx), of the charged particles;
- (iii) a specialised system to identify the nature of the charged particles based on the Cherenkov effect;

- (iv) a calorimeter for the measurement of the electromagnetic showers produced by photons and electrons;
- (v) an instrumented magnetic flux return used for the identification of muons and the detection of K_L mesons.

Despite the relatively long lifetime of the B mesons, their mean flight length transverse to the beam directions is only $30\mu m$, and about $250\mu m$ in the beam direction. So the B mesons decay in the beam pipe and only the decay products reach the various sub-detectors.

The semileptonic decays are reconstructed starting from the identification of an high-momentum lepton. Typically the minimum lepton momentum is required to be few hundreds of MeV. For some analysis this momentum can be pushed down, but there is a minimum momentum under which the identification is not reliable. And electron has to reach the calorimeter to be clearly identified from the measurement of $E/|\vec{p}|$, the ratio between the measured energy released in the calorimeter and the measured momentum of the associated track. In general the minimum energy is close to 0.5 GeV. A muon needs to reach the muon detector to be identified. Its identification relies on the calorimeter energy measurement, that needs to be compatible with minimum ionizing particles, and the number of the detecting plane traversed in the iron. A muon traverses more planes and releases less hits per plane than a pion. For both electrons and muons, the most relevant source of wrongly identified leptons are the pions. Pions that interact strongly in the calorimeter can mimic the energy released by an electron. The distribution of the energy released in the calorimeter is exploited to separate electrons from pions.

Pions can mimic a muons because there is a finite probability that they go through the iron absorber without interacting (punch through). Moreover pions can decay in flight and generate a muon which is identified in the main detector. Because of the small mass difference between pions and muons, the kink resulting from the pion decay in flight is in most of the cases too small to be detected. At small energy the background from pion decay in flight is dominant and prevents the reliability of the identified low momentum muons.

The performances of the lepton identification is done using control samples of electrons and muons. The cleanest source of electrons and muons are

- (i) Bhabha and di-muon processes, $e^+e^- \rightarrow e^+e^-(\gamma)$ and $e^+e^- \rightarrow \mu^+\mu^-(\gamma)$;
- (ii) decays of the J/ψ into e^+e^- and $\mu^+\mu^-$.

*4.2.1. Soft pion from D^** The study of the exclusive $B \rightarrow D^*\ell\nu$ decays requires the reconstruction of the D^{*+} or D^{*0} . These mesons are reconstructed usually through the decay chains $D^{*+} \rightarrow D^0\pi^+$ and $D^{*0} \rightarrow D^0\pi^0$. Because of the little phase space available in $D^* \rightarrow D\pi$ decays, the emitted π has a slow momentum in the D^* rest frame. As consequence the momentum of the π is correlated with the variable w , and

any inefficiency in reconstructing these pions in the low transverse momentum region, affects the signal reconstruction in the zero-recoil phase space region.

Low momentum π^+ does not cross the full tracking device, so its tracking efficiency is strongly dependent on the momentum. For transverse momentum of magnitude p_T around 100 MeV, the tracking relies entirely on the inner silicon trackers. Below 60 MeV, the reconstruction is not possible because the track does not traverse enough layers. A good knowledge of the soft π^+ efficiency is required for precise measurements. At B -Factories the low p_T track reconstruction efficiency is based on an approach used for the first time by the CLEO collaboration and described in detail in [121]. This approach exploits the distribution of the π^+ helicity angle θ^* as a function of the D^{*+} momentum. The helicity angle θ^* is defined as the angle between the slow π^+ momentum in the D^* rest frame and the D^* direction in the laboratory frame. The distribution of θ^* is expected to be symmetrical and can be described by $dN/d\cos\theta^* \propto (1 + \alpha \cos^2\theta^*)$. The angle θ^* is connected with the slow π^+ momentum in the laboratory frame by $p_\pi = \gamma(p_\pi^* \cos\theta^* - \beta E_\pi^*)$ where β and γ are the D^* boost parameters. From the last relation, any asymmetry in the θ^* distribution can be related to the reconstruction efficiency in a region of the slow π^+ momenta.

4.2.2. B tagging At the B -Factories the decay products of the two B mesons originated from the decays of the $\Upsilon(4S)$ overlap and it can happen than one or more particles can be assigned to the wrong B meson. This source of background, called *combinatorial*, can be relevant and the approach to evaluate and eventually suppress its contributions depends strongly on the analysis.

In the $\Upsilon(4S) \rightarrow B\bar{B}$ decay, there are only two B -mesons in the final state. Reconstructing one B in exclusive decays modes it is possible to reduce the combinatorial background and also the continuum. This technique, called *B tagging*, has been widely and successfully used at B -Factories. In addition to the background reduction, the kinematics information of the tagged B (B_{tag}) can be used to constrain the kinematic of the full event and improve the resolution in the kinematic quantity of the signal B meson (B_{sig}) decay analysis. The main disadvantage of the B tagging approaches is the small efficiency for the reconstruction of B_{tag} , usually well below 1%. This is because there are many B decay modes, all with small branching fractions and with high multiplicity in the final state, resulting in overall small detection efficiency.

The B tagging approaches can be classified in two main categories:

- (i) **hadronic tagging:** the B_{tag} is fully reconstructed in a mixture of many different hadronic decay modes. The reconstruction of the B_{tag} starts reconstructing a set of charm mesons (called *seeds*), like D^0 , D^+ , D^{*+} , D^{*0} , D_s , D_s^* or J/ψ from their decay modes. Usually many decay modes of these seeds are added up together to increase efficiency. A seed is then combined with additional charmless mesons, (π^\pm , K^\pm , π^0 and K_s) to form a possible B candidates. The two variables used to test the compatibility with a B meson are

- (a) $\Delta E = E_B^* - E_{beam}^*$, the difference between the energy of the B candidate in $\Upsilon(4S)$ and the expected B candidate energy fixed by the energy of the beams;
- (b) the energy substituted mass, $m_{ES} = \sqrt{E_{beam}^{*2} - |\vec{p}_B^*|^2}$, where \vec{p}_B^* is the momentum of the B candidate.

A correctly identified B meson gives $\Delta E \approx 0$ and $m_{ES} \approx m_B$. The quantity m_{ES} exploits the feature that the energy of the B mesons are precisely determined by the beam energy, which is known with a resolution better than 2 MeV. The tagging efficiency depends on the multiplicity and the kind of particles present in the analyzed final state. The purity, defined as the probability that a specific decay chain is correctly reconstructed, is very different depending on the decay mode considered. In case of more B_{tag} candidates, the one with the highest purity is in general chosen. To gain in efficiency, usually more than a thousand possible decay modes are considered. The hadronic B -tagging approach has been improved over time by both BaBar and Belle. In BaBar more decays modes and wider mass windows have been implemented according to the specif mode considered. Belle instead made use of a novel algorithm described in [122]. This algorithm uses a set of different neural-networks, properly trained, to estimate the probability that a seed has been correctly reconstructed. The output of the final neural network is used to rank the various B_{tag} candidates. At the end, the average overall efficiency is about 0.3 – 0.5% for the tagging B^+ and about 0.3% for the B^0 , with purity of about 10 – 30%. The reconstruction of the four-momentum of the B_{tag} allows to determine clearly the four-momentum of the signal B_{sig} , even in B_{sig} with missing particles, using:

$$p_{B_{sig}} = p_{\Upsilon(4S)} - p_{B_{tag}}, \quad (60)$$

where $p_{\Upsilon(4S)} = p_{e^+} + p_{e^-}$ is the four-momentum of the initial $\Upsilon(4S)$, determined by the energy of the initial electron and positron beams. The charge and the flavour of the reconstructed B_{tag} are also exploited to clean the sample and reduce the backgrounds.

- (ii) **semileptonic tagging:** the B_{tag} is reconstructed using both $B \rightarrow D^* \ell \nu_\ell$ and $B \rightarrow D \ell \nu_\ell$ decays. The branching fractions of these decays are among the highest in B decays. Moreover, the efficiency to reconstruct semileptonic decays is higher than the one to reconstruct fully hadronic B decays. The final efficiency of the semileptonic B tagging run between 0.5 – 1.0%. The final efficiency is higher than the hadronic B tagging, but the background is also higher. Another disadvantage of the semileptonic tagging is that it does not allow tight kinematic constraints for the presence of neutrino in the tag side.

4.3. Semileptonic measurements at LHCb

LHCb is a dedicated experiment that exploits the fact that the $b\bar{b}$ production rate is larger in the forward direction, as described in section 4.1.2. Because the $c\bar{c}$ production

has similar production mechanism, and it has a cross section about twenty times higher than the $b\bar{b}$, also a huge amount of c -hadrons are produced in the forward direction. The fact that all species of heavy hadrons are produced, makes LHCb a unique facility for heavy flavour physics.

The LHCb detector [115, 123] is a single-arm forward spectrometer that covers the pseudorapidity range $2 < \eta < 5$. It consists of the following subdetectors:

- (i) a precise vertex detector for the identification of the vertex (primary vertex, PV) where the inelastic pp collision occurs, and the reconstruction of the decay vertex of the B hadrons;
- (ii) two detectors specialized for the identification of protons, pions and kaons;
- (iii) an electromagnetic calorimeter for electrons and photon identification and energy measurement, and an hadronic calorimeter for the identification of high p_T hadrons;
- (iv) a detector for muon identification.

The study of semileptonic B decays, because of the presence of the unreconstructable neutrino, presents an experimental challenges in LHCb. The momentum of the B hadrons in production is not known. The identification of semileptonic events exploits the very good identification of the B flight direction. The situation is complementary to that of the B -Factories, where, in untagged measurements, the magnitude of the B momenta is known but their direction. The reconstruction of the kinematic for semileptonic B decays is described in the next section 4.3.1.

In the forward direction, the B hadrons are highly boosted so they have a mean flight length of about 1 cm. This property, associated with the great vertex resolution, is crucial for a clean reconstruction of the signal event. In particular, the large separation between the B decay vertex and the PV reduces the combinatorial background. Moreover, the decay products of the second B hadron, produced usually within the LHCb acceptance, are in general well separated in η , so the mis-assignment of tracks from B hadrons is in general negligible.

The majority, more than 99%, of inelastic pp collisions does not produce b -quarks and are a relevant source of backgrounds, so the triggering of the events is crucial: it has to be efficient for B -hadrons, and has to have a high reject rate for backgrounds. The trigger in LHCb exploits the fact that the B hadrons are long lived, and that, having a relatively large mass, give decay products with an average p_T larger than the typical particle produced in a pp collisions. The trigger consists in a combination of an hardware trigger stage (L0) and a software one. The L0 trigger relies mainly on the muon detector and the calorimeters response.

For the study of semileptonic decays in LHCb, the presence of a muon is very well suited because the L0 trigger line for muons is very efficient. The L0 muon trigger requires the presence of muons of p_T greater than about 1 GeV. This low threshold ensures a large efficiency for B semileptonic decays. For comparison, at CMS and ATLAS this threshold is more than 5 GeV. The trigger for electrons is not as efficient because its identification has to rely on the electromagnetic calorimeter where the trigger

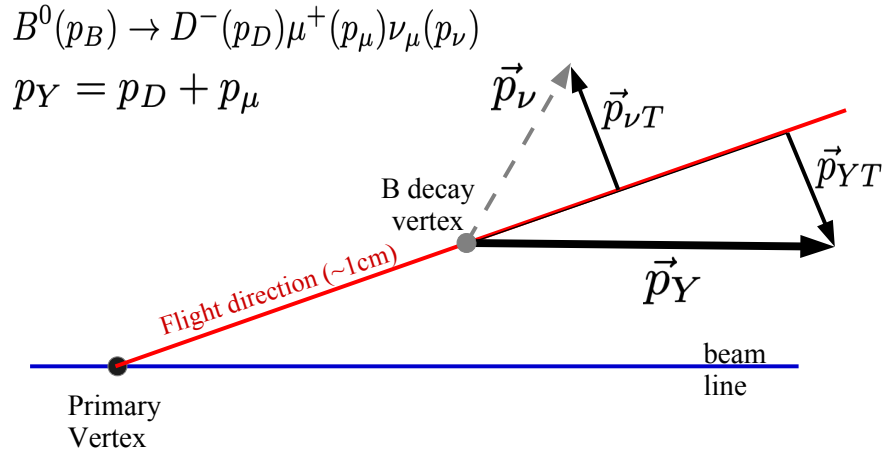


Figure 7. In LHCb the average flight length of the B hadrons is about 1 cm. The good resolution in the vertex reconstruction allows to determine the flight direction.

threshold has to be increased to avoid large backgrounds. Moreover, electrons are affected by bremsstrahlung that deteriorates their momentum reconstruction. For these reasons, usually only semileptonic decays into muons are exploited in LHCb.

At the luminosity of LHC, a large number of multiple pp collision occur in the same bunch crossing. On average about 40 inelastic pp collisions (called *pile-up*) are produced. The study of the B -hadron properties requires the detection of the decay vertex and the production vertex, and large pile-up can pollute the clear identification of the PV, and increase the occupancy in the various subdetectors, worsening the B reconstruction. This problem in LHCb is overcome decreasing locally the luminosity by about a factor 20. This reduces the average number of visible collision per bunch crossing to about 1.8.

4.3.1. Techniques for kinematic reconstruction As mentioned above, the precise determination of the flight direction, from the identification of the PV and the decay B vertex, can be used to constrain the decay kinematic of semileptonic decays [124]. In the hypothesis of a single missing particle with known mass, the unknowns are the components of the 3-momentum of the missing particle. Two constraints are obtained by the momentum conservation in the plane transverse to the decay flight, and the third is determined by the assumed mass of decaying B hadron. Because this last constrain is quadratic, there are two possible solutions.

In figure 7 we illustrate the ingredients exploited to constrain the kinematics. Lets consider the decay $B(p_B) \rightarrow D(p_D)\mu(p_\mu)\nu_\mu(p_\nu)$, where the four-momentum of the various particles are given in parenthesis. The visible system $Y \equiv D\mu$, has a four-momentum given by $p_Y = p_D + p_\mu$. It is useful to decompose p_Y in the longitudinal (p_{YL}) and transverse (p_{YT}) components along the B flight direction. If there is only a missing particle, like a neutrino, its transverse component is known just balancing the

visible transverse component, $\vec{p}_{\nu T} = -\vec{p}_{YT}$. The only unknown is the magnitude of the longitudinal component $|\vec{p}_{\nu L}|$, or, equivalently, the momentum $|\vec{p}_B|$ of the decaying B meson. The B four-momentum is given by $p_B = p_Y + p_\nu$, so we can write

$$p_\nu = p_B - p_Y \implies m_\nu^2 = m_B^2 + m_Y^2 - 2(E_Y E_B - |\vec{p}_B| |\vec{p}_Y| \cos \theta_{BY}), \quad (61)$$

where θ_{BY} is the angle of Y respect to the flight direction. After setting the mass of the B to its value, substituting $E_B = \sqrt{m_B^2 + |\vec{p}_B|^2}$ in (61), squaring and solving for $|\vec{p}_B|$, we arrive to a simple second degree equation

$$(|\vec{p}_Y|^2 \cos^2 \theta_{BY} - E_Y^2) |\vec{p}_B|^2 + (2M |\vec{p}_Y| \cos \theta_{BY}) |\vec{p}_B| + (M^2 - m_B^2 - E_Y^2) = 0, \quad (62)$$

where $M = [(m_B^2 + m_Y^2) - m_\nu^2]/2$. The equation (62) yields two solutions for the B momentum, thus all the kinematic quantities we determine for the decay are affected by this ambiguity; for instance, in the example above, the are two possible $q^2 = (p_B - p_D)^2$ values. Furthermore, the limited vertex resolution gives a fraction of decays with non physical solution, which are usually excluded in the analyses. The fraction of these events depends by the decay considered but it is usually between 20 and 30%.

The two solutions are equally probable and cannot be distinguished. However, after the signal selection requirements are applied, the one that gives the systematically smaller $|\vec{p}_B|$ usually has an higher chance to be the correct solution. Thus in practice, resolutions on q^2 of the order of 10-20% can be achieved by selecting only this solution.

Other approaches to improve the kinematic resolution have been used. In [125] it has been proposed a regression algorithm that uses the information of the flight decay length and the production angles to increase the chance to select the right solution. Another possibility is to consider B decays that come from decays of narrow excited B hadron states. The constraint that comes from the mass difference between the excited state and the B meson removes the ambiguity. This approach has been exploited for example in the analysis [126], where the $B^+ \rightarrow D/D^*/D^{**} \mu \nu_\mu$ relative fraction have been measured by tagging the B^+ mesons from the $B_{s2}^* \rightarrow B^+ K^-$ decay. The price is a reduced signal efficiency due to the low rate of production of the excited B_{2s}^* state.

5. Inclusive $|V_{cb}|$ determination

In section 3.1 we have introduced the inclusive $B \rightarrow X_c \ell \nu$ decays. The total semileptonic rate for $B \rightarrow X_c \ell \nu$ decays is expressed in the framework of the HQE (see section 3.1.1), which allows to disentangle coefficients and corrections calculable in QCD perturbation theory from genuinely non perturbative parameters. The same holds for the moments of distributions of charged-lepton energy and hadronic invariant mass, defined in (36) and (37), respectively. As underlined in section 3.1.2, the inclusive analysis requires a suitable definition of the quark mass in a coherent framework, or scheme.

The shapes of the kinematic distributions in the $B \rightarrow X_c \ell \nu$ decays are sensitive to the masses of the b and c quarks, and the non-perturbative HQE parameters, thus their knowledge is needed to extract $|V_{cb}|$ from data. Non perturbative parameters can be extracted together with $|V_{cb}|$ in a simultaneous fit (global fit) based on experimentally

measured distributions and momenta. Global fit analyses differ by the data sets they are based onto, the theoretical scheme employed, the order of truncation of the HQE expansion. Challenges are experimental selections applied to the data as well as to properly account for correlations.

In the following we describe the measurements of the moments of the charged lepton energy spectrum and the hadronic invariant mass distribution, which, together with the total rate, are the ingredients to extract $|V_{cb}|$ in global fits.

5.1. Moment measurements

The moments of the observables in $B \rightarrow X_c \ell \nu$ inclusive decays have been measured by various experiments. A list of the inputs included in the extraction of $|V_{cb}|$ performed by HFLAV [79] is reported in table 2.

Table 2. Experimental measurements used in the global analysis of $\bar{B} \rightarrow X_c \ell^- \bar{\nu}_\ell$. n is the order of the moment, c is the threshold value of the lepton momentum in GeV.

Exp.	Hadron moments $\langle m_X^{2n} \rangle$	Lepton moments $\langle E_\ell^n \rangle$	Remarks
BaBar [127] [128]	$n = 1, c = 0.9, 1.1, 1.3, 1.5$ $n = 2, c = 0.8, 1.0, 1.2, 1.4$ $n = 3, c = 0.9, 1.3$	$n = 0, c = 0.6, 1.2, 1.5$ $n = 1,$ $c = 0.6, 0.8, 1.0, 1.2, 1.5$ $n = 2, c = 0.6, 1.0, 1.5$ $n = 3, c = 0.8, 1.2$	Lepton momentum spectrum is obtained with an inclusive measurements. The hadronic moments are determined in hadronic tagged B meson sample.
Belle [129] [130]	$n = 1, c = 0.7, 1.1, 1.3, 1.5$ $n = 2, c = 0.7, 0.9, 1.3$	$n = 0, c = 0.6, 1.4$ $n = 1, c = 1.0, 1.4$ $n = 2, c = 0.6, 1.4,$ $n = 3, c = 0.8, 1.2$	Both lepton and hadronic moments measured using the hadronic B tagged events.
CDF [131]	$n = 1, c = 0.7$ $n = 2, c = 0.7$		Hadronic mass measurement obtained from the $D^* \pi$ mass distribution in $B \rightarrow D^{(*)} \pi \ell \nu$ decays, combined with the known $B \rightarrow D^{(*)} \ell \nu$ rates.
CLEO [132]	$n = 1, c = 1.0, 1.5$ $n = 2, c = 1.0, 1.5$		The kinematics of the hadronic part is inferred from the measurement of the neutrino momentum inclusively from the global event missing momentum.
DELPHI [133]	$n = 1, c = 0.0$ $n = 2, c = 0.0$ $n = 3, c = 0.0$	$n = 1, c = 0.0$ $n = 2, c = 0.0$ $n = 3, c = 0.0$	Exploiting the large boost of the B meson produced, the moments are measured without cuts on the lepton energy.

We have already introduced experimental techniques used for the study of semileptonic decays in section 4.2. In the following we provide additional experimental

details on some of the measurements performed at the B -Factories.

5.1.1. Hadron moments The BaBar analysis [127] uses the hadronic B tagging technique. After the reconstruction of the B_{tag} , an identified lepton (electron or muon) is required in the event. The momentum of the lepton is required to be greater than 0.8 GeV in the rest frame of the signal B meson. All the tracks and clusters not associated with the B_{tag} and the lepton are combined to reconstruct the four-momentum of the hadronic system X_c . The resolution on the resulting hadronic mass m_X is improved using a kinematic fit of the full event, considering the conservation of the four-momentum and setting the missing mass to zero. The hadronic moments $\langle m_X^{2n} \rangle$ are reconstructed from the measured m_X spectrum, for different cuts on the minimum lepton energy. The distribution of the mass spectrum for two minimum value of the lepton moments, are reported in figure 8 (left). The different exclusive contributions to the $B \rightarrow X_c \ell \nu$ decay are not disentangled, because of the limited resolution, due mainly to lost or misidentified particles. The reconstructed m_X distribution has to be corrected for the detector efficiency and resolution effects. The true values for the hadronic moments are obtained using a *per-event* corrections to the reconstructed moments, which are determined from simulations. The corrections depend on the lepton energy, the X_c multiplicity and the missing mass in the event.

The Belle analysis [129] also uses the hadronic B tagging method. Belle sets the minimum lepton momentum at 0.7 GeV . The true value of the hadronic moments, is extracted using an unfolding procedure based on the SVD algorithm [134]. This approach requires the knowledge of the migration matrix that connects the reconstructed and the true values of m_X , which is obtained using simulations.

5.1.2. Lepton moments In general the lepton energy momentum $\langle E_\ell^n \rangle$ can be measured with higher precision than the hadronic mass moments. The BaBar analysis [128] uses an inclusive approach where the $B\bar{B}$ candidates are selected requiring two leptons in the event. In this analysis, to reduce the background due to the hadron misidentification for low energy leptons, only electrons are used. A tagging electron is required to have a momentum in the $1.4 - 2.3\text{ GeV}$ range. The second electron in the event, the signal, is studied from momentum greater than 0.6 GeV . The background from the continuum is reduced with the global shape variables. The main source of background is due to lepton from secondary decay of charm mesons. This is reduced by requiring the charge correlation between signal and tagging lepton, and exploiting the kinematic properties of the two leptons. In general the moments have to be computed in the B meson rest frame so in this inclusive analysis further corrections are needed to account for the small motion of the B in the $\Upsilon(4S)$ rest frame.

The Belle analysis of the lepton moments [130] also is limited to electrons, and uses the hadronic B tagging method. One advantage of the tagging approach, is that the four-momentum of the B_{sig} is known from the fully reconstructed B_{tag} so the moments are directly computed in the B rest frame. The moments are extracted

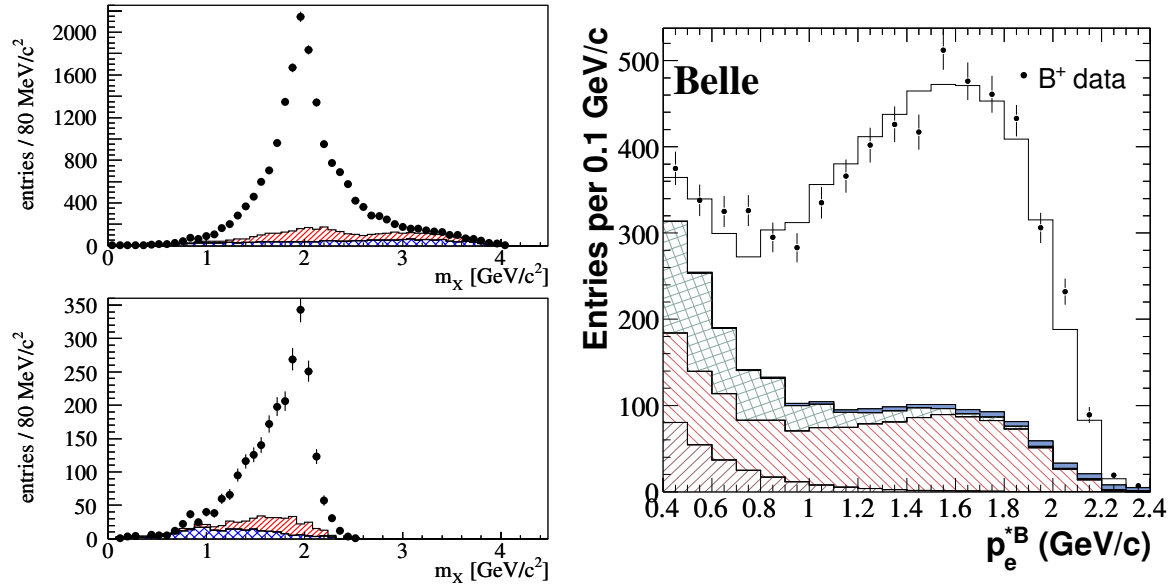


Figure 8. Left: Mass spectra for a lepton momentum cut of $p_\ell^* > 0.6$ GeV (top) and $p_\ell^* > 1.4$ GeV (bottom) obtained by BaBar prior the background subtraction. Plot from [127]. Right: lepton momentum from Belle in the B^+ decays. Plot from [130].

from the minimum lepton momentum cut of $p - e^* > 0.4$ GeV, computed in the B rest frame. The distribution of the lepton momentum, for the B^+ sample, is reported in figure 8 (right).

5.2. Results

A recent global analysis of the inclusive $B \rightarrow X_c \ell \nu$ has been done by HFLAV [79]. In this fit the hadronic mass moments $\langle m_X^{2n} \rangle$ of orders $n = 1, 2, 3$ and the lepton energy moments $\langle E_\ell^n \rangle$ of order $n = 0, 1, 2, 3$ are used. The lepton energy moments of order $n = 0$ are just the partial branching fractions. The moments are determined with different lower values of the lepton energy (E_{cut}). Because the moments of the same order and with different E_{cut} are strongly correlated, only a sub-sample of the measured moments are used in the global analysis. The list of the moments used is reported in table 2.

The moments of the $B \rightarrow X_c \ell \nu$ decay allow to determine a linear combination of the b and c quark masses. Additional inputs can be used for a precise determination of m_b . The additional information can come from the moments of the photon energy in $B \rightarrow X_s \gamma$ decay, or from an external determination of the c quark mass.

In the framework of kinetic scheme, $|V_{cb}|$ is extracted together with the b and c quark masses and 4 non-perturbative parameters (namely μ_π^2 , μ_G^2 , ρ_D^3 and ρ_{LS}^3). The subset of measurements used and the general approach follow the ones described in [135]. The fit is based on theoretical calculations described in [11, 136]. In this analysis the c quark mass is constrained to the value obtained in [137], which is $m_c^{\overline{\text{MS}}}(3 \text{ GeV}) = 0.989 \pm 0.013 \text{ GeV}$. The result of the fit, projected on some of the lepton energy and hadronic mass moments,

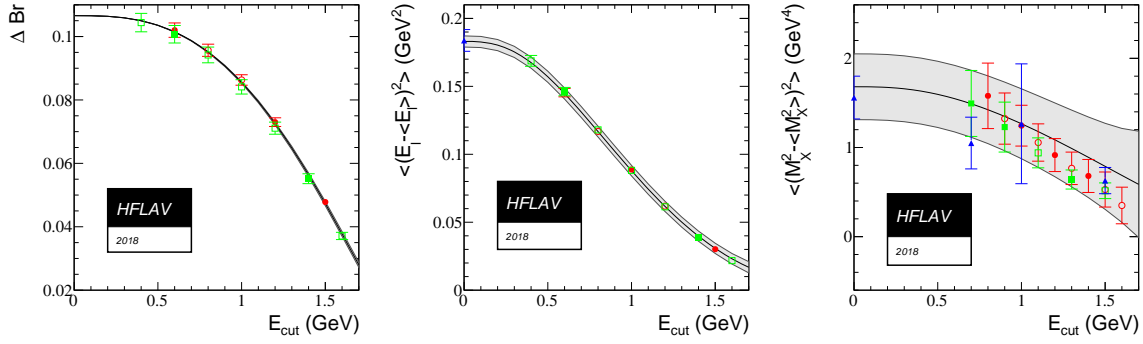


Figure 9. Distributions of the partial semileptonic branching fraction (left), one central lepton momentum (middle) and one hadronic mass central moment (right), with the result of the global fit in the kinetic mass scheme superimposed. The gray band is the theory prediction, fixing the HQE parameters at the fitted value, with the theory uncertainty. Babar data are shown by circles (red), Belle by squares (green) and other experiments (DELPHI, CDF and CLEO) by triangles (blue). Open symbols (no internal color) are measurements not included in the fit.

is shown in figure 9. Let us report also the resulting values for $|V_{cb}|$ and m_b^{kin}

$$\begin{aligned} |V_{cb}| &= (42.19 \pm 0.78) \times 10^{-3}, \\ m_b^{\text{kin}} &= 4.554 \pm 0.018 \text{ GeV} \end{aligned} \quad (63)$$

where the quoted uncertainties include both the experimental and the theoretical uncertainties. It is worth to mention that the theoretical uncertainties are dominating. The excellent fit quality points toward the validity of the HQE fit, but the small χ^2 per degree of freedoms of $\chi^2/ndf = 0.32$, could be a signal of some overestimated theoretical uncertainties, or overestimated correlations between the various moments. These points have been discussed extensively for previous version of the global fit in [135].

An analysis performed in the framework of the 1S scheme, and based on the calculation of the lepton and hadron moments described in [138], gives, for $|V_{cb}|$ and the b quark 1S mass

$$\begin{aligned} |V_{cb}| &= (41.98 \pm 0.45) \times 10^{-3}, \\ m_b^{1S} &= 4.691 \pm 0.037 \text{ GeV}. \end{aligned} \quad (64)$$

This analysis uses the same list of lepton and hadron moments reported in table 2 and in addition the moments of the photon spectrum in $B \rightarrow X_s \gamma$ decays as further constraints. The central values of $|V_{cb}|$ in (63) and (64) are in good agreement, but the uncertainties are different. The uncertainty on $|V_{cb}|$ from the global fits is 1.8% in the kinetic scheme and only 1.1% in the 1S scheme. However, a direct comparison between these two results is not significant, since the two schemes are not equivalent, as sketched in section 3.1.2, and [138] does not include all contributions of order $O(\alpha_s \Lambda_{QCD}^2/m_b^2)$.

All the analyses considered above include only the minimal set of four matrix elements which appear until order $O(1/m_b^3)$. At higher order, the large increase of HQE parameters complicates a great deal the extraction from data. A model approach

that estimates the effects of orders $O(1/m_b^4)$ and $O(1/m_b^5)$, in the so-called Lowest Lying State Approximation, was employed in a recent global fit [139]. Their results indicate that such higher-order terms induce a sub-percent reduction in $|V_{cb}|$, which is not appreciable at the current level of precision. Another recent suggestion is to use a symmetry within the HQE, the reparametrization invariance, to achieve a reduction of independent parameters in some specific observables, that could be measured at e^+e^- colliders and used to extract $|V_{cb}|$ at order $O(1/m_b^4)$ [140].

6. Exclusive $|V_{cb}|$ determination

6.1. Unitarity bounds

As mentioned in section. 3.2, the extraction of $|V_{cb}|$ involves an extrapolation to the zero-recoil point, for which a parametrization of the form factors in terms of w is needed. In this section we describe briefly parameterizations built on the basis of dispersion relations and unitarity bounds. Since more than 50 years, it has been known that nontrivial constraints on an hadronic form factor can be derived starting from a given inequality on a suitable integral of the square modulus of the form factor, along the unitarity cut. Let $F(t)$ denote a generic form factor, depending on a variable t , which is real analytic in the complex t -plane cut along the positive real axis from the lowest unitarity branch point t_+ to ∞ . The essential inequality just mentioned is expressed as

$$\int_{t_+}^{\infty} dt \rho(t) |F(t)|^2 < I \quad (65)$$

where both the function $\rho(t) \geq 0$ and the quantity I are known. Such integral condition can be provided by an observable or, alternatively, by the dispersion relation satisfied by a suitable correlator. The positive spectral function of the correlator has, by unitarity, a lower bound involving the modulus squared of the relevant form factor. Therefore, the constraints derived in this framework are often referred to as “unitarity bounds”. Through complex analysis, this condition leads to constraints on the values at interior points or on the expansion parameters.

Many applications of this approach to the heavy-to-heavy and heavy-to-light form factors, the light-meson form factors, the electro-magnetic form factor of the pion, the strangeness changing $K\pi$ form factors, and so on, can be found in literature (for a review see f.i. [141]). Here we sketch the application to $B \rightarrow D^{(*)}$ decays; details and demonstrations can be found elsewhere (f.i in [142–145] and therein). The two-point QCD function Π^{2P} of a flavor-changing current J is rendered finite by making one or two subtractions, leading to dispersion relations. For one subtraction one can write

$$\chi \equiv \frac{\partial}{\partial q^2} \Pi^L(q^2) = \frac{1}{\pi} \int_0^{\infty} dt \frac{\text{Im} \Pi^L(t)}{(t - q^2)^2} \quad (66)$$

where $\Pi^{2P}(q^2) = 1/q^2(q^\mu q^\nu - q^2 g^{\mu\nu}) \Pi^T(q^2) + q^\mu q^\nu / q^2 \Pi^L(q^2)$. Similarly for $\Pi^T(q^2)$. The functions χ may be computed reliably in perturbative QCD for values of q^2 far from the kinematic region where the current can produce manifestly nonperturbative effects,

like pairs of hadrons. For heavy quarks a reasonable choice is $q^2 = 0 \ll (m_b + m_c)^2$. The spectral functions $\text{Im } \Pi$ are evaluated by unitarity, inserting into the unitarity sum a complete set of states X that couple the current to the vacuum

$$\text{Im } \Pi^L = \frac{1}{2} \sum_X (2\pi)^4 \delta^4(q - p_X) |< 0|J|X>|^2 \quad (67)$$

Since the sum is semipositive definite, by taking a subset of hadronic states, namely the states with only the two heavy mesons, one can obtain a strict inequality. We recover an upper bound of the form of (65) in the pair-production region, that is

$$\frac{1}{\pi\chi} \int_{t_+}^{\infty} dt \frac{W(t)|F(t)|^2}{(t - q^2)^2} \leq 1 \quad (68)$$

where $W(t)$ is a computable function, expressed as a product of phase-space factors, and $t_+ = m_B + m_{D^{(*)}}$ is the unitarity threshold. A similar result holds for Π^T . This inequality makes clear how the perturbative calculation constrains the magnitude of the form factor in the pair-production region, but to turn it into a constraint in the semileptonic region requires that the integrand is analytic below the pair-production threshold $t \leq t_+$. The form factor $F(t)$ may have poles arising from the contribution of bound states, the B_c resonances with the appropriate quantum numbers. Let us consider a conformal variable transformation as

$$z(t; t_0) \equiv \frac{\sqrt{t_+ - t_0} - \sqrt{t_+ - t}}{\sqrt{t_+ - t} + \sqrt{t_+ - t_0}} = \frac{t - t_0}{(\sqrt{t_+ - t} + \sqrt{t_+ - t_0})^2} \quad (69)$$

This transformation maps the complex t -plane, which contains a branch cut extending from t_+ to ∞ , onto the unit disc $|z| < 1$ in the $z(t)$ plane. The branch point t_+ is mapped onto $z = 1$ and the two edges of the unitarity cut $t \geq t_+$ map to the boundary $|z| = 1$. We can see that z is real for $t \leq t_+$ and a pure phase for $t \geq t_+$; t_0 represents the point mapped onto the origin of the z plane. Let us observe that a simple pole in t_0 can be eliminated by multiplying by $z(t; t_0)$. The change of variable (69) simplifies the next step, aimed at isolating factors that encode the nonanalytic behavior of the form factor $F(t)$, so that the inequality (68) becomes

$$\frac{1}{2\pi i} \int_C \frac{dz}{z} |\phi(z)P(z)F(z)|^2 \leq 1 \quad (70)$$

where C is the unit circle in the complex z plane. Here $\phi(z)$ is an outer function, defined in complex analysis as an analytic function lacking zeros in $|z| < 1$, and $P(z)$ is known as a Blaschke factor (or inner function), a products of suitable chosen $z(t; t_0)$ removing singularities due to the resonances below the pair-production threshold. Since $\phi(z)P(z)F(z)$ is analytic on the whole unit disc, we have managed to isolate the analytic structure of the form factor and can write an expansion as

$$F(t) = \frac{1}{\phi(t; t_0)|P(t)|} \sum_{n=0}^{\infty} a_n z^n(t; t_0) \quad (71)$$

with unknown coefficients a_n . These coefficients are different for each form factor, and must be determined by experiment. Inserting (71) back into (70) gives the constraint

$$\sum_{n=0}^{\infty} a_n^2 \leq 1, \quad (72)$$

which is known as the weak unitarity constraint, and holds for each set of form factors sharing parity and spin quantum numbers. All possible functional dependence of the form factor $F(t)$ consistent with the analyticity, unitarity, and explicit QCD information discussed before are now encoded into the coefficients a_n , which are highly constrained by (72). A randomly chosen shape for a form factor would almost inevitably have some $a_n > 1$, disallowing the bound given by (72). In case the allowed kinematic range for z has $|z| \ll 1$, as for semileptonic $B \rightarrow D^{(*)}$ decays, the convergence of the series is geometrically fast, and only the first few a_n coefficients are relevant to the shape of the form factor. In that case the sum in (72) is well approximated by a sum limited by a finite number, depending on the form factor analysed, rather than by ∞ .

One can further constrain the coefficients of the z expansion by considering several decays related by crossing symmetry; these additional constraints are known as the strong unitarity constraints.

We conclude this section by observing that in case of semileptonic $B \rightarrow D^{(*)}$ decay the above formalism is generally expressed in terms of parent and daughter velocity 4-vectors, and the parameter w . Such kinematic variables turns out to be more convenient than the momentum transfer variable $t = (p_B - p_{D^{(*)}})^2$ in the framework of heavy quark symmetries. The conformal transformation $t \rightarrow z$ in (69) becomes $w \rightarrow z$, and we have [143]

$$z(w; \mathcal{N}) \equiv \frac{\sqrt{1+w} - \sqrt{2\mathcal{N}}}{\sqrt{1+w} + \sqrt{2\mathcal{N}}} \quad \mathcal{N} \equiv \frac{t_+ - t_0}{t_+ - t_-} \quad (73)$$

where $z(w; \mathcal{N})$ maps the physical region $1 < w < 1.5$ onto $0 < z < 0.056$ and vanishes at $w = 2\mathcal{N} - 1$. There are several parametrizations of the form factors for semileptonic $B \rightarrow D^{(*)}$ decays based on the approach outlined in this section; we discuss two examples in the next section.

6.2. BGL and CLN parametrizations

The unitarity and dispersion relations outlined in section 6.1 are at the basis of several different parameterization for the exclusive semileptonic $B \rightarrow D^{(*)}$ decays.

Let us consider the $B \rightarrow D^*$ channel. In the so-called Boyd, Grinstein and Lebed (BGL) parameterization [46, 47, 146], it is convenient to set

$$\begin{aligned} H_0(w) &= F_1(w)/\sqrt{q^2} , \\ H_{\pm}(w) &= f(w) \mp m_B m_{D^*} \sqrt{w^2 - 1} g(w) \end{aligned} \quad (74)$$

These equalities define the form factors $F_1(z)$, $f(z)$, and $g(z)$ in terms of the helicity amplitudes; looking at (50), we observe that $F_1(z)$ and $f(z)$ are connected to axial form factors, and $g(z)$ to the vector one. These new form factors can be expressed by series in the variable z , as seen in section 6.1

$$f(z) = \frac{1}{P_{1+}(z)\phi_f(z)} \sum_{n=0}^{\infty} a_n^f z^n ,$$

$$\begin{aligned}
F_1(z) &= \frac{1}{P_{1+}(z)\phi_{F_1}(z)} \sum_{n=0}^{\infty} a_n^{F_1} z^n, \\
g(z) &= \frac{1}{P_{1-}(z)\phi_g(z)} \sum_{n=0}^{\infty} a_n^g z^n
\end{aligned} \tag{75}$$

The ϕ functions are the outer functions [143]. The $P_{1\pm}$ factors are the Blaschke factors, which take into account the sub-threshold B_c resonances with the same quantum numbers as the current involved in the definition of the form factor, and depend on the masses of such resonances. Recent determinations can be found in Refs. [82, 88]. The coefficients a_n are the parameters that need to be fitted on data, subject to unitary constraints

$$\sum_{n=0}^{n_g} (a_n^g)^2 < 1, \quad \sum_{n=0}^{n_f} (a_n^f)^2 + \sum_{n=0}^{n_{F_1}} (a_n^{F_1})^2 < 1 \tag{76}$$

They ensure the convergence of the series over the whole physical region $0 < z < 0.056$ [88]. The series are truncated at different n_i . A similar analysis can be done for the $B \rightarrow D$ channel.

Another common parameterization is the so-called Caprini, Lellouch and Neubert (CLN) parameterization [45]. This parameterization is based on the same unitarity bounds as the BGL parametrization, but it employs strong unitarity constraints to reduce the number of parameters of the more general expansion. It makes use of the relations among the form factors due to heavy quark symmetries (HQS), in particular of the connection, at the leading order in the $1/m_b$ expansion, of all the form factors to the single Isgur-Wise function $\xi(w)$. In the heavy-quark limit, all form factors become identical and equal to $\xi(w)$ (see (45)). In order to incorporate corrections to that limit, one form factor, $F_{ref}(w)$, is chosen a reference form factor and expanded around $w = 1$. Its derivatives are bounded by unitarity relations of the kind of (72). The first derivative, the slope, is defined as

$$\rho^2 = - \left. \frac{\partial F_{ref}(w)}{\partial w} \right|_{w=1} \tag{77}$$

The ratio of all other form factors with the reference one are obtained by including the leading short-distance and $1/m_b$ corrections, and expressed in terms of the reference parameters as ρ . Roughly speaking we have, for each form factor $F(w)$

$$F(w) = \left(\frac{F}{F_{ref}} \right)_{HQS} F_{ref}(w) \tag{78}$$

For $B \rightarrow D^* \ell \nu$ decays, in the CLN parametrisation, the more convenient variables are the leading form factor $h_{A_1}(w)$ and the ratios of form factors $R_1(w)$, and $R_2(w)$ defined in Eqs. (48). The form factor $h_{A_1}(w)$ up to symmetry-breaking corrections coincides with the Isgur-Wise function, while the two form-factor ratios are equal to 1 in the heavy flavour limit, independently of w . The reference form factor is taken to be the axial vector form factor, see formula (35) in [45]. These parameters are expanded

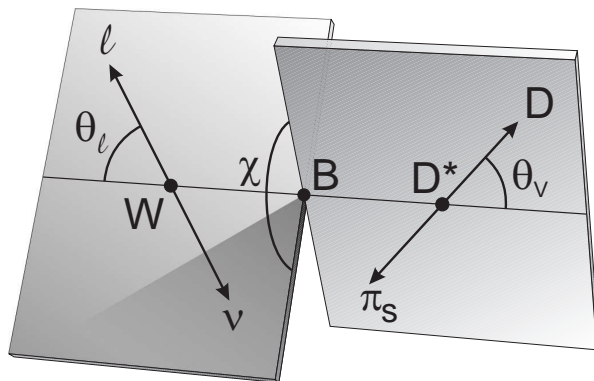


Figure 10. The helicity angles θ_V , θ_ℓ and χ in the $B \rightarrow D^* \ell \nu_\ell$ with the subsequent $D^* \rightarrow D\pi$ decay.

for $w \rightarrow 1$, fixing the series coefficients using dispersive bounds. They are given by [45]

$$\begin{aligned} h_{A_1}(w) &= h_{A_1}(1)[1 - 8\rho^2 z + (53\rho^2 - 15)z^2 - (231\rho^2 - 91)z^3] , \\ R_1(w) &= R_1(1) - 0.12(w - 1) + 0.05(w - 1)^2 , \\ R_2(w) &= R_2(1) + 0.11(w - 1) - 0.06(w - 1)^2 \end{aligned} \quad (79)$$

where $z = (\sqrt{w+1} - \sqrt{2})/(\sqrt{w+1} + \sqrt{2})$. In the $B \rightarrow D^* \ell \nu_\ell$ decays, the reference function is taken to be $\mathcal{G}(w)$, yielding, in the z variable [45]

$$\mathcal{G}(z) = \mathcal{G}(1)[1 - 8\rho_D^2 z + (51\rho_D^2 - 10)z^2 - (252\rho_D^2 - 84)z^3] \quad (80)$$

In this section, we have restricted our discussion to BGL and CLN parameterizations, whose comparison has excited lively discussions since a couple of years. Indeed, in 2017 the reliability of the CLN approach has been questioned in both $B \rightarrow D \ell \nu_\ell$ [80] and $B \rightarrow D^* \ell \nu_\ell$ channels [147, 148]. Details and updates on the current situation are given in section 6.4.2.

6.3. The $B \rightarrow D^* \ell \nu_\ell$ channel

The $B \rightarrow D^* \ell \nu_\ell$ channel, with a branching fraction of about 5%, is the most abundant semileptonic decays of the B mesons. The D^* is reconstructed in the $D^* \rightarrow D\pi$ or $D^* \rightarrow D\gamma$ decay modes, so the $B \rightarrow D^* \ell \nu_\ell$ decay can be seen as a four-body decay. A full description of this decay requires four independent kinematic variables. A customary choice of variables are w , the helicity angle of the D meson (θ_V), the helicity angle of the charged lepton ℓ (θ_ℓ), and the angle χ between the hadronic and leptonic two-body decay planes. These angles are shown in figure 10. Here the set $\cos \theta_V$, $\cos \theta_\ell$ and χ will be collectively called w .

The determination of $|V_{cb}|$ using the $B \rightarrow D^* \ell \nu_\ell$ decays has been performed by many experiments in various environments: CLEO, ALEPH, DELPHI, OPAL, and modern B -Factories, BaBar and Belle. The measurements performed by CLEO and LEP experiments, and also the first ones at the B -Factories, extracted $\eta_{EW}|V_{cb}|$ and

some parameters of the form factor $\mathcal{F}(w)$ in (42), by measuring only the differential decay rate $d\Gamma$ as a function of w only. Since the fully differential rate in w and w depends on the three helicity amplitudes, in these measurements further assumptions are needed. For example, using the CLN parameterization, one relies on external determinations of the $R_1(1)$ and $R_2(1)$ ratios.

The first measurement that extracted information on all the form factors was done by CLEO [149]. In this pioneering measurement, the joint distribution of w and w was fit using an unbinned maximum likelihood method. By assuming a linear dependence on w of $h_{A_1}(w)$, and $R_1(w)$ and $R_2(w)$ independents of w , the following values were measured: $R_1 = 1.18 \pm 0.30 \pm 0.12$, $R_2 = 0.71 \pm 0.22 \pm 0.07$ and $\rho^2 = 0.81 \pm 0.15 \pm 0.06$, where the first uncertainty is statistical and the second is systematic. The parameters R_1 and R_2 were found consistent with the heavy quark symmetry limit of $R_1 = R_2 = 1$. The measurement was limited by the statistics available, based only on 2 fb^{-1} only, but it was the first observation that the corrections to the heavy-quark symmetry limit are quite small.

BaBar and Belle have measured these form factors and $|V_{cb}|$ with significant improved precision thanks to the larger statistics, the improved analysis techniques and the better knowledge of the background from the decay into excited D^{**} final states. At B -Factories the $B \rightarrow D^* \ell \nu_\ell$ decay has been studied using both the untagged approach and the hadronic B -tagging technique. In the following we describe in more details the two most recent measurements, one by Belle [150], using the untagged approach, and one from BaBar [87], based on the hadronic B -tagging.

6.3.1. Belle untagged measurement The Belle experiment has measured the shape of the form factors and $|V_{cb}|$ from $B^0 \rightarrow D^{*-} \ell^+ \nu_\ell$ using both the CLN and the BGL parameterizations [150]. This analysis, based on the full dataset of 711 fb^{-1} , extracts the parameters of interests from one-dimensional projections on w and the angles w .

A positron or an anti-muon with momentum in the range $0.3\text{-}2.4 \text{ GeV}$ or $0.6\text{-}2.4 \text{ GeV}$ in the laboratory frame, is combined with a D^{*-} candidate. The D^{*-} is reconstructed from a \bar{D}^0 and slow pion π^- . The invariant mass difference between the $\bar{D}^0 \pi^-$ combination and the \bar{D}^0 candidates, $\Delta m = m(\bar{D}^0 \pi^-) - m(\bar{D}^0)$, is required to be less than 165 MeV . To reduce the combinatorial background, the \bar{D}^0 is reconstructed only in the $K^+ \pi^-$ decay mode, which has a branching fraction of about 3.8% and it is the experimentally cleanest mode.

The most relevant backgrounds leftover, after the selection requirements, are

- Continuum background: $e^+ e^- \rightarrow c \bar{c}$, where \bar{c} gives a D^{*-} ;
- Combinatorial background: fake D^{*-} candidates;
- D^{**} : resonant $B \rightarrow D^{**} \ell \nu_\ell$ decays, where D^{**} decays to a D^* , and non-resonant $B \rightarrow D^{(*)} \pi \ell \nu_\ell$ decays;
- Misidentified lepton: D^{*-} candidate is combined with an hadron identified incorrectly as electron or muon;

- Correlated background: when the D^{*-} and the lepton come from the same B , like $B \rightarrow D^* \tau \nu_\tau$, $\tau \rightarrow \ell \nu \nu$; $B \rightarrow D^* X_c$ where $X_c \rightarrow \ell Y$;
- Uncorrelated background: when the D^{*-} and the lepton come from different B 's.

The signal and the background yields for the various sources are extracted performing a binned maximum likelihood fit of the $D^* \ell$ candidates in the variables Δm , $\cos \theta_{BY}$ and p_ℓ . The momentum of the lepton p_ℓ is sensitive to the form factors themselves, thus, to avoid biasing the measurement, it is divided only in two regions, below and above 0.6 GeV. This choice has been useful to constrain the residual lepton misidentification background that affects mainly the low lepton momentum region. The invariant mass difference Δm is sensitive to the combinatorial background. The most powerful variable that allows to separate signal from the D^{**} and the correlated background, is $\cos \theta_{BY}$. In the assumption that the decay is $B \rightarrow D^* \ell \nu$, in the $\Upsilon(4S)$ rest frame, the B direction can be constrained in a cone around the axis given by the $Y \equiv D^* \ell$ direction,

$$\cos \theta_{BY} = \frac{2E_B^* E_Y^* - m_B^2 - m_Y^2}{2|\vec{p}_B^*| |\vec{p}_Y^*|}, \quad (81)$$

where E_B^* and $|\vec{p}_B^*|$ are given by the beam energy and all the other quantities are determined only by the visible system Y . In (81) all the kinematic quantities are computed in the $\Upsilon(4S)$ rest frame. For the signal, $\cos \theta_{BY}$ is constrained in the physical region $(-1.0 \div 1.0)$, instead for the $B \rightarrow D^{**} \ell \nu$ and $B \rightarrow D^* \pi \ell \nu$, where one or more further particles are emitted, it is easy to show that $\cos \theta_{BY}$ is only constrained to be less than +1.0. Thus for D^{**} background $\cos \theta_{BY}$ has a long tail below the -1.0 value. The uncorrelated background is also constrained from $\cos \theta_{BY}$ because its shape extends to the region with $\cos \theta_{BY} > 1.0$. The distribution of $\cos \theta_{BY}$ for the most important physical backgrounds is shown in figure 11 (left).

Because of the bremsstrahlung that affects the electrons, and the finite resolution in the momentum reconstruction of the visible energy, $\cos \theta_{BY}$ for the signal also extends over the physical range. An important source of uncertainty in the computation of $\cos \theta_{BY}$ is due to the beam energy spread of few MeV that affects the computation of p_B^* and E_B^* hence smearing the $\cos \theta_{BY}$ variable.

The signal yields extraction, from a simultaneous fit to Δm , $\cos \theta_{BY}$ and p_ℓ , is performed for each bin of the kinematic variables considered (w and the angles w). After the background subtraction, a total number of 180×10^3 candidates is obtained.

Because of the presence of the neutrino, the B -direction is not known, so these kinematic quantities cannot be calculated directly. From the value of $\cos \theta_{BY}$ per event, it is known only that the B must lie on a cone around the direction of the Y system. Various approaches have been used in different analyses to constrain the B direction on the cone. In this analysis Belle exploits the rest of the events to build a rough estimation of the direction of the other B inclusively. The B direction is chosen as the one on the cone closest to opposite of the other B meson direction. In figure 11(right) is illustrated how the technique works. With this algorithm the resolutions of the kinematic variables

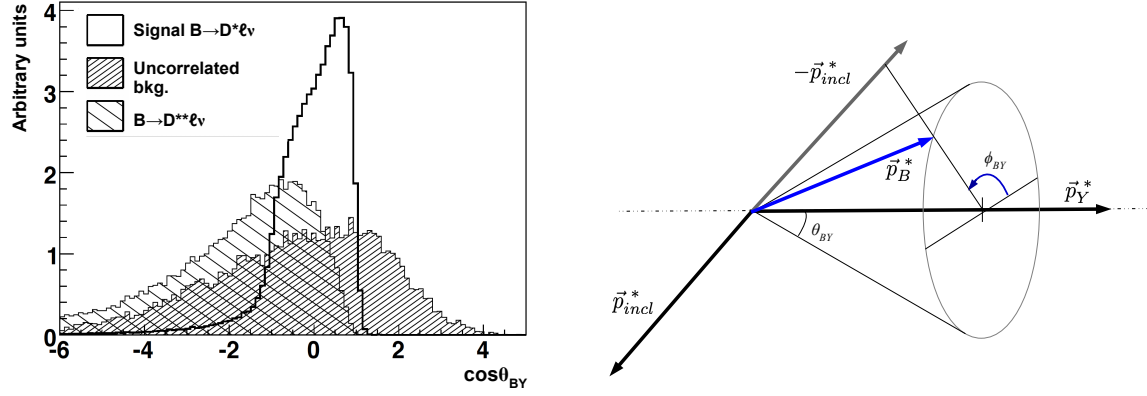


Figure 11. Left: the $\cos\theta_{BY}$ distribution for the signal $B \rightarrow D^* e \nu_e$, the D^{**} and the uncorrelated background. The differences in shapes show the discriminating power of this variable. Because of the bremsstrahlung the tail extend in the $\cos\theta_{BY} < -1$ region. Right: illustration on how the direction of the B meson is determined. The quantity \vec{p}_{incl}^* is given summing the three-momentum of the particles not associated to the signal. The direction of the signal B , \vec{p}_B^* , is the one that minimizes the distance with the $-\vec{p}_{incl}^*$ vector.

are 0.020 for w , 0.038 for $\cos\theta_\ell$, 0.044 for $\cos\theta_V$ and 0.210 for χ . The data are divided in 10 equidistant bins for each of four variables. The distributions of these variables, after the fit, are shown in figure 12. The signal yields in the four one-dimensional projections are simultaneously fitted to extract the shape of the form factors. Because the same events enter into the four projections, the correlation between all the various bins has to be carefully evaluated for both signal and backgrounds.

The measured yields are normalized to the total number of B^0 in the sample analyzed, which is given by $N_{B^0} = 2 \cdot f_{00} \cdot N_{BB}$, where N_{BB} is the total number of BB pairs collected by Belle, known with a precision of 1.4%, and f_{00} is the branching ratio of $\Upsilon(4S) \rightarrow B^0 \bar{B}^0$ determined to be $f_{00} = 0.486 \pm 0.006$ [89].

The results of the fit on $\eta_{EW} \mathcal{F}(1) |V_{cb}|$ with the CLN parameterization are given in table 4, together with the results from other measurements obtained with the CLN. This result, consistent with the other measurements, is the most precise and dominates the HFLAV average. It is dominated by the systematic uncertainties which give a contribution of 1.6%, while the statistic uncertainty is only 0.4%. The dominant source of systematics is the tracking efficiency, mainly the soft pion one, the lepton identification and the uncertainty on the total number of $\Upsilon(4S)$ candidates. Also the external parameters, $\mathcal{B}(D \rightarrow K\pi)$ and f_{+-}/f_{00} , give significant contributions.

The results of the fit with the BGL parameterization is reported in table 3. The series in the expansion of the form factors are truncated at $n = 1$ for $f(z)$ and $g(z)$, instead $\mathcal{F}_1(z)$ is truncated at $n = 2$. Following the notation used in [88], this BGL configuration is called $\text{BGL}^{(121)}$ and has five free parameters, one more than the CLN one. This parameterization describes the data very well and the data are not sensitive

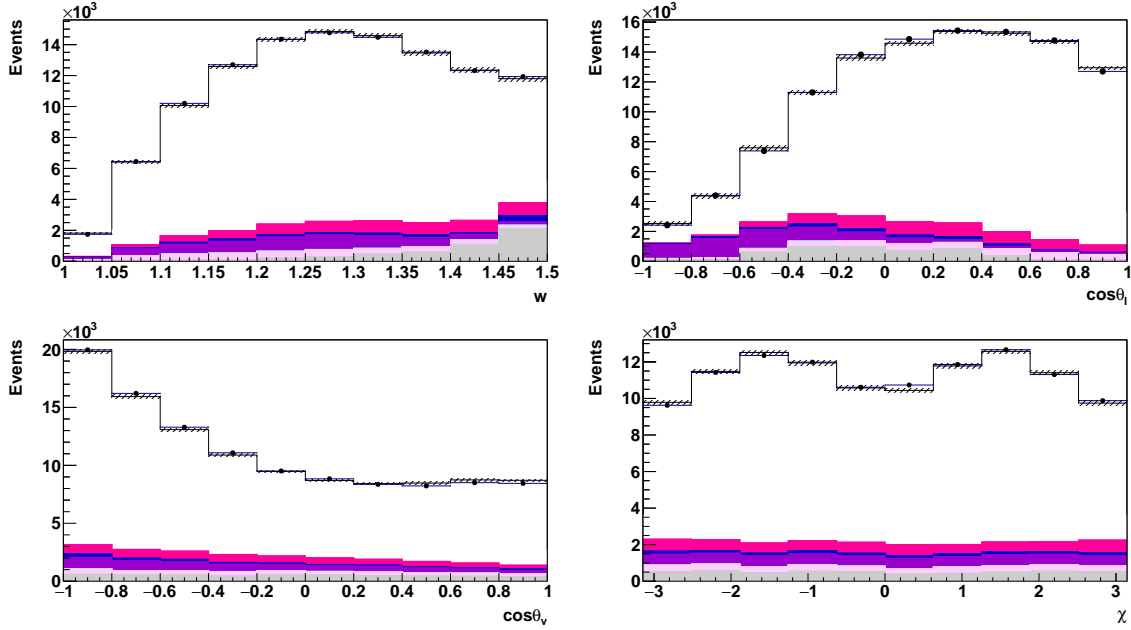


Figure 12. Distribution of the variables w , the cosine of the angles θ_V , θ_ℓ , and the angle χ for the Belle analysis of $B \rightarrow D^* \ell \nu_\ell$. The fit results using the CLN parameterization is superimposed. From [150].

to higher orders coefficients. The unitarity constraints has not been applied. The result on $|V_{cb}|$ obtained with the BGL parametrization is compatible with the CLN one, but has a larger statistical uncertainty. And the χ^2/ndf of the fit to Belle data, in both CLN and BGL cases, are acceptable, so the data available are not sensitive to the different parametrizations.

6.3.2. BaBar tagged measurement BaBar has measured the shape of the form factors of $B^0 \rightarrow D^{*-} \ell^+ \nu_\ell$ decays using both CLN and BGL parameterizations [87]. This analysis is based on the full dataset of $450 fb^{-1}$, and exploits a sample where one of the B is fully reconstructed. The hadronic B -tagging is described in section 4.2. The knowledge of the kinematic of the B_{tag} event by event, and the beam properties, allows to determine the four-momentum of the neutrino from the missing four-momentum $p_{miss} = p_{e^+} + p_{e^-} - p_{B_{tag}} - p_{D^* \ell}$.

In this analysis two decay chains are considered: $B^0 \rightarrow D^{*-} \ell^+ \nu_\ell$ with $D^{*-} \rightarrow \bar{D}^0 \pi^-$, and $B^+ \rightarrow D^{*0} \ell^+ \nu_\ell$ with $D^{*0} \rightarrow \bar{D}^0 \pi^0$.

The \bar{D}^0 is reconstructed in the three cleanest modes $K^+ \pi^-$, $K^+ \pi^- \pi^0$, $K^+ \pi^- \pi^+ \pi^-$. As usual the D^* is selected requiring Δm to be consistent with the expectation. The lepton is required to have momentum in the laboratory frame greater than 0.2 GeV or 0.3 GeV for it is an electron or a muon, respectively. Besides the B_{tag} , the D^* and the lepton, no additional tracks are allowed in the event. The full decay chain $e^+ e^- \rightarrow \Upsilon(4S) \rightarrow B_{tag} B_{sig} (\rightarrow D^* \ell \nu_\ell)$ is considered in a kinematic fit that includes constraints on the beam spot, the secondary vertices, the masses of B_{tag} , B_{sig} , D^*

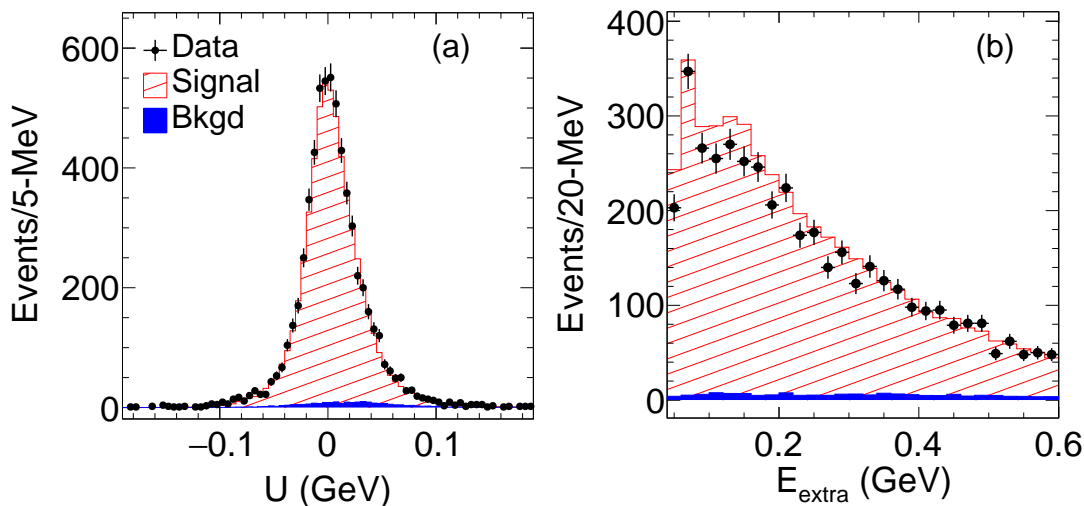


Figure 13. Comparison between data and simulation in the variables U (a) and E_{extra} (b). From [87].

and the missing neutrino. The probability of the χ^2 of this constrained fit is the main discriminating variables against the backgrounds. The sample is further cleaned rejecting candidates with large values for E_{extra} , which is defined as the sum of the energy of the photons not associated with the signal. The overall background level is only 2% and it is due to $B\bar{B}$ events decaying generically. The agreement between the signal and simulations for the E_{extra} and the variable $U = E_{miss} - |\vec{p}_{miss}|$ is very good, as can be seen in figure 13. After all the selection requirements, a total of about 5900 signal candidates is obtained.

The shape of the form factors is extracted using an unbinned maximum likelihood fit where the signal events are described by the four dimensional decay rate $d\Gamma/dwdw$. All events in the signal region, defined by $|U| < 90$ MeV, are considered in the likelihood as signal, and the small residual background is subtracted using information from large sample of $B\bar{B}$ simulated events.

The extraction of $|V_{cb}|$ is performed indirectly by adding to the likelihood the constraint that the integrated rate $\Gamma = \mathcal{B}/\tau_B$, where \mathcal{B} is the $B \rightarrow D^*\ell\nu$ branching fraction and τ_B is the B -meson lifetime. The values of these external inputs are taken from HFLAV [79].

The result with the BGL parametrization is reported in table 3 and with the CLN one in table 4. They are perfectly compatible and also compatible with the HFLAV average. Because of the limited signal statistics, the form factors are truncated at $n = 1$, BGL⁽¹¹¹⁾, and the unitarity constraint is not applied.

The dominant source of systematic uncertainty on the measurement of $|V_{cb}|$ is due to the remnant background that contaminates the angular distributions. The resolution on the kinematic variables, which is not considered in the fit, is about a factor five better than the one possible with the untagged measurement. The impact of the finite resolution is evaluated using the simulation and turns out to be negligible.

6.3.3. Results Table 4 reports a summary of the measurements of $\eta_{EW}\mathcal{F}(1)|V_{cb}|$ obtained with the CLN parametrization, together with the HFLAV average. Using the FLAG 2019 value for the normalization of the form factor $\eta_{EW}\mathcal{F}(1) = 0.910 \pm 0.013$, the HFLAV average for $|V_{cb}|$ is

$$|V_{cb}| = (38.76 \pm 0.42 \pm 0.55) \times 10^{-3} \quad (82)$$

where the first error is experimental and the second is due to the form factor normalization. The results obtained with CLN and BGL parameterizations are consistent.

In the 2017 the Belle collaboration released an analysis, not published, of $B \rightarrow D^* \ell \nu$ using the hadronic B -tagging [85]. The form factors and $|V_{cb}|$ were extracted from the projections on w and the angles w with a fit similar to the one described before for the untagged analysis. The result of the fit, performed using the CLN parameterization, was consistent with previous measurements. The Belle collaboration released also the spectra of the projections on the four kinematic variable, unfolded for the resolution and corrected for the efficiencies. Some groups took this opportunity to fit the Belle data using not only the CLN parametrization but also the BGL one [83, 147, 148, 155]. They observed that the central value of $|V_{cb}|$ using the BGL parameterization was systematically higher than the value obtained with the CLN one, and that, depending on the choice of constraints and inputs of the analysis, could be lifted up to 6 – 7%. For illustration, we report in table 3 the BGL results of [147]. The fact that the BGL result became compatible with the inclusive determination of $|V_{cb}|$ disclosed the possibility that a suitable choice of the parametrization could be enough to solve the $|V_{cb}|$ puzzle. However, some inconsistencies were observed in the fits exploiting the BGL approach;

Table 3. Fit results with the BGL parameterization of some recent analyses. The notation is $\text{BGL}^{n_f, n_{F1}, n_g}$ where n_f , n_{F1} and n_g are the order of the z -expansions for the $f(z)$, $F_1(z)$ and $g(z)$ respectively. The parameters cannot be compared directly because different constants are used, in particular the B_c^* masses value in the Blasckhe factor.

BGL	Bigi et al. [147]	Belle [150]	BaBar [87]	Gambino et al. [88]
	BGL^{222}	BGL^{120}	BGL^{111}	BGL^{222}
$ V_{cb} \times 10^{-3}$	$41.7^{+2.0}_{-2.1}$	38.3 ± 0.97	38.36 ± 0.90	$39.6^{+1.1}_{-1.0}$
a_0^f	0.01223 ± 0.00018	0.0131 ± 0.0002	0.0129 ± 0.0003	0.01221 ± 0.00016
a_1^f	$-0.054^{+0.058}_{-0.043}$	0.0169 ± 0.0050	0.0163 ± 0.0010	$0.006^{+0.032}_{-0.045}$
a_2^f	$0.20^{+0.7}_{-1.2}$	-	-	$-0.2^{+1.2}_{-0.8}$
$a_1^{F_1}$	$-0.0100^{+0.0061}_{-0.0056}$	0.0070 ± 0.0018	0.0003 ± 0.0011	0.0042 ± 0.0022
$a_2^{F_1}$	0.012 ± 0.010	0.085 ± 0.034	-	$-0.069^{+0.041}_{-0.037}$
a_0^g	$0.012^{+0.011}_{-0.008}$	-0.0241 ± 0.0058	0.0274 ± 0.0011	$0.024^{+0.021}_{-0.009}$
a_1^g	$0.7^{+0.3}_{-0.4}$	-	0.0833 ± 0.0667	$0.05^{+0.39}_{-0.72}$
a_2^g	$0.8^{+0.2}_{-1.7}$	-	-	$1.0^{+0.0}_{-2.0}$

for example it was shown in [155] that the form factor ratio $R_1(w)$ determined from the results of the fits strongly contradict the HQS predictions.

More data were eagerly needed. They have been provided in 2018 by Belle [150] and in 2019 by Babar [87]. These analyses, detailed in section 6.3.1 and 6.3.2, respectively, show no sign of discrepancy on $|V_{cb}|$ between the BGL and CLN parameterizations, within the uncertainties. Belle also in this case released the data in a format that

Table 4. Results of $B \rightarrow D^* \ell \nu_\ell$ measurements with the CLN parameterization and the current HFLAV average [79]. Only $\eta_{EW} \mathcal{F}(1) |V_{cb}| (\times 10^3)$ and ρ^2 are reported.

	$\eta_{EW} \mathcal{F}(1) V_{cb} (\times 10^3)$	ρ^2	Remarks
BaBar [151]	$33.77 \pm 0.29 \pm 0.98$ $1.184 \pm 0.048 \pm 0.029$		Untagged measurement of the $B^0 \rightarrow D^{*-} \ell^+ \nu_\ell$ decay. Fit to the four projections: w and the three helicity angles. Data fitted with the CLN. Extracted also $R_1(1)$ and $R_2(1)$, together with ρ^2 . The form factors are further constrained to a dedicated measurement performed by BaBar which uses only clean $B^0 \rightarrow D^{*+} e \nu$ data samples [152].
BaBar [153]	$34.81 \pm 0.58 \pm 1.06$ $1.125 \pm 0.058 \pm 0.053$		Untagged measurement of $B^+ \rightarrow D^{*0} \ell^+ \nu_\ell$ with D^{*0} reconstructed in $\bar{D}^0 \pi^0$ decay mode. One-dimensional fit of w using only CLN. Parameters $R_1(1)$ and $R_2(1)$ taken from external inputs.
BaBar [154]	$35.75 \pm 0.20 \pm 1.09$ $1.180 \pm 0.020 \pm 0.061$		Global analysis of $B \rightarrow D^* \ell \nu_\ell$ and $B \rightarrow D \ell \nu_\ell$ using inclusive samples of $B \rightarrow D^- \ell \nu_\ell X$ and $B \rightarrow \bar{D}^0 \ell \nu_\ell X$ decays. The fit is performed multidimensional on p_ℓ^* , p_D^* and $\cos \theta_{BY}$ variables. Only the CLN parameterization was used.
Belle [150]	$35.07 \pm 0.15 \pm 0.56$ $1.106 \pm 0.031 \pm 0.008$		Untagged measurement of $B^0 \rightarrow D^{*-} \ell^+ \nu_\ell$. Fit to the four projections. Data fitted with the CLN. Extracted also $R_1(1)$ and $R_2(1)$, together with ρ^2 . Results also using the BGL. Published also the background subtracted spectra of the four projections with all the information, like efficiencies and migration matrix, needed for subsequent refitting.
HFLAV [79]	$35.27 \pm 0.11 \pm 0.36$ $1.122 \pm 0.015 \pm 0.019$		The average includes also older measurements from CLEO and LEP experiments: DELPHI, ATLAS and OPAL. The average Confidence Level is only 0.8%.
Belle [85]	$34.93 \pm 0.23 \pm 0.59$		Tagged measurement of $B^0 \rightarrow D^{*-} \ell^+ \nu_\ell$, not published. For the first time the spectrum of the projections on q^2 and the angular variables was released. The spectrum unfolded and corrected for the efficiency was also released.
BaBar [87]	34.94 ± 0.50 0.96 ± 0.08		Tagged measurement of $B^+ \rightarrow D^{*0} \ell^+ \nu_\ell$ and $B^0 \rightarrow D^{*-} \ell^+ \nu_\ell$ decays. Not included yet in the HFLAV average. The uncertainties include both the statistical and systematics. Fit is unbinned to q^2 and the angular variables. Data fitted using both CLN and BGL. This measurement is not normalized, so $ V_{cb} $ is extracted from the measured $B^+ \rightarrow D^{*0} \ell \nu$ branching fractions [79].

allows them to be fitted by outside groups, prompting a new analysis by some among the authors of the 2017 fits [88]. The new fits, which include also the previous Belle analysis, have been performed with both CLN and BGL parameterizations, in different configurations, and the results found to be consistent. Also the BGL discrepancy with HQS mentioned before seems to be overcome. The BGL value is reported in table 3, for comparison with the results of Belle and Babar.

Nevertheless the initial discrepancies have been useful to revisit the assumptions under the widely used CLN parameterization. The possible systematics due to the parameterization itself had never been considered in the $|V_{cb}|$ extraction. Theoretical analyses have investigated constraints and subtleties of the different approaches, including the studies on the optimal number of parameters of the BGL fit, and the risk of overfitting [88, 156]. Moreover, with only few exceptions, most of the experimental analyses were using only the CLN parameterization. With the increasing precision, it is crucial to describe the shape of the form factors in a model independent way. It is worth to mention now that, when calculation of the form factor at $w > 1$ will be available, the role of parameterizations will become less relevant, because the extrapolation to $w = 1$ will reduce to an interpolation between experimental results and different theory points.

6.4. $B \rightarrow D\ell\nu_\ell$ channel

The analysis of $B \rightarrow D\ell\nu_\ell$ decays is difficult because of the large background from $B \rightarrow D^*\ell\nu_\ell$ where the D^* decays in $D\pi$ or $D\gamma$, with the soft pion or gamma lost or not detected. This kind of background is usually called *down-feed* in the literature. In the past, untagged approaches have been used, similar to the one described above for the $B \rightarrow D^*\ell\nu_\ell$, by the CLEO [157] and Belle [158] collaborations. CLEO has used both $B^+ \rightarrow \bar{D}^0\ell^+\nu_\ell$ and $B^0 \rightarrow D^-\ell^+\nu_\ell$ decays. In general, the signal selection relies mostly on the selection of a good D meson candidate, so the combinatorial background is large. The consequence is that only few, low multiplicity D decay modes can be exploited. CLEO in fact uses the $\bar{D}^0 \rightarrow K^+\pi^-$ and $D^- \rightarrow K^+\pi^-\pi^-$ decay modes, which are the cleanest. The $B^+ \rightarrow \bar{D}^0\ell^+\nu_\ell$ decays with the untagged approach is the most difficult because of the large down-feed: the \bar{D}^0 can come from both $B^+ \rightarrow D^{*0}\ell^+\nu_\ell$, with D^{*0} decaying in \bar{D}^0 almost all the time, and $B^0 \rightarrow D^{*-}\ell^+\nu_\ell$ with $D^{*-} \rightarrow \bar{D}^0\pi^-$, which has a branching fraction of 68%. The $B^0 \rightarrow D^-\ell^+\nu_\ell$ instead is easier because the D^- comes only from $B^+ \rightarrow D^{*0}\ell^+\nu_\ell$ with $D^{*0} \rightarrow D^-\pi^0$, which has a branching fraction of only 31%. For this reason Belle analyzed only the $B^0 \rightarrow D^-\ell^+\nu_\ell$. The larger phase space suppression in the region close to $w \rightarrow 1$ for the $B \rightarrow D$ decays, compared with the $B \rightarrow D^*$, implies a large background in the region crucial for the $|V_{cb}|$ extraction.

The hadronic B -tagging is particularly suitable for the $B \rightarrow D\ell\nu_\ell$, as shown in the BaBar analysis [159], where both $B^0 \rightarrow D^-\ell^+\nu_\ell$ and $B^+ \rightarrow \bar{D}^0\ell^+\nu_\ell$ are studied. The hadronic tagging allows to reduce the combinatorial background in the \bar{D}^0 and D^- reconstruction, and also the down-feed from D^* and D^{**} decays, because the tagging allows to separate clearly $\Upsilon(4S) \rightarrow B^+B^-$ from $\Upsilon(4S) \rightarrow B^0\bar{B}^0$ decay modes.

6.4.1. Belle tagged analysis The most precise measurement has been done by Belle [160] and uses an improved hadronic b -tagging approach. The tracks and the clusters of the event, remaining after the identification of the B_{tag} , are used to identify the $B \rightarrow D\ell\nu_\ell$ signal decay. The lepton is required to have a momentum greater than 0.3 GeV for the electron case, and 0.6 GeV for the muon case. The low signal efficiency, due to the reconstruction of the hadronic tag, is partially compensated by the possibility to reconstruct D mesons in many different decays modes, also including π^0 and K_s particles. In particular, the D^- meson is reconstructed in 10 possible final states, covering about 29% of the total rate, and the \bar{D}^0 is reconstructed in 13 final states, corresponding to more than 40% of the total rate.

The discriminating variable used to separate the signal $B \rightarrow D\ell\nu_\ell$ from background is the missing mass squared M_{miss}^2 . The distribution of M_{miss}^2 for a bin in w is reported in figure 14 separately for B^0 and B^+ decays. The signal extraction is performed separately in ten bins in w , in the range from 1 to 1.6, with the Barlow and Beeston algorithm [161], that accounts for statistical uncertainties in both data and simulation. The shapes of the backgrounds and the signal are determined from simulations and fixed in the fit. The fit to extract the signal yields is simultaneous in the four samples: $B^0 \rightarrow D^- e^+ \nu_e$, $B^+ \rightarrow \bar{D}^0 e^+ \nu_e$, $B^0 \rightarrow D^- \mu^+ \nu_\mu$, $B^+ \rightarrow \bar{D}^0 \mu^+ \nu_\mu$. The largest source of systematic uncertainty is due to the calibration of the hadronic B -tagging sample. This calibration is required because the composition and the efficiency of the various hadronic B decay modes used in the B -tagging definition have to be adapted to the data. The other relevant sources of uncertainties are the knowledge of the branching ratios of D^- and \bar{D}^0 mesons, and of the tracking efficiency.

The distribution of the measured differential decay width $d\Gamma/dw$, is shown in figure 15 (left) with the result of the fit using the BGL parameterisation, superimposed. The fit also exploits the available lattice calculations from FNAL/MILC [63] and HPQCD [64] for the values of $w \in (1, 1.08, 1.16)$. The lattice calculations are obtained for both $f_+(z)$ and $f_0(z)$, while the experimental $d\Gamma/dw$ depends only on $f_+(z)$. Nevertheless, exploiting the kinematic constraint between f_+ and f_0 at maximum recoil, $f_0(q_{min}^2) = f_+(q_{min}^2)$, the lattice data on $f_0(z)$ help to reduce the uncertainties on $|V_{cb}|$. The fit result depends on the truncation order n of the $f_{+,0}(z)$ series. The default result is obtained with $n = 3$ because the fit stabilizes for $n \geq 3$. The result is $|V_{cb}| = (40.83 \pm 1.13) \times 10^{-3}$. By fitting $d\Gamma/dw$ with the CLN parameterization, and taking $\mathcal{G}(1) = 1.0541 \pm 0.0083$ [41], the results is $|V_{cb}| = (39.86 \pm 1.33) \times 10^{-3}$. The result with the CLN parameterization is less precise than BGL one because in the latter additional lattice point are used.

6.4.2. Results A summary of the measurements of $\eta_{EW}\mathcal{G}(1)|V_{cb}|$ obtained with the CLN parameterization is reported in table 5, together with the HFLAV average. Using the $\mathcal{G}(1)$ from [41], the HFLAV average is

$$|V_{cb}| = (39.58 \pm 0.94 \pm 0.37) \times 10^{-3} \quad (83)$$

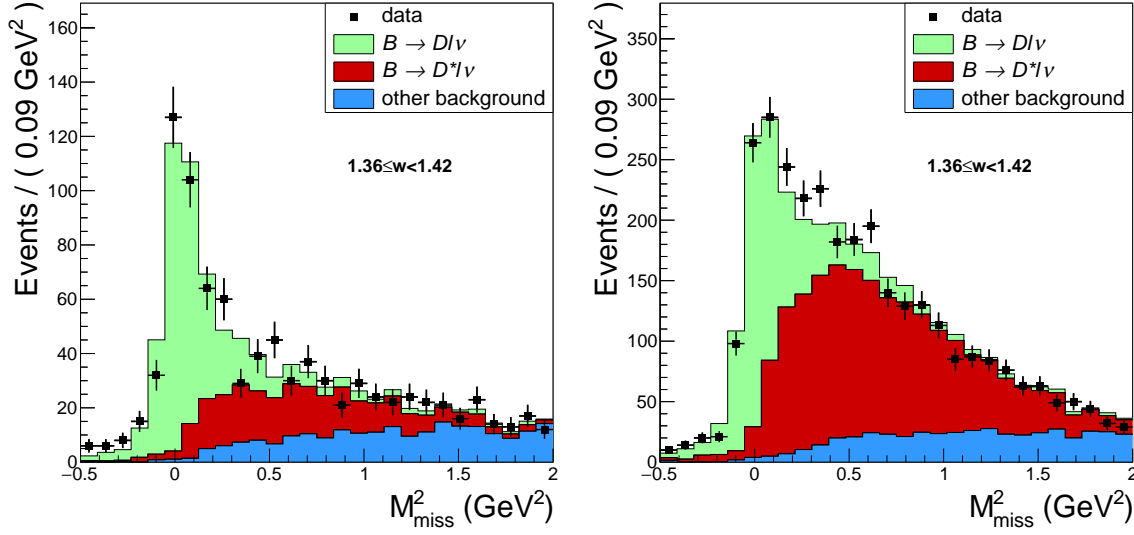


Figure 14. Distribution of M_{miss}^2 from the Belle tagged analysis [160]. The distribution corresponds to the bin with $1.36 < w < 1.42$ separately for $B^0 \rightarrow D^- e^+ \nu_e$ decays (left) and $B^+ \rightarrow \bar{D}^0 e^+ \nu_e$ decays (right). The larger down-feed due to D^* background present in the B^+ sample is clearly visible.

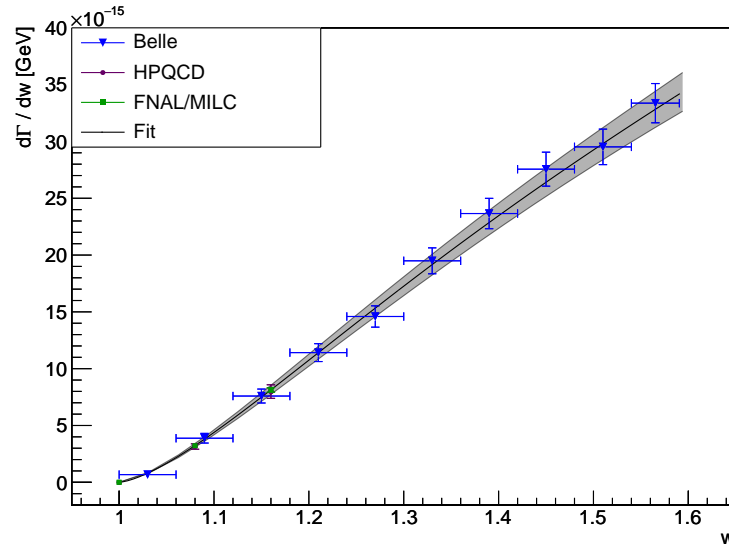


Figure 15. Differential decay width of $B \rightarrow D \ell \nu_\ell$ decay obtained by Belle [160], and results of the combined fit between data and lattice calculations from FNAL/MILC and HPQCD.

where the first error is experimental and the second is due to the form factor normalization. This result is compatible with the result from $B \rightarrow D^* \ell \nu_\ell$ given in section 82. A fit of both BaBar and Belle data, combined with lattice calculation and performed using both BGL and CLN parameterizations, gives consistent results, even if the BGL value, $|V_{cb}| = (40.49 \pm 0.97) \times 10^{-3}$, is slightly higher than the one obtained with CLN [80].

Table 5. Results of $B \rightarrow D\ell\nu_\ell$ measurements with the CLN parameterization and the current HFLAV average [79]. Both $\eta_{EW}\mathcal{G}(1)|V_{cb}|$ and ρ^2 are reported.

	$\eta_{EW}\mathcal{G}(1) V_{cb} $ ρ^2	Remarks
BaBar [154]	$42.76 \pm 1.71 \pm 1.26$ $1.200 \pm 0.088 \pm 0.043$	Global analysis of $B \rightarrow D^*\ell\nu_\ell$ and $B \rightarrow D\ell\nu_\ell$ using inclusive samples of $B \rightarrow D^-\ell\nu_\ell X$ and $B \rightarrow \bar{D}^0\ell\nu_\ell X$ decays. The fit is multidimensional on p_ℓ^* , p_D^* and $\cos\theta_{BY}$ variables. Only the CLN parameterization was used.
BaBar [159]	$42.76 \pm 1.71 \pm 1.26$ $1.200 \pm 0.088 \pm 0.043$	Tagged measurement using both B^0 and B^+ . The sample is normalized to the inclusive $B \rightarrow X\ell\nu$ which is known with an uncertainty of only 1%. The fit is based on CLN.
Belle [160]	$42.22 \pm 0.60 \pm 1.21$ $1.090 \pm 0.036 \pm 0.019$	Tagged measurement using both B^0 and B^+ . Both fit use CLN and BGL, as well as the lattice data points at non-zero recoil from FNAL/MILC [63] and HPQCD [64]. This analysis published also the unfolded w spectrum corrected for the efficiency.
HFLAV [79]	$42.00 \pm 0.45 \pm 0.89$ $1.131 \pm 0.024 \pm 0.023$	The average includes also an older measurement from CLEO.

6.5. Direct measurement of $|V_{ub}/V_{cb}|$

The LHCb collaboration has measured the ratio of the branching fractions $\Lambda_b^0 \rightarrow p\mu^-\bar{\nu}_\mu$ and $\Lambda_b^0 \rightarrow \Lambda_c^+\mu\bar{\nu}_\mu$ [162], from which they have determined the first direct measurement of the ratio $|V_{ub}/V_{cb}|$. The measured ratio of branching fractions is related to $|V_{ub}/V_{cb}|$ through the relation

$$\frac{|V_{ub}|}{|V_{cb}|} = \sqrt{R_{FF} \frac{\mathcal{B}(\Lambda_b^0 \rightarrow p\mu\nu_\mu)}{\mathcal{B}(\Lambda_b^0 \rightarrow \Lambda_c^+\mu\nu_\mu)}}, \quad (84)$$

where R_{FF} is the ratio of the relevant form factors, which have to be calculated using non perturbative approaches. In lattice QCD, unquenched results for the form factors away from the static limit have been performed in 2015 [163].

In the normalization channel $\Lambda_b^0 \rightarrow \Lambda_c^-\mu\nu_\mu$, the baryon Λ_c^- is reconstructed requiring $\Lambda_c^+ \rightarrow pK^-\pi^+$. With the choice of this normalization channel, many systematic uncertainties cancel, in particular the uncertainty on the Λ_b^0 production rate, the muon and the proton identification efficiency. Only the efficiency of the kaon and the pion required to reconstruct the Λ_c^- , and the slight differences in the detector acceptances of the proton and muon due to the slightly different kinematics, have to be properly accounted. Both the signal and the normalization reconstruction require isolated, well separated vertexes for both $p\mu$ and $p\Lambda_c^+$ from the primary vertex. This reduces most of the combinatorial background and down-feed from B -hadron decays with additional charged tracks. The remaining background comes from down-feed events with neutral or unreconstructed charged particles. For example, for the signal $\Lambda_b^0 \rightarrow p\mu\nu_\mu$, it comes mainly from $\Lambda_b^0 \rightarrow \Lambda_c\mu\nu_\mu$, where $\Lambda_c \rightarrow pX$ and $\Lambda_b^0 \rightarrow N^*\mu\nu_\mu$, with an excited baryon

N^* decaying in proton and missing particles. A powerful variable, useful to discriminate the signal from down-feed background categories, is the corrected mass defined as $m_{corr} = \sqrt{m_Y^2 + |\vec{p}_\perp|^2} + |\vec{p}_\perp|$, where \vec{p}_\perp is the transverse momentum (to the flight direction) of the visible system Y , that is $p\mu$ or $\Lambda_c\mu$. The variable m_{corr} peaks at the mass of the Λ_b^0 when there is a single massless particle missing, and peaks at lower values for down-feed backgrounds $\dagger\dagger$. The available lattice QCD calculation [163] is more accurate in the high q^2 region, in particular the predicted ratio $1/R_{FF} = 1.471 \pm 0.095 \pm 0.109$, where the first uncertainty is statistical and the second systematic, is given in the regions $q^2 > 15 \text{ GeV}^2$ and $q^2 > 7 \text{ GeV}^2$ for $\Lambda_b^0 \rightarrow p\mu\nu_\mu$ and $\Lambda_b^0 \rightarrow \Lambda_c^-\mu\nu_\mu$ respectively. The measurement is performed in both regions, where also the signal extraction is cleaner. The q^2 reconstruction is performed as described in section 4.3.1. The problem of having two equally probable solutions (see section 4.3.1) for each reconstructed Λ_b^0 momentum affects the resolution of q^2 . As a consequence, the measured partially fractions computed in the high q^2 range have to be corrected for the effect of the limited q^2 resolution. To avoid biases in the measurement, the ratio of branching fractions is extracted only for events where both the solutions are within the q^2 ranges considered. Even if this choice results in a loss of efficiency, it has been beneficial for the control of the systematic uncertainties.

The measurement of the branching fraction of the normalization channel relies on the known absolute branching fraction $\mathcal{B}(\Lambda_c \rightarrow pK\pi) = (6.28 \pm 0.32)\%$ [89], whose value is based on the average of the two most precise available measurements [164, 165], by Belle and BESIII, respectively. It is worth to mention that these measurements are only marginally consistent, and more effort should be pursued, using BaBar and LHCb data.

Updating the measured ratio in [162] with the most recent value of $\mathcal{B}(\Lambda_c \rightarrow pK\pi)$ [89], one obtains

$$\frac{|V_{ub}|}{|V_{cb}|} = 0.079 \pm 0.004 \pm 0.004, \quad (85)$$

where the first uncertainty is experimental and the second one is from the lattice QCD calculation. Even if this is not a direct measurement of $|V_{cb}|$, by taking $|V_{ub}|$ from external inputs it is possible to determine $|V_{cb}|$. For instance, using the exclusive determination of the $B \rightarrow \pi\ell\nu_\ell$ decay rate from HFLAV [79], one obtains $|V_{cb}| = (46.4 \pm 3.8) \times 10^{-2}$, which is compatible with the inclusive measurement, as reported in section 5.2. This measurement of $|V_{ub}/V_{cb}|$ relies only on a single lattice QCD calculation, but the predicted q^2 shape for the normalization channel has been validated by a LHCb measurement of the q^2 spectrum of $\Lambda_b^0 \rightarrow \Lambda_c^+\mu\nu_\mu$ decays [166].

The LHCb analysis, besides being the first one made at hadronic colliders, and the first one to use B -baryon decays, opened the possibility to extract $|V_{ub}/V_{cb}|$ from the ratio $\mathcal{B}(B_s \rightarrow K\mu\nu_\mu)/\mathcal{B}(B_s \rightarrow D_s\mu\nu_\mu)$, a measurement which is ongoing at LHCb.

$\dagger\dagger$ It is interesting to mention that m_{corr} can be generalized also to the case of a massive missing particle, assuming $B \rightarrow YX$ where Y is the visible system, and X a single particle with mass m_X . In this case, under the same assumptions behind the standard formula, one has $m_{corr} = \sqrt{m_Y^2 + |\vec{p}_\perp|^2} + \sqrt{m_X^2 + |\vec{p}_\perp|^2}$.

6.6. The $|V_{cb}|$ puzzle

As we have seen, the inclusive and exclusive semileptonic searches rely on different theoretical tools and experimental techniques. The agreement among $|V_{cb}|$ values from inclusive and exclusive decays can be regarded as an interesting test of our capability to investigate weak interactions and QCD dynamics. From this prospective, a lot of attention has been devoted to a discrepancy which, since more than three decades, is observed between the values extracted from exclusive and inclusive decays. It is referred as the $|V_{cb}|$ puzzle.

In figure 16 we summarize exclusive and inclusive determinations of $|V_{cb}|$ and compare with the analogous determinations of $|V_{ub}|$.

The most precise estimates of $|V_{cb}|$ stem from the $B \rightarrow D^* \ell \nu_\ell$ channel with inputs from lattice, followed by determinations based on inclusive measurements. Their uncertainties all stay around 1.8%. In figure 16 the vertical bands represent the different determinations of $|V_{cb}|$. We have separated the bands relative to exclusive $|V_{cb}|$ determination with $B \rightarrow D^* \ell \nu_\ell$ and $B \rightarrow D \ell \nu_\ell$ decays. Both show a discrepancy with the the band relative to the inclusive determination. The bands relative to the exclusive $B \rightarrow D$ and $B \rightarrow D^*$ decays are the HFLAV averages done with the CLN parameterizations. Also considering the slightly larger uncertainty associated with the BGL fit to $B \rightarrow D^* \ell \nu_\ell$ decays described before, the discrepancy with the inclusive determinations remains significant. The tension amounts to about 3σ .

It is also possible to determine $|V_{cb}|$ indirectly, using the CKM unitarity relations together with CP violation and flavour data, excluding direct informations on decays. The indirect fits provided by the CKMfitter collaboration [5] and by the UTfit collaboration [6] are in agreement between them and seem to prefer the inclusive value for $|V_{cb}|$, as shown in figure 16.

In figure 16 we report also the world average values of the CKM parameter $|V_{ub}|$ obtained by HFLAV collaboration. Precise values for $|V_{ub}|$ are also obtained from semileptonic decays. The CKM-suppressed decay $B \rightarrow \pi \ell \nu_\ell$ is the typical exclusive channel used to extract $|V_{ub}|$, being better controlled both experimentally and theoretically. We report also the band constrained by the $|V_{ub}|/|V_{cb}|$ ratio measurement reported in (85). The LHCb measurement is consistent with the prediction from the indirect determination.

As it can be seen in figure 16, $|V_{ub}|$ shares with $|V_{cb}|$ the discrepancy between inclusive and exclusive values, which is labelled, similarly, the $|V_{ub}|$ puzzle (for concise reviews see f.i. [167–170]). Most of the theoretical and experimental considerations presented in this review apply also to the $|V_{ub}|$ determination. The main differences between $|V_{cb}|$ and $|V_{ub}|$ determinations emerge in inclusive decays. Due to the large background to $B \rightarrow X_u \ell \nu_\ell$ decays represented by $B \rightarrow X_c \ell \nu_\ell$ decays, the phase space region is strongly limited by the experimental cuts needed to reduce the background. This requires to address theoretical issues absent in the inclusive $|V_{cb}|$ determination, since the experimental cuts enhance the relevance of a region in the phase space,

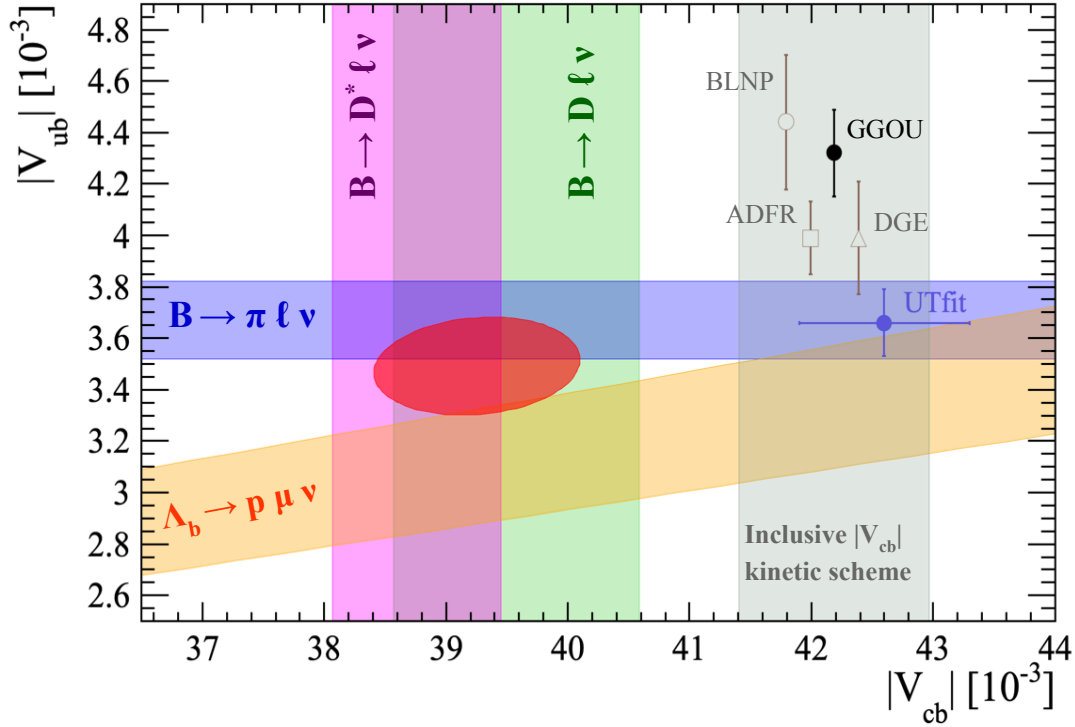


Figure 16. The combined $V_{ub} - V_{cb}$ average obtained by HFLAV including the exclusive measurements of $|V_{ub}|$ from $B \rightarrow \pi \ell \nu$ (blue), $|V_{cb}|$ from $B \rightarrow D^* \ell \nu_\ell$ (magenta) and $B \rightarrow D \ell \nu_\ell$ (green) decays, and $|V_{ub}/V_{cb}|$ (orange) from $\Lambda_b \rightarrow p \mu \nu$ decay. The grey band refers to inclusive $|V_{cb}|$ in the kinetic scheme. The result on inclusive $|V_{ub}|$ with different calculations are the four points with vertical error bars. The shift along the x-axis of these four points is just arbitrary and has no meaning. The blue point are the result of the indirect predictions of $|V_{ub}|$ and $|V_{cb}|$ obtained by the UTfit collaboration [6] and based on the global fit to the unitarity triangle.

the so-called threshold region, where the applicability of HQE is compromised. In place of a widely accepted theoretical tool as the HQE, several models or schemes have been devised. They are all tailored to analyze data in the threshold region, but differ in their treatment of perturbative corrections and the parametrization of non-perturbative effects. In figure 16 we show the results for the four theoretical approaches included in the HFLAV averages [79]: ADFR (Aglietti, Di Lodovico, Ferrera, Ricciardi) [171–173], BLNP (Bosch, Lange, Neubert, Paz) [174–176], DGE (Dressed Gluon Exponentiation) [177] and GGOU (Gambino, Giordano, Ossola, Uraltsev) [178]. The results are based on the same experimental inputs (apart the one from ADFR which does not include the latest result from BaBar [179]), and are slightly above the exclusive $|V_{ub}|$ value, extracted from both $B \rightarrow \pi \ell \nu_\ell$ and $\Lambda_b \rightarrow p \mu \nu_\mu$ decays.

7. Future prospects

The pattern of quark and lepton masses and mixings remains one of the most debated and interesting open questions in particle physics, in spite of a plethora of new experimental results. The precise determination of the CKM matrix elements connects flavour physics with the Higgs sector, since they represent the couplings of the Higgs boson to fermions. Generations of dedicated experiments have provided us with more and more precise measurements and exposed a flavor pattern of an highly non-generic structure, begging for an underlying organizing principle, which is still unveiled. Experimental hints for deviations from SM predictions in flavour processes are one of our best hopes to direct research towards the right energy scale of new physics. As suggested by the 2020 EPPSU update [180], flavor physics should remain at the forefront of the European particle physics strategy. In this wide perspective, the search for very high precision in $|V_{cb}|$ determination is actively pursued on both experimental and theoretical sides.

In exclusive decays, the larger theoretical uncertainties in the $|V_{cb}|$ determination, amounting to about 1.4%, concern the extraction from $B \rightarrow D^* \ell \nu_\ell$ decays, while the experimental error is maximum, about 2%, for values extracted from $B \rightarrow D \ell \nu_\ell$ decays, as can be seen in the averages (82) and (83). A theoretical research area with direct impact on future experimental programmes is lattice gauge theory, the only systematically improvable method for nonperturbative calculations in QCD. Like in the case of the exclusive $|V_{cb}|$ determination from $B \rightarrow D \ell \nu_\ell$ decays, determinations from $B \rightarrow D^* \ell \nu_\ell$ decays are expected to improve significantly as soon as lattice calculations of the form factors at non-zero recoil will become fully available. The pivotal importance of precise information on the form factors is a clear outcome of the analyses on form factors parametrization in exclusive determinations, discussed in section 6.3.3. For example, it has been noted [88] that a possible steeper slope of the form factor $\mathcal{F}(w)$ at zero recoil could lift the value of the exclusive $|V_{cb}|$ determination towards agreement with inclusive determinations.

While lattice unquenched results for the form factors of $B \rightarrow D^{(*)}$ semileptonic decays have been available since at least 10 years, lattice analyses for inclusive decays move now their first significant steps. On lattice it is not straightforward to extract inclusive observables, i.e. quantities that are summed over all multiparticle final states. Major challenges are that the lattice calculations are performed in a finite volume and naturally formulated in the Euclidean space, which complicates the analyses of correlation functions for the case of multi-particle states in the kinematical region accessible on the lattice. A large body of work has already gone into developing algorithms and theory to overcome these and similar limitations, with significant implications also on other branches of physics and mathematics (for details see f.i. [181]). A different suggestion, specific to inclusive semileptonic B decays, is to analytically continue the amplitude from the experimentally accessible physical kinematic region to an unphysical region in which the lattice calculation can be performed [182].

As mentioned in section 3.2.2, another interesting exclusive channel is the semileptonic $B_s \rightarrow D_s \ell \nu_\ell$, where form factors are already available, while the experimental analyses are still in progress. Future theoretical advances are also expected for B decays to excited D meson states. The required accuracy could come from Belle II, which has the potential to precisely isolate all four orbitally excited modes and characterize their sub-decay modes, constraining and measuring the branching ratios with higher accuracy [183]. Form factors must be determined in all modes through precise differential measurements. Complementary information on the decay rates of orbitally excited modes should be extracted from hadronic B decays and include multi-pion and other light quark meson transitions. Lattice studies are in progress with realistic charm mass, and results on $\bar{B} \rightarrow D^{**} l \nu$ form factors are available, still at a preliminary stage, since 2013 [184]. For recent and more complete reviews on open charmed systems see f.i. [185, 186].

A promising field of study are Λ_b baryons, which represent approximately 20% of all bottom hadrons produced at the LHC. The measurement of the ratio of $\Lambda_b^0 \rightarrow p \mu^- \bar{\nu}_\mu$ and $\Lambda_b^0 \rightarrow \Lambda_c^+ \mu^- \bar{\nu}_\mu$ decay rates at LHCb, combined with a lattice QCD calculation of the $\Lambda_b \rightarrow p$ and $\Lambda_b \rightarrow \Lambda_c$ form factors [163], has allowed the first determination of $|V_{ub}|/|V_{cb}|$ at a hadron collider [162]. We have shown the band of results in figure 16. Right now, theory uncertainties are approximately 5%, comparable with the experimental uncertainty. As the experimental uncertainty is expected to reach about 2% with the expected integrated luminosity of 50 fb^{-1} and the foreseen improvements in the $\Lambda_c \rightarrow p K \pi$ branching fraction uncertainty, further theoretical progress is needed, which could come from lattice improvements to the form factors computation. The baryonic decays are sensitive to both the vector and axial-vector currents in the weak effective Hamiltonian, and their measurements can also represent a check of right-handed couplings beyond the Standard Model.

The Belle II experiment at KEK started recently to take data from the renewed e^+e^- KEK-B accelerator (SuperKEKB), designed to reach an instantaneous luminosity 50 times higher than KEK-B. The final goal of Belle II is to collect 50 ab^{-1} by 2025. The precise study of semileptonic B meson decays will be part of the Belle II program [183]. However, the increase in luminosity is not enough by itself, because most of the measurements that we have presented above, are limited by systematics and not by the statistical uncertainties.

For the exclusive $|V_{cb}|$, the most precise measurement is the Belle untagged analysis of $B \rightarrow D^* \ell \nu_\ell$ decays, where the systematic uncertainty is 2.5 times the statistical uncertainty. The largest contribution to the systematics are due to the tracking and the particle identification, and the second largest one is due to the external inputs like the branching fraction of $D^0 \rightarrow K \pi$ and f_{00} . The tagged analyses of $B \rightarrow D^* \ell \nu_\ell$ are reaching the precision of the untagged measurements, but are at present affected by large uncertainties due to the calibration of the hadronic B tagging. The reduction of all these sources of systematics is paramount to exploit the huge statistics available at Belle-II. Also the analyses approaches have to be revisited. For instance, as we have

shown before, the BaBar tagged measurement, which performed a truly four-dimensional fit despite the fact that the signal yield was only 1/30 of the Belle signal yields, has reached comparable good precision.

The semileptonic B decays we have considered are tree-level processes in the SM, which are generally assumed, in all analyses, unaffected by NP contributions. Because of their pivotal role in precise measurements of the CKM matrix elements, it is not without importance to ascertain the validity of this assumption, given also the tensions underlined above, f.i. the $|V_{cb}|$ puzzle. There are several analyses addressing this issue, but their results do not support evidence of NP in decays driven by $b \rightarrow c\ell\nu_\ell$ transitions, where ℓ is a light lepton (see f.i. [187–189]). Particular attention deserves $R(D^{(*)})$, discussed in section 3.3, whose measured value differs from the SM prediction. A better understanding of this discrepancy could shed light on possible NP and as such it is a priority for Belle-II and for the future planned LHCb upgrade.

Acknowledgments

It is a pleasure to thank Aoifa Barucha and Francesco Polci for their invitation to give GDR-InF lectures at the Institut Henri Poincaré (Paris, France), where part of this work was performed, and for providing a stimulating environment. G.R. acknowledges partial financial support from MIUR under Project No. 2015P5SBHT and from the INFN research initiative ENP.

8. Bibliography

- [1] Buras A J, De Fazio F and Girrbach J 2014 *Eur. Phys. J.* **C74** 2950 (*Preprint* 1404.3824)
- [2] Wolfenstein L 1983 *Phys. Rev. Lett.* **51** 1945
- [3] Buras A J, Lautenbacher M E and Ostermaier G 1994 *Phys. Rev.* **D50** 3433–3446 (*Preprint* hep-ph/9403384)
- [4] Jarlskog C 1985 *Phys. Rev. Lett.* **55** 1039
- [5] Charles J, Hocker A, Lackner H and Laplace S, Le Diberder F R, Malcles J, Ocariz J, Pivk M and L R (CKMfitter Group) updated results URL http://ckmfitter.in2p3.fr/www/html/ckm_main.html
- [6] Alpigiani C, Bevan A, Bona M, Ciuchini M, Derkach D, Franco E, Lubicz V, Martinelli G, Parodi F, Pierini M, Schiavi C, Silvestrini L, Sordini V, Stocchi A, Tarantino C and Vagnoni V (Ufit Group) updated results URL <http://www.utfit.org/UTfit/WebHome>
- [7] Shifman M A 2001 Quark hadron duality *At the frontier of particle physics. Handbook of QCD. Vol. 1-3* World Scientific (Singapore: World Scientific) pp 1447–1494 [3,1447(2000)] (*Preprint* hep-ph/0009131) URL <http://jhep.sissa.it/archive/prhep/preproceeding/hf8/013>
- [8] Bigi I I Y and Uraltsev N 2001 *Int. J. Mod. Phys.* **A16** 5201–5248 (*Preprint* hep-ph/0106346)
- [9] Manohar A V and Wise M B 2000 *Camb. Monogr. Part. Phys. Nucl. Phys. Cosmol.* **10** 1–191
- [10] Melnikov K 2008 *Phys. Lett.* **B666** 336–339 (*Preprint* 0803.0951)
- [11] Gambino P 2011 *JHEP* **09** 055 (*Preprint* 1107.3100)
- [12] Trott M 2004 *Phys. Rev.* **D70** 073003 (*Preprint* hep-ph/0402120)
- [13] Aquila V, Gambino P, Ridolfi G and Uraltsev N 2005 *Nucl. Phys.* **B719** 77–102 (*Preprint* hep-ph/0503083)
- [14] Pak A and Czarnecki A 2008 *Phys. Rev. Lett.* **100** 241807 (*Preprint* 0803.0960)

- [15] Pak A and Czarnecki A 2008 *Phys. Rev.* **D78** 114015 (*Preprint* 0808.3509)
- [16] Biswas S and Melnikov K 2010 *JHEP* **02** 089 (*Preprint* 0911.4142)
- [17] Benson D, Bigi I I, Mannel T and Uraltsev N 2003 *Nucl. Phys.* **B665** 367–401 (*Preprint* hep-ph/0302262)
- [18] Becher T, Boos H and Lunghi E 2007 *JHEP* **12** 062 (*Preprint* 0708.0855)
- [19] Alberti A, Ewerth T, Gambino P and Nandi S 2013 *Nucl. Phys.* **B870** 16–29 (*Preprint* 1212.5082)
- [20] Alberti A, Gambino P and Nandi S 2014 *JHEP* **01** 147 (*Preprint* 1311.7381)
- [21] Mannel T, Pivovarov A A and Rosenthal D 2015 *Phys. Lett.* **B741** 290–294 (*Preprint* 1405.5072)
- [22] Mannel T, Pivovarov A A and Rosenthal D 2015 *Phys. Rev.* **D92** 054025 (*Preprint* 1506.08167)
- [23] Gremm M and Kapustin A 1997 *Phys. Rev.* **D55** 6924–6932 (*Preprint* hep-ph/9603448)
- [24] Mannel T and Pivovarov A A 2019 (*Preprint* 1907.09187)
- [25] Bigi I I, Uraltsev N and Zwicky R 2007 *Eur. Phys. J.* **C50** 539–556 (*Preprint* hep-ph/0511158)
- [26] Breidenbach C, Feldmann T, Mannel T and Turczyk S 2008 *Phys. Rev.* **D78** 014022 (*Preprint* 0805.0971)
- [27] Bigi I, Mannel T, Turczyk S and Uraltsev N 2010 *JHEP* **04** 073 (*Preprint* 0911.3322)
- [28] Dassinger B M, Mannel T and Turczyk S 2007 *JHEP* **03** 087 (*Preprint* hep-ph/0611168)
- [29] Mannel T, Turczyk S and Uraltsev N 2010 *JHEP* **11** 109 (*Preprint* 1009.4622)
- [30] Heinonen J and Mannel T 2014 *Nucl. Phys.* **B889** 46–63 (*Preprint* 1407.4384)
- [31] Beneke M 1999 *Phys. Rept.* **317** 1–142 (*Preprint* hep-ph/9807443)
- [32] Bigi I I Y, Shifman M A, Uraltsev N G and Vainshtein A I 1995 *Phys. Rev.* **D52** 196–235 (*Preprint* hep-ph/9405410)
- [33] Bigi I I Y, Shifman M A, Uraltsev N and Vainshtein A I 1997 *Phys. Rev.* **D56** 4017–4030 [*205(1996)*] (*Preprint* hep-ph/9704245)
- [34] Bigi I I Y, Shifman M A and Uraltsev N 1997 *Ann. Rev. Nucl. Part. Sci.* **47** 591–661 (*Preprint* hep-ph/9703290)
- [35] Beneke M 1998 *Phys. Lett.* **B434** 115–125 (*Preprint* hep-ph/9804241)
- [36] Hoang A H, Ligeti Z and Manohar A V 1999 *Phys. Rev. Lett.* **82** 277–280 (*Preprint* hep-ph/9809423)
- [37] Hoang A H, Ligeti Z and Manohar A V 1999 *Phys. Rev.* **D59** 074017 (*Preprint* hep-ph/9811239)
- [38] Hoang A H and Teubner T 1999 *Phys. Rev.* **D60** 114027 (*Preprint* hep-ph/9904468)
- [39] Uraltsev N 2004 Heavy quark expansion in beauty: Recent successes and problems *Continuous advances in QCD. Proceedings, Conference, Minneapolis, USA, May 13-16, 2004* pp 100–114 (*Preprint* hep-ph/0409125)
- [40] Sirlin A 1982 *Nucl. Phys.* **B196** 83–92
- [41] Bailey J A *et al.* (Fermilab Lattice, MILC) 2014 *Phys. Rev.* **D89** 114504 (*Preprint* 1403.0635)
- [42] Ball P and Zwicky R 2001 *JHEP* **10** 019 (*Preprint* hep-ph/0110115)
- [43] Ball P and Zwicky R 2005 *Phys. Rev.* **D71** 014015 (*Preprint* hep-ph/0406232)
- [44] Becirevic D and Kaidalov A B 2000 *Phys. Lett.* **B478** 417–423 (*Preprint* hep-ph/9904490)
- [45] Caprini I, Lellouch L and Neubert M 1998 *Nucl. Phys.* **B530** 153–181 (*Preprint* hep-ph/9712417)
- [46] Boyd C G, Grinstein B and Lebed R F 1995 *Phys. Rev. Lett.* **74** 4603–4606 (*Preprint* hep-ph/9412324)
- [47] Bourrely C, Caprini I and Lellouch L 2009 *Phys. Rev.* **D79** 013008 [Erratum: *Phys. Rev.* D82,099902(2010)] (*Preprint* 0807.2722)
- [48] Isgur N and Wise M B 1989 *Phys. Lett.* **B232** 113–117
- [49] Isgur N and Wise M B 1990 *Phys. Lett.* **B237** 527–530
- [50] Caswell W E and Lepage G P 1986 *Phys. Lett.* **167B** 437–442
- [51] Harrison J, Davies C and Wingate M (HPQCD) 2018 *Phys. Rev.* **D97** 054502 (*Preprint* 1711.11013)
- [52] McLean E, Davies C T H, Lytle A T and Koponen J 2019 *Phys. Rev.* **D99** 114512 (*Preprint* 1904.02046)

- [53] de Divitiis G M, Petronzio R and Tantalo N 2009 *Nucl. Phys.* **B807** 373–395 (*Preprint* 0807.2944)
- [54] Vaquero Avilés-Casco A, DeTar C, Du D, El-Khadra A, Kronfeld A S, Laiho J and Van de Water R S 2018 *EPJ Web Conf.* **175** 13003 (*Preprint* 1710.09817)
- [55] Avilés-Casco A V, DeTar C, El-Khadra A X, Kronfeld A S, Laiho J and Van de Water R S (Fermilab Lattice, MILC) 2019 *PoS LATTICE2018* 282 (*Preprint* 1901.00216)
- [56] Bailey J A, Bhattacharya T, Gupta R, Jang Y C, Lee W, Leem J, Park S and Yoon B (LANL-SWME) 2018 *EPJ Web Conf.* **175** 13012 (*Preprint* 1711.01786)
- [57] Kaneko T, Aoki Y, Colquhoun B, Fukaya H and Hashimoto S (JLQCD) 2018 *PoS LATTICE2018* 311 (*Preprint* 1811.00794)
- [58] Gambino P, Mannel T and Uraltsev N 2010 *Phys. Rev.* **D81** 113002 (*Preprint* 1004.2859)
- [59] Gambino P, Mannel T and Uraltsev N 2012 *JHEP* **10** 169 (*Preprint* 1206.2296)
- [60] Gubernari N, Kokulu A and van Dyk D 2019 *JHEP* **01** 150 (*Preprint* 1811.00983)
- [61] Bordone M, Jung M and van Dyk D 2019 (*Preprint* 1908.09398)
- [62] de Divitiis G M, Molinaro E, Petronzio R and Tantalo N 2007 *Phys. Lett.* **B655** 45–49 (*Preprint* 0707.0582)
- [63] Bailey J A *et al.* (MILC) 2015 *Phys. Rev.* **D92** 034506 (*Preprint* 1503.07237)
- [64] Na H, Bouchard C M, Lepage G P, Monahan C and Shigemitsu J (HPQCD) 2015 *Phys. Rev.* **D92** 054510 [Erratum: *Phys. Rev.*D93,no.11,119906(2016)] (*Preprint* 1505.03925)
- [65] Bailey J A *et al.* 2012 *Phys. Rev.* **D85** 114502 [Erratum: *Phys. Rev.*D86,039904(2012)] (*Preprint* 1202.6346)
- [66] Monahan C J, Na H, Bouchard C M, Lepage G P and Shigemitsu J 2017 *Phys. Rev.* **D95** 114506 (*Preprint* 1703.09728)
- [67] Atoui M, Morénas V, Bećirevic D and Sanfilippo F 2014 *Eur. Phys. J.* **C74** 2861 (*Preprint* 1310.5238)
- [68] Flynn J M, Hill R C, Jüttner A, Soni A, Tsang J T and Witzel O 2019 *PoS LATTICE2018* 290 (*Preprint* 1903.02100)
- [69] McLean E, Davies C T H, Koponen J and Lytle A T 2019 (*Preprint* 1906.00701)
- [70] Matyja A *et al.* (Belle) 2007 *Phys. Rev. Lett.* **99** 191807 (*Preprint* 0706.4429)
- [71] Lees J P *et al.* (BaBar) 2012 *Phys. Rev. Lett.* **109** 101802 (*Preprint* 1205.5442)
- [72] Lees J P *et al.* (BaBar) 2013 *Phys. Rev.* **D88** 072012 (*Preprint* 1303.0571)
- [73] Huschle M *et al.* (Belle) 2015 *Phys. Rev.* **D92** 072014 (*Preprint* 1507.03233)
- [74] Aaij R *et al.* (LHCb) 2015 *Phys. Rev. Lett.* **115** 111803 [Erratum: *Phys. Rev. Lett.*115,no.15,159901(2015)] (*Preprint* 1506.08614)
- [75] Sato Y *et al.* (Belle) 2016 *Phys. Rev.* **D94** 072007 (*Preprint* 1607.07923)
- [76] Caria G *et al.* (Belle) 2019 (*Preprint* 1910.05864)
- [77] Hirose S *et al.* (Belle) 2017 *Phys. Rev. Lett.* **118** 211801 (*Preprint* 1612.00529)
- [78] Aaij R *et al.* (LHCb) 2018 *Phys. Rev. Lett.* **120** 171802 (*Preprint* 1708.08856)
- [79] Amhis Y S *et al.* (HFLAV) 2019 updated results and plots available at <https://hflav.web.cern.ch/> (*Preprint* 1909.12524)
- [80] Bigi D and Gambino P 2016 *Phys. Rev.* **D94** 094008 (*Preprint* 1606.08030)
- [81] Bernlochner F U, Ligeti Z, Papucci M and Robinson D J 2017 *Phys. Rev.* **D95** 115008 [erratum: *Phys. Rev.*D97,no.5,059902(2018)] (*Preprint* 1703.05330)
- [82] Bigi D, Gambino P and Schacht S 2017 *JHEP* **11** 061 (*Preprint* 1707.09509)
- [83] Jaiswal S, Nandi S and Patra S K 2017 *JHEP* **12** 060 (*Preprint* 1707.09977)
- [84] Fajfer S, Kamenik J F and Nisandzic I 2012 *Phys. Rev.* **D85** 094025 (*Preprint* 1203.2654)
- [85] Abdesselam A *et al.* (Belle) 2017 (*Preprint* 1702.01521)
- [86] Aoki S *et al.* (Flavour Lattice Averaging Group) 2019 (*Preprint* 1902.08191)
- [87] Lees J P *et al.* (BaBar) 2019 *Phys. Rev. Lett.* **123** 091801 (*Preprint* 1903.10002)
- [88] Gambino P, Jung M and Schacht S 2019 *Phys. Lett.* **B795** 386–390 (*Preprint* 1905.08209)
- [89] Tanabashi M *et al.* (Particle Data Group) 2018 *Phys. Rev.* **D98** 030001

- [90] Abe K *et al.* (Belle) 2004 *Phys. Rev.* **D69** 112002 (*Preprint hep-ex/0307021*)
- [91] Aubert B *et al.* (BaBar) 2009 *Phys. Rev.* **D79** 112004 (*Preprint 0901.1291*)
- [92] Aaij R *et al.* (LHCb) 2015 *Phys. Rev.* **D91** 092002 [Erratum: *Phys. Rev.* D93,no.11,119901(2016)] (*Preprint 1503.02995*)
- [93] Aaij R *et al.* (LHCb) 2015 *Phys. Rev.* **D92** 032002 (*Preprint 1505.01710*)
- [94] Aaij R *et al.* (LHCb) 2016 *Phys. Rev.* **D94** 072001 (*Preprint 1608.01289*)
- [95] Aubert B *et al.* (BaBar) 2008 *Phys. Rev. Lett.* **101** 261802 (*Preprint 0808.0528*)
- [96] Liventsev D *et al.* (Belle) 2008 *Phys. Rev.* **D77** 091503 (*Preprint 0711.3252*)
- [97] del Amo Sanchez P *et al.* (BaBar) 2010 *Phys. Rev.* **D82** 111101 (*Preprint 1009.2076*)
- [98] Aaij R *et al.* (LHCb) 2013 *JHEP* **09** 145 (*Preprint 1307.4556*)
- [99] Aubert B *et al.* (BaBar) 2008 *Phys. Rev. Lett.* **100** 151802 (*Preprint 0712.3503*)
- [100] Le Yaouanc A, Oliver L, Pene O and Raynal J C 1996 *Phys. Lett.* **B387** 582–592 (*Preprint hep-ph/9607300*)
- [101] Uraltsev N 2001 *Phys. Lett.* **B501** 86–91 [,195(2000)] (*Preprint hep-ph/0011124*)
- [102] Morenas V, Le Yaouanc A, Oliver L, Pene O and Raynal J C 1996 *Phys. Lett.* **B386** 315–327 (*Preprint hep-ph/9605206*)
- [103] Morenas V, Le Yaouanc A, Oliver L, Pene O and Raynal J C 1997 *Phys. Rev.* **D56** 5668–5680 (*Preprint hep-ph/9706265*)
- [104] Ebert D, Faustov R N and Galkin V O 1998 *Phys. Lett.* **B434** 365–372 (*Preprint hep-ph/9805423*)
- [105] Ebert D, Faustov R N and Galkin V O 2000 *Phys. Rev.* **D61** 014016 (*Preprint hep-ph/9906415*)
- [106] Segovia J, Albertus C, Entem D R, Fernandez F, Hernandez E and Perez-Garcia M A 2011 *Phys. Rev.* **D84** 094029 (*Preprint 1107.4248*)
- [107] Leibovich A K, Ligeti Z, Stewart I W and Wise M B 1998 *Phys. Rev.* **D57** 308–330 (*Preprint hep-ph/9705467*)
- [108] Bigi I I, Blossier B, Le Yaouanc A, Oliver L, Pene O, Raynal J C, Oyanguren A and Roudeau P 2007 *Eur. Phys. J.* **C52** 975–985 (*Preprint 0708.1621*)
- [109] Lees J P *et al.* (BaBar) 2016 *Phys. Rev. Lett.* **116** 041801 (*Preprint 1507.08303*)
- [110] Klein R, Mannel T, Shahriaran F and van Dyk D 2015 *Phys. Rev.* **D91** 094034 (*Preprint 1503.00569*)
- [111] Bernlochner F U, Ligeti Z and Turczyk S 2012 *Phys. Rev.* **D85** 094033 (*Preprint 1202.1834*)
- [112] Bećirević D, Le Yaouanc A, Oliver L and Raynal J C 2017 *Phys. Rev.* **D96** 036018 (*Preprint 1705.05667*)
- [113] Bevan A J *et al.* (BaBar, Belle) 2014 *Eur. Phys. J.* **C74** 3026 (*Preprint 1406.6311*)
- [114] Nason P *et al.* 1999 Bottom production 1999 CERN Workshop on standard model physics (and more) at the LHC, CERN, Geneva, Switzerland, 25-26 May: Proceedings pp 231–304 (*Preprint hep-ph/0003142*)
- [115] Alves Jr A A *et al.* (LHCb) 2008 *JINST* **3** S08005
- [116] Aaij R *et al.* (LHCb) 2017 *Phys. Rev. Lett.* **118** 052002 [Erratum: *Phys. Rev. Lett.* 119,no.16,169901(2017)] (*Preprint 1612.05140*)
- [117] Aaij R *et al.* (LHCb) 2019 *Phys. Rev.* **D100** 031102 (*Preprint 1902.06794*)
- [118] Aubert B *et al.* (BaBar) 2002 *Nucl. Instrum. Meth.* **A479** 1–116 (*Preprint hep-ex/0105044*)
- [119] Aubert B *et al.* (BaBar) 2013 *Nucl. Instrum. Meth.* **A729** 615–701 (*Preprint 1305.3560*)
- [120] Bondar A (Belle) 1998 *Nucl. Instrum. Meth.* **A408** 64–76
- [121] Allmendinger T *et al.* 2013 *Nucl. Instrum. Meth.* **A704** 44–59 (*Preprint 1207.2849*)
- [122] Feindt M, Keller F, Kreps M, Kuhr T, Neubauer S, Zander D and Zupanc A 2011 *Nucl. Instrum. Meth.* **A654** 432–440 (*Preprint 1102.3876*)
- [123] Aaij R *et al.* (LHCb) 2015 *Int. J. Mod. Phys.* **A30** 1530022 (*Preprint 1412.6352*)
- [124] Dambach S, Langenegger U and Starodumov A 2006 *Nucl. Instrum. Meth.* **A569** 824–828 (*Preprint hep-ph/0607294*)
- [125] Ciezarek G, Lupato A, Rotondo M and Vesterinen M 2017 *JHEP* **02** 021 (*Preprint 1611.08522*)

- [126] Aaij R *et al.* (LHCb) 2019 *Phys. Rev.* **D99** 092009 (*Preprint* 1807.10722)
- [127] Aubert B *et al.* (BaBar) 2010 *Phys. Rev.* **D81** 032003 (*Preprint* 0908.0415)
- [128] Aubert B *et al.* (BaBar) 2004 *Phys. Rev.* **D69** 111104 (*Preprint* hep-ex/0403030)
- [129] Schwanda C *et al.* (Belle) 2007 *Phys. Rev.* **D75** 032005 (*Preprint* hep-ex/0611044)
- [130] Urquijo P *et al.* (Belle) 2007 *Phys. Rev.* **D75** 032001 (*Preprint* hep-ex/0610012)
- [131] Acosta D *et al.* (CDF) 2005 *Phys. Rev.* **D71** 051103 (*Preprint* hep-ex/0502003)
- [132] Csorna S E *et al.* (CLEO) 2004 *Phys. Rev.* **D70** 032002 (*Preprint* hep-ex/0403052)
- [133] Abdallah J *et al.* (DELPHI) 2006 *Eur. Phys. J.* **C45** 35–59 (*Preprint* hep-ex/0510024)
- [134] Hocker A and Kartvelishvili V 1996 *Nucl. Instrum. Meth.* **A372** 469–481 (*Preprint* hep-ph/9509307)
- [135] Gambino P and Schwanda C 2014 *Phys. Rev.* **D89** 014022 (*Preprint* 1307.4551)
- [136] Alberti A, Gambino P, Healey K J and Nandi S 2015 *Phys. Rev. Lett.* **114** 061802 (*Preprint* 1411.6560)
- [137] Chetyrkin K G, Kuhn J H, Maier A, Maierhofer P, Marquard P, Steinhauser M and Sturm C 2009 *Phys. Rev.* **D80** 074010 (*Preprint* 0907.2110)
- [138] Bauer C W, Ligeti Z, Luke M, Manohar A V and Trott M 2004 *Phys. Rev.* **D70** 094017 (*Preprint* hep-ph/0408002)
- [139] Gambino P, Healey K J and Turczyk S 2016 *Phys. Lett.* **B763** 60–65 (*Preprint* 1606.06174)
- [140] Fael M, Mannel T and Keri Vos K 2019 *JHEP* **02** 177 (*Preprint* 1812.07472)
- [141] Abbas G, Ananthanarayan B, Caprini I, Sentitemsu Imsong I and Ramanan S 2010 *Eur. Phys. J.* **A45** 389–399 (*Preprint* 1004.4257)
- [142] Bourrely C, Machet B and de Rafael E 1981 *Nucl. Phys.* **B189** 157–181
- [143] Boyd C G, Grinstein B and Lebed R F 1997 *Phys. Rev.* **D56** 6895–6911 (*Preprint* hep-ph/9705252)
- [144] Boyd C G and Savage M J 1997 *Phys. Rev.* **D56** 303–311 (*Preprint* hep-ph/9702300)
- [145] Grinstein B and Lebed R F 2015 *Phys. Rev.* **D92** 116001 (*Preprint* 1509.04847)
- [146] Boyd C G, Grinstein B and Lebed R F 1996 *Nucl. Phys.* **B461** 493–511 (*Preprint* hep-ph/9508211)
- [147] Bigi D, Gambino P and Schacht S 2017 *Phys. Lett.* **B769** 441–445 (*Preprint* 1703.06124)
- [148] Grinstein B and Kobach A 2017 *Phys. Lett.* **B771** 359–364 (*Preprint* 1703.08170)
- [149] Duboscq J E *et al.* (CLEO) 1996 *Phys. Rev. Lett.* **76** 3898–3902
- [150] Waheed E *et al.* (Belle) 2019 *Phys. Rev.* **D100** 052007 (*Preprint* 1809.03290)
- [151] Aubert B *et al.* (BaBar) 2008 *Phys. Rev.* **D77** 032002 (*Preprint* 0705.4008)
- [152] Aubert B *et al.* (BaBar) 2006 *Phys. Rev.* **D74** 092004 (*Preprint* hep-ex/0602023)
- [153] Aubert B *et al.* (BaBar) 2008 *Phys. Rev. Lett.* **100** 231803 (*Preprint* 0712.3493)
- [154] Aubert B *et al.* (BaBar) 2009 *Phys. Rev.* **D79** 012002 (*Preprint* 0809.0828)
- [155] Bernlochner F U, Ligeti Z, Papucci M and Robinson D J 2017 *Phys. Rev.* **D96** 091503 (*Preprint* 1708.07134)
- [156] Bernlochner F U, Ligeti Z and Robinson D J 2019 *Phys. Rev.* **D100** 013005 (*Preprint* 1902.09553)
- [157] Bartelt J E *et al.* (CLEO) 1999 *Phys. Rev. Lett.* **82** 3746 (*Preprint* hep-ex/9811042)
- [158] Abe K *et al.* (Belle) 2002 *Phys. Lett.* **B526** 258–268 (*Preprint* hep-ex/0111082)
- [159] Aubert B *et al.* (BaBar) 2010 *Phys. Rev. Lett.* **104** 011802 (*Preprint* 0904.4063)
- [160] Glattauer R *et al.* (Belle) 2016 *Phys. Rev.* **D93** 032006 (*Preprint* 1510.03657)
- [161] Barlow R J and Beeston C 1993 *Comput. Phys. Commun.* **77** 219–228
- [162] Aaij R *et al.* (LHCb) 2015 *Nature Phys.* **11** 743–747 (*Preprint* 1504.01568)
- [163] Detmold W, Lehner C and Meinel S 2015 *Phys. Rev.* **D92** 034503 (*Preprint* 1503.01421)
- [164] Zupanc A *et al.* (Belle) 2014 *Phys. Rev. Lett.* **113** 042002 (*Preprint* 1312.7826)
- [165] Ablikim M *et al.* (BESIII) 2016 *Phys. Rev. Lett.* **116** 052001 (*Preprint* 1511.08380)
- [166] Aaij R *et al.* (LHCb) 2017 *Phys. Rev.* **D96** 112005 (*Preprint* 1709.01920)
- [167] Ricciardi G 2017 *Mod. Phys. Lett.* **A32** 1730005 (*Preprint* 1610.04387)
- [168] Ricciardi G 2014 *Mod. Phys. Lett.* **A29** 1430019 (*Preprint* 1403.7750)

- [169] Ricciardi G 2013 *Mod. Phys. Lett.* **A28** 1330016 (*Preprint* 1305.2844)
- [170] Ricciardi G 2012 *Mod. Phys. Lett.* **A27** 1230037 (*Preprint* 1209.1407)
- [171] Aglietti U and Ricciardi G 2004 *Phys. Rev.* **D70** 114008 (*Preprint* hep-ph/0407225)
- [172] Aglietti U, Ferrera G and Ricciardi G 2007 *Nucl. Phys.* **B768** 85–115 (*Preprint* hep-ph/0608047)
- [173] Aglietti U, Di Lodovico F, Ferrera G and Ricciardi G 2009 *Eur. Phys. J.* **C59** 831–840 (*Preprint* 0711.0860)
- [174] Lange B O, Neubert M and Paz G 2005 *Phys. Rev.* **D72** 073006 (*Preprint* hep-ph/0504071)
- [175] Bosch S W, Lange B O, Neubert M and Paz G 2004 *Nucl. Phys.* **B699** 335–386 (*Preprint* hep-ph/0402094)
- [176] Bosch S W, Neubert M and Paz G 2004 *JHEP* **11** 073 (*Preprint* hep-ph/0409115)
- [177] Andersen J R and Gardi E 2006 *JHEP* **01** 097 (*Preprint* hep-ph/0509360)
- [178] Gambino P, Giordano P, Ossola G and Uraltsev N 2007 *JHEP* **10** 058 (*Preprint* 0707.2493)
- [179] Lees J P *et al.* (BaBar) 2017 *Phys. Rev.* **D95** 072001 (*Preprint* 1611.05624)
- [180] Ellis R K *et al.* 2019 (*Preprint* 1910.11775)
- [181] Lehner C *et al.* (USQCD) 2019 *Eur. Phys. J.* **A55** 195 (*Preprint* 1904.09479)
- [182] Hashimoto S 2017 *PTEP* **2017** 053B03 (*Preprint* 1703.01881)
- [183] Altmannshofer W *et al.* (Belle-II) 2018 (*Preprint* 1808.10567)
- [184] Atoui M, Blossier B, Morénas V, Pène O and Petrov K 2015 *Eur. Phys. J.* **C75** 376 (*Preprint* 1312.2914)
- [185] Chen H X, Chen W, Liu X, Liu Y R and Zhu S L 2017 *Rept. Prog. Phys.* **80** 076201 (*Preprint* 1609.08928)
- [186] Le Yaouanc A and Pène O 2015 *Int. J. Mod. Phys.* **A30** 1543009 [171(2014)] (*Preprint* 1408.5104)
- [187] Jung M and Straub D M 2019 *JHEP* **01** 009 (*Preprint* 1801.01112)
- [188] Crivellin A and Pokorski S 2015 *Phys. Rev. Lett.* **114** 011802 (*Preprint* 1407.1320)
- [189] Colangelo P and De Fazio F 2018 *JHEP* **06** 082 (*Preprint* 1801.10468)